Beach-dune morphodynamics and climatic variability in Gwaii Haanas National Park Reserve and Haida Heritage Site, British Columbia, Canada.

by

Rebecca Miville Cumming
B.Sc.Hon., University of Victoria, 2005

A Thesis Submitted in Partial Fulfillment
of the Requirements for the Degree of

MASTER OF SCIENCE

in the Department of Geography

Beach-dune morphodynamics and climatic variability in Gwaii Haanas National Park Reserve and Haida Heritage Site, British Columbia, Canada.

by

Rebecca Miville Cumming
B.Sc.Hon., University of Victoria, 2005

Supervisory Committee

Dr. Ian J. Walker, Supervisor
(Department of Geography)

Dr. Dan Smith, Departmental Member
(Department of Geography)

Dr. Stephen Wolfe, Departmental Member
(Department of Geography)

Dr. John Harper, Outside Member
(School of Earth and Ocean Science)

Supervisory Committee

Dr. Ian J. Walker, Supervisor
(Department of Geography)

Dr. Dan Smith, Departmental Member
(Department of Geography)

Dr. Stephen Wolfe, Departmental Member
(Department of Geography)

Dr. John Harper, Outside Member
(School of Earth and Ocean Science)

ABSTRACT

This thesis describes the geomorphology and morphodynamics of two embayed, sandy, macrotidal beach-dune systems in the Cape St. James region of Gwaii Haanas National Park Reserve and Haida Heritage Site. Gilbert Bay beach is a small embayment with a southwest aspect that exhibits prograding dune ridges. Woodruff Bay beach, a larger system with a SE aspect, is characterized by large erosional scarps on the established foredune. Aspect to erosive conditions and embayment size control the distinct morphologic responses of these beach-dune systems. The morphodynamic regime at Cape St. James consists of high onshore sediment transport potential combined with an increasingly erosive water level regime that is forced by PDO and ENSO climatic variability events. Conceptual models of potential future responses of these beaches to sea level rise show a possible landward migration of up to 3.5 m at Gilbert Bay beach and up to 4 m at Woodruff Bay beach.

Table of Contents

List of Tables

List of Figures

List of Equations

List of Acronyms

AWL – average water level

AAWL – annual average water level

ALPI – Aleutian Low Pressure Index

BC – British Columbia

CHS – Canadian Hydrographic Service

CSJ – Cape St. James

DP – Drift Potential

EC – Environment Canada

ENSO - El Niño Southern Oscillation

GH-NPR – Gwaii Haanas National Park Reserve and Haida Heritage Site

HG – Haida Gwaii

HHWLT – Higher High Water Low Tide

LLWLT – Lower Low Water Low Tide

MaxWL – maximum water level

MEI – Multivariate ENSO Index

MSR – mean spring tide range

MWL – mean water level

NE – northeast

NOI – Northern Oscillation Index

PDO – Pacific Decadal Oscillation

PR - Price Rupert

RDD – Resultant Drift Direction

RDP – Resultant Drift Potential

RS – Rose Spit

SST – sea surface temperature

VU – vector units

Acknowledgements

This thesis would not have been possible without the support of numerous individuals and organizations. Firstly, I would like to thank my supervisor, Dr. Ian J. Walker, for providing me with the opportunity to undertake this exciting project and for always providing me with invaluable insight, feedback, and friendship. I would also like to thank my supervisory committee members Drs. Dan Smith and Stephen Wolfe and my external examiner Dr. John Harper for their advice and feedback. I would also like to offer much deserved credit to Ole Heggen, our in-house graphics guru, for the wonderful site maps and figures that he happily produced for me.

The fieldwork for this project would not have been possible without the support of the Council of the Haida Nation and Parks Canada (co-managers of Gwaii Haanas National Park Reserve and Haida Heritage Site). In particular, Park wardens Clint, Richard, Jon, and Debby, and the patrol officers provided great field support and, of course, good times.

Financial support from the National Science and Engineering Research Council (NSERC) Canada Graduate Scholarship, the UVic Geography department, and the Derrick Sewell Graduate Scholarship was essential to completing my thesis in a timely and relatively low-stress manner.

Many thanks also to Trevor, my family, the Hoskins family, and my wonderful friends for all their encouragement, opportunities for distraction, and unwavering support during this two-year adventure!

1.0 Introduction and Research Objectives

1.1 Introduction

Although most coastal scholarship agrees that the morphologies of macrotidal (i.e., tide range >5m) beach-dune systems are controlled by interacting wind, wave, and tide regimes, the morphodynamics of these coasts remain understudied and not thoroughly understood (Davis and Hayes, 1984; Masselink and Short, 1993; Anthony and Orford, 2002; Bernabeu et al., 2003a, 2003b; Cooper et al., 2004; Psuty, 2004). In particular, research addressing the morphodynamics of Canada's Pacific Coast macrotidal, high-energy beach-dune systems is lacking. Meso-macrotidal ranges (i.e., 2 to 6 m) create an expansive zone of energy transfer across the beach, resulting in cross-shore variations in beach-dune morphodynamics and sediment transport. The result is a dynamic cross-shore profile morphology that reflects onshore, offshore, and alongshore transfers of sediment by wave, tidal, and aeolian processes.

Most beaches on the northeast (NE) Pacific coast are also geomorphically distinct due to their high-energy wind and wave regimes and their responsiveness to climate variability and change events (e.g., increased storminess and sea-level rise) (Allan and Komar, 2002, 2006; Walker and Barrie, 2006; Abeysirigunawardena and Walker, unpublished data, 2007). Climate variability affects wind, wave, and water level regimes, which, in turn, are reflected in seasonal to interannual changes in beach-dune dynamics. It is suggested that high-energy, macrotidal beach-dune systems require extreme water level events, such as those associated with high-intensity El Niño Southern Oscillation (ENSO) events (Storlazzi and Griggs, 2000;

Allan and Komar, 2002, 2006), to cause significant morphological change (Cooper et al., 2004; Ruz and Meur-Ferec, 2004).

The coastal waters of Haida Gwaii (HG), also known as the Queen Charlotte Islands, are influenced by climate variability events such as the 4-7 year ENSO and the 20-30 year Pacific Decadal Oscillation (PDO)(Abeysirigunawardena and Walker, unpublished data, 2007). These oscillations are associated with changes in storminess, sea levels, and coastal erosion on the west coast of North America (Ruggiero et al., 1997, 2001; Storlazzi et al., 2000; Allan and Komar, 2002; Barrie and Conway, 2002; Abeysirigunawardena and Walker, unpublished data, 2007) (see Section 2.4). As such, an understanding of the teleconnections between local hydrodynamic processes and regional climate variability modes is critical for understanding the morphological history and future state of these beach-dune systems.

Parks Canada (2000) has indicated there is a need for increased monitoring and understanding of sandy beach-dune systems located within Canada's coastal National Parks. Gwaii Haanas National Park Reserve and Haida Heritage Site (GH-NPR) in HG is host to several understudied, high-energy, sandy beach-dune systems. The work presented in this thesis is part of the initial phase of a 5-year project intended to monitor key geoindicators (Welch, 2002) of climate change impacts (e.g., coastal erosion, sea-level rise, and extreme storm events) within GH-NPR (See Table 1.1 for detailed list of geoindicators). The thesis aims to provide a deepened understanding of the geomorphic features and the morphodynamic response of sandy beach-dune systems in GH-NPR through a detailed assessment of regional wind,

climate, and water level regimes, coastal and aeolian processes, and local geomorphology.

Table 1.1: Key geoindicators for monitoring coastal change including relevant geomorphic measures, linkages to climate variability/change via formative process regimes, and overall relevance and practicality for ecological integrity monitoring (modified from Welch (2002) as in Walker, 2007: Tables 6,8)(Δ= change in).

Geoindicator	Geomorphic measures(s)	Process linkage to CV/CC	Relevance & Practicality
dunes	➢ size, type, position ➢ migration rates	➢ Δ wind regime with ENSO	High, High
wind erosion	➢ aeolian drift potential ➢ sand traps, erosion pins	➢ Δ wind regime with ENSO	Medium, High
shorelines	➢ position, slope, features, sediments, beach width	➢ Δ WL &/or wave regimes, SLR ➢ linked to ENSO	High, Medium
relative sea-level	➢ total water level (TWL) = tide +/- surge ➢ land rise/subsidence	➢ Δ TWL with storms, ENSO, PDO ➢ eustatic SLR	Low(?), Low
soil/sediment erosion	➢ erosion/deposition pins, topographic profiles, sand traps	➢ Δ WL, wave &/or wind regimes, SLR ➢ linked to ENSO	High, Low
*marine nearshore env.	➢ profiles, swath bathymetry, sediments, features	➢ Δ WL &/or wave regimes, SLR ➢ linked to ENSO	Medium, Low
*extreme events	➢ TWL, winds, waves, erosion ➢ relative to geomorphic thresholds or encroachment on built environments or infrastructure	➢ Δ WL, wave &/or wind regimes ➢ linked to ENSO, PDO	Medium(?), Medium
*built environments	➢ footprint areas, distance from shorelines/dunes/flood zones	➢ Δ WL &/or wave regimes, SLR	High, High
*proxy (paleo) record	➢ soil/sed. pits, tree rings, ^{14}C materials, geoarch, optical dating	➢ Δ climate, WL, wind, wave regimes ➢ linked to ENSO, PDO	Low, Medium
**indicators not found in the original IUGS (1996) classification (see Welch. 2002)*			

1.2 Study Site

GH-NPR is located approximately 80 km off the central coast of the British Columbia (BC) mainland, in the southern portion of the HG archipelago (Figure 1.1). During a preliminary field season in June 2005, 13 coastal sites were selected for a preliminary erosion and climate change impacts assessment for GH-NPR (Walker,

2007). For this thesis, the two largest sandy beach-dune sites, Gilbert Bay beach and Woodruff Bay beach (Figure 1.2), were selected for a comparative geomorphic assessment. Both sandy, embayed, macrotidal beach-dune systems are in the Cape St. James (CSJ) region and were chosen because of their distinct geomorphic features (e.g., prograding vs. eroded foredunes) and differing aspects to regional wind and wave regimes (e.g., Gilbert Bay beach - SW, Woodruff Bay beach - SE).

Research addressing the morphodynamic response of high-energy, macrotidal systems to storm events is rare compared to low-energy sites (Cooper et al., 2004). The research presented in this thesis contributes to the growing understanding of beach-dune morphodynamics in embayed, high-energy, macrotidal environments. Introductory site descriptions for each beach are outlined below (based on Walker, 2007), with more detailed geomorphic assessments presented in Chapter 4.

Figure 1.1: Regional map of the central coast of British Columbia showing Haida Gwaii and the locations of the Environment Canada climate stations at Rose Spit and Cape St. James.

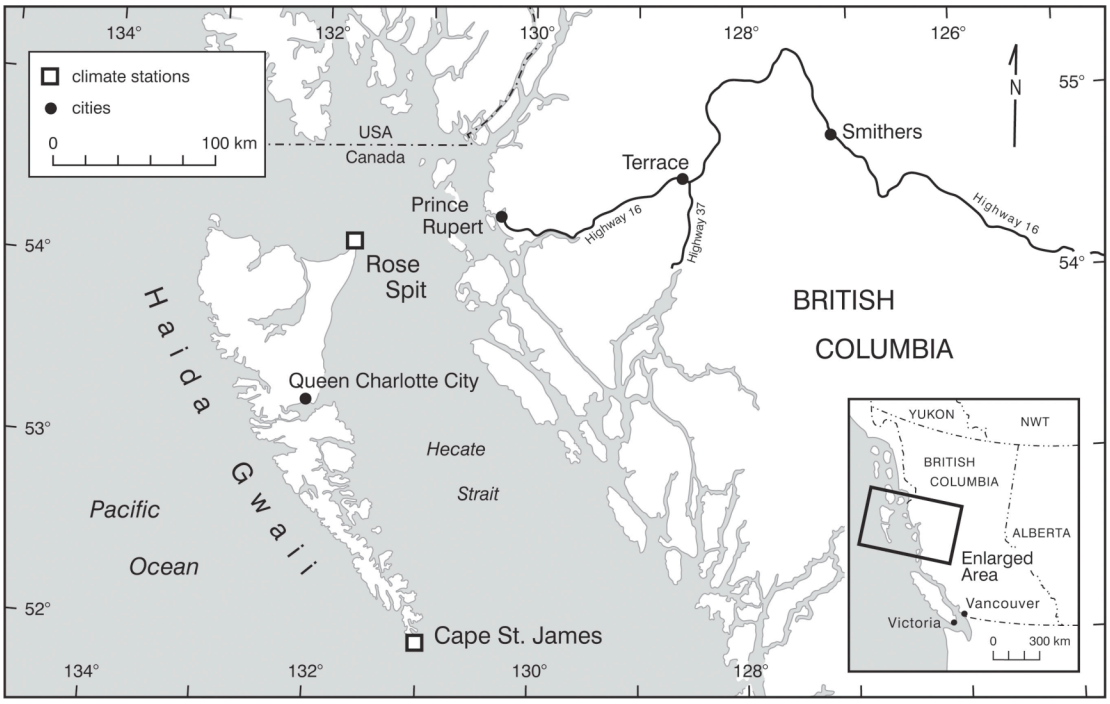

Figure 1.2: Map of South Moresby and Kunghit Islands within Gwaii Haanas National Park Reserve showing the two study sites, Gilbert Bay and Woodruff Bay, and including the location of the Environment Canada offshore South Moresby wave buoy (#46147).

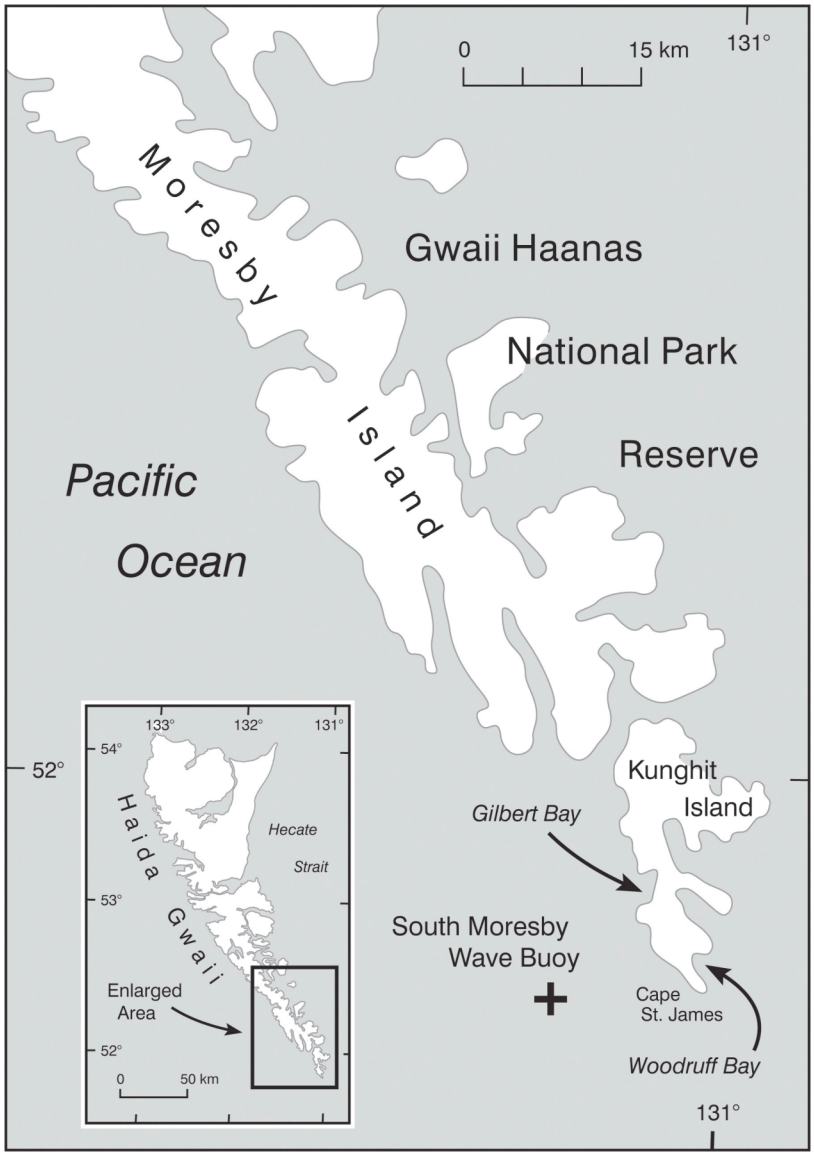

1.2.1 Gilbert Bay Beach

Gilbert Bay beach (centred at UTM Zone 9, 357011E, 5767558N) is an embayed, high-energy, macrotidal, sandy beach on the west coast of Kunghit Island, northwest of Cape St. James (CSJ) (Figures 1.2, 1.3, and 1.4). The beach lies on the north side of Gilbert Bay, has a SW aspect, and is ~500 m long. The beach-dune system is characterized by large, well-developed, prograding foredunes, an active driftwood jam accretion zone (5-10 m wide) in the backshore, and a dynamic backshore river system to the east (see site photos in Chapter 4). The active, vegetated dune ridge (~6-12 m tall) is bounded to the west by outcropped basalt bedrock and to the east by the river outflow. Several larger stabilized parabolic dune ridges (~700-800 m wide, ~5-25 m high) occur in the forest behind the beach, indicating past seaward progradation. Migration of the river is actively eroding the base of the relict foredunes, and appears to deliver sand to the nearshore. This site was chosen primarily for its prograding, terraced dune ridges in the backshore, which contrast the recent erosional features of Woodruff Bay beach.

Figure 1.3: Aerial photograph of Kunghit Island, Gwaii Haanas National Park Reserve showing the locations of Gilbert and Woodruff Bay beaches. [#BCC04002, 2004, with permission].

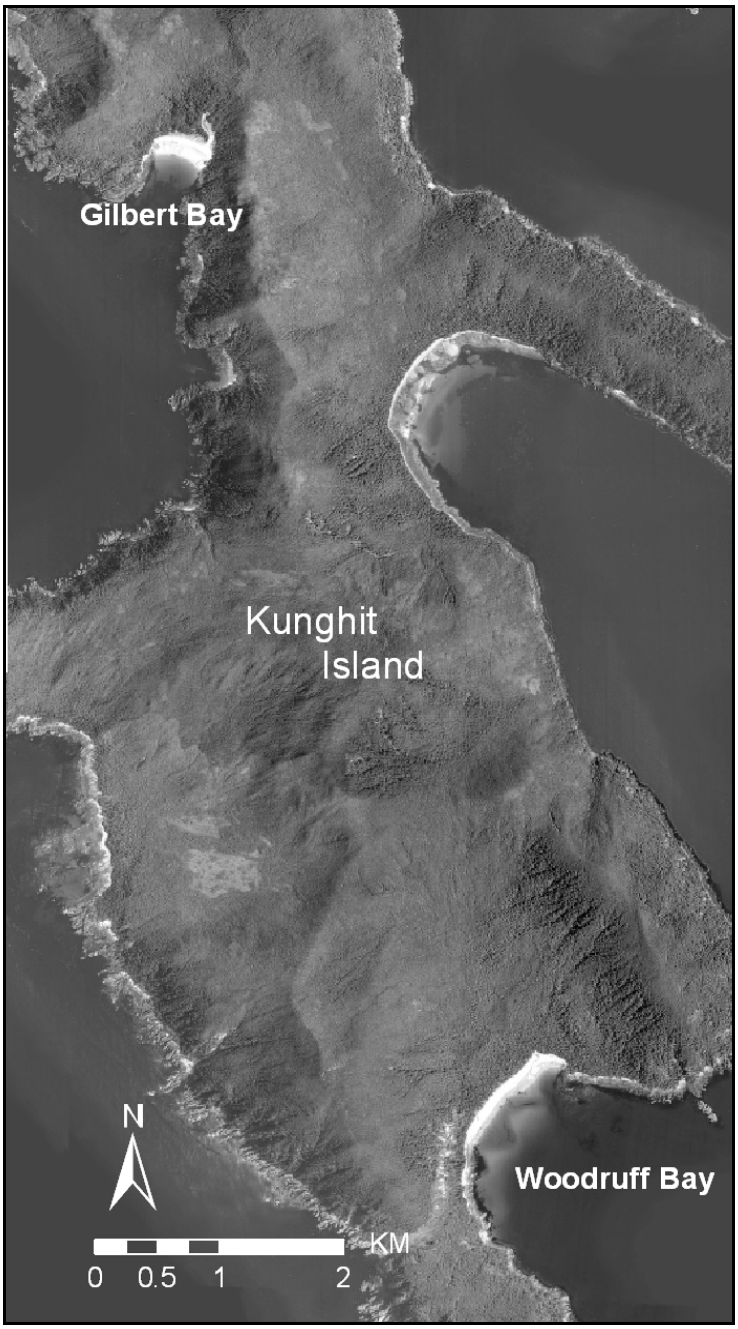

Figure 1.4 Topographic map of Kunghit Island showing: A) Gilbert Bay, and B) Woodruff Bay. 100 m contour lines. [Retrieved and modified from http://www.geogratis.cgdi.gc.ca on July 5, 2007].

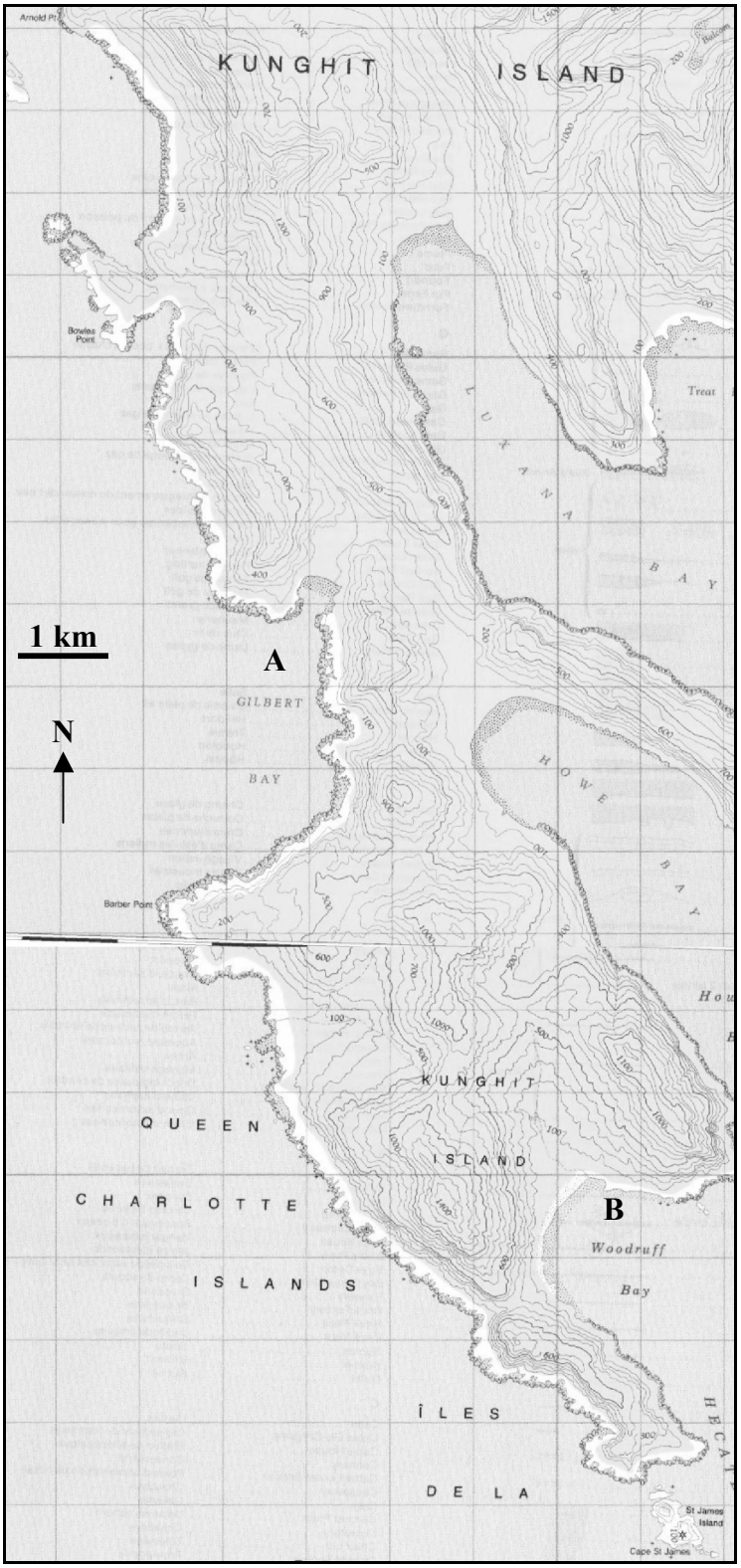

1.2.2 Woodruff Bay Beach

Woodruff Bay beach (centred at UTM Zone 9, 360276E, 5760182N) is a larger (~1 km long) macrotidal, embayed, high-energy beach located northeast of CSJ with a SE aspect facing Queen Charlotte Sound (Figures 1.2, 1.3, and 1.4). The beach is bounded on both sides by outcropped basalt bedrock. This coarse, well-sorted sandy beach has a well-developed vegetated foredune ridge (~10-12 m tall), characterized by a large seaward face scarp fronted by a smaller, remnant foredune (~4-6 m tall) with a driftwood jam core (see site photos in Chapter 4). Small dune ridges (1-3 m tall) atop the large dune scarp suggest past dune progradation. Large Sitka spruce (*Picea sitchensis*) trees (~5-7 m circumference) are rooted on several large relict foredune ridges (~700-800 m wide) that extend as far as 500 m inland. This site was chosen for its prominent dune scarp, which provides evidence for a major erosive event.

1.3 Research Purpose and Objectives

The purpose of this research is to assess geomorphic features, modern morphodynamics, and potential climate variability responses of two embayed macrotidal beach-dune systems in GH-NPR. The following objectives will guide this assessment:

i) To describe and classify the geomorphic features and controls of two embayed, macrotidal, high-energy beach-dune systems, Gilbert Bay beach and Woodruff Bay beach, using aerial photographs and field observations (e.g., topographic surveys, sediment analysis, site photographs, and bathymetric surveys).

ii) To estimate the erosional and depositional regimes of GH-NPR using statistical analysis of the regional water level record, and wave runup analysis and Fryberger's (1979) model of regional aeolian sand drift

potential. Future erosive water level scenarios will be projected into beach-dune profiles to forecast possible future states for the beaches at Gilbert and Woodruff Bays.

iii) To identify regional climatic variability and climate change-induced signals in the total water level regime of the Cape St. James region and to compare these to the longer-term regional signals at Prince Rupert, BC.

1.3.1 Thesis Outline

This thesis consists of seven chapters. Chapter 2 outlines the research context through a broad review of key literature in coastal geomorphology, aeolian sediment transport, beach classification and modeling, and climate variability and impacts. Chapter 3 details the methods used to achieve each of the objectives described above. Chapter 4 documents and describes the geomorphology of Woodruff and Gilbert Bay beaches, setting the environmental context for the final chapters. Chapter 5 assesses the erosional and rebuilding regimes of the CSJ region using analysis of aeolian activity, water level trends, and wave runup. Chapter 6 examines climate variability signals in the water level record from the CSJ region. The final chapter provides a brief summary, conclusions, and recommendations for future research directions.

2.0 Research Context

Assessing the morphodynamic regime of sandy beach-dune environments requires consideration of the numerous factors underlying these dynamic systems and the interactions between them. This chapter details the broad literature context for the research presented in this thesis. The first section addresses important components of ocean-beach interaction including intertidal sediment transport, nearshore bar morphology, and erosive water levels. The second section addresses a variety of concepts related to beach-dune morphodynamics including morphodynamic classification of beaches, embayed beach-dune systems, beach rotation, and aeolian sediment transport. Finally, the third section discusses climate change, climate variability modes, and corresponding geomorphic/oceanographic responses.

2.1 Ocean-beach dynamics

2.1.1 Longshore sediment transport

The morphodynamic regime of macrotidal beach-dune systems is influenced by sediment transport patterns in the intertidal zone (i.e., between the high and low tide marks). Intertidal sediment transport patterns can be identified using surface grain-size statistics such as mean grain size, sorting, and skewness. The sediment grain-size distribution of a given surface sample is affected by a variety of factors including: selective entrainment, mode of transport, and depositional environment. Selective entrainment occurs when sediment is picked up into the flow through fluid-induced stresses and forces on the seabed. When this occurs, sedimentary deposits will tend to become better sorted in the direction of transport.

McLaren (1981) presents a sediment transport model for marine environments based on three grain-size parameters: mean (μ), sorting (σ^2), and skewness (Sk). Based on the assumption that light sediment grains have a greater probability of being eroded and transported than heavier grains, McLaren and Bowles (1985) conclude that there are two possible trends in sedimentary transport. First, erosion of source sediment followed by deposition, resulting in finer, better sorted, and more negatively skewed sediments than the source (FB-). Second, the remaining lag from the eroded sediment is coarser, better sorted, and more positively skewed (CB+). McLaren and Bowles (1985) conclude that sediment in transport is always finer and more negatively skewed than its source and the remaining deposit is always coarser and more positively skewed than its source (See details in McLaren and Bowles, 1985).

Sediment transport pathways will only be identified if two key assumptions and environmental conditions are met:

1) Sediment supply to the beach-dune systems must be consistent, not episodic.

2) The temporal and spatial scales of littoral mixing must be significantly smaller than the source to sink transport cycle.

As such, using the McLaren and Bowles (1985) to understand nearshore sediment dynamics is limited to environments where these assumptions can be met. On beach-dune systems with an inconsistent sediment supply or with a lot of nearshore mixing (e.g., high-energy, embayed systems) the intertidal sediment pathways may not be clearly identified using the McLaren and Bowles (1985) approach.

2.1.2 Nearshore bar morphology

In addition to the longshore movement of sediments, it is important to consider the role of nearshore bars in beach-dune sediment dynamics on macrotidal systems. These features, found ubiquitously on low-angle, sandy, storm-wave dominated upper shorefaces, store and cycle nearshore sediments, and are maintained by high-energy wave action and longshore currents (Houser and Greenwood, 2005; Walker and Barrie, 2006). These bars are reworked periodically by storms and, in some areas, show a rhythmic pattern from the presence of rips (Anthony and Orford, 2002). Under large storm waves nearshore bars move seaward towards the local dissipation maximum (Dally and Dean, 1984; Houser and Greenwood, 2005). The cross-shore location of the outermost bar is determined by the largest storm waves reaching the beach (assuming no measurable changes in sea level) (Houser and Greenwood, 2005). The spatial and temporal pattern of the local wave energy regime influences nearshore bar growth, decay, and on/offshore migration (Houser and Greenwood, 2005). On macrotidal beaches, intertidal bars can provide enhanced sediment supply to the dunes and, via aeolian action, greatly influence beach-dune morphodynamics (Anthony, 2000; Walker and Barrie, 2006).

2.1.3 Water levels and erosive events

Coastal morphodynamic models must also consider the potential influence of water level variations on aeolian sand transport and coastal dune evolution (Anthony, 1998; Ruz and Meur-Ferec, 2003). Water levels can be used to estimate potentially erosive events and upper beach-dune evolution (Ruz and Meur-Ferec, 2003). Potentially erosive events are defined as periods of time when the beach-dune

junction can be reached by high total water levels (e.g., when high spring tides coincide with strong onshore winds) (Figure 2.1) (Ruz and Meur-Ferec, 2003). Erosive events caused by storm surges are common on sandy shorelines (Carter et al., 1990; Arens, 1996, Ruz and Meur-Ferec, 2003). Ruz and Meur-Ferec (2003) suggest a seasonal cycle of beach-dune evolution characterized by summer accumulation and fall/winter storm-induced erosion. Following high water dune-scarping storm events, sediment is transferred from the dune to the nearshore and then returned to the dune via aeolian transport in the beach-dune recovery cycle. Ruz and Meur-Ferec (2003) conclude that upper beach/dune evolution is mainly controlled by the frequency and magnitude of storm-induced high water levels and, therefore, high water levels are a major forcing parameter in beach-dune morphodynamics.

Figure 2.1: Basic schematic illustration of quantities used to assess wave runup on beach systems. E_j is the elevation of the beach-dune junction, E is the elevation of the total water level, E_T is the elevation of the observed water level, and R is wave runup. R is composed of wave setup and swash action. [Modified from Ruggiero et al., 1997].

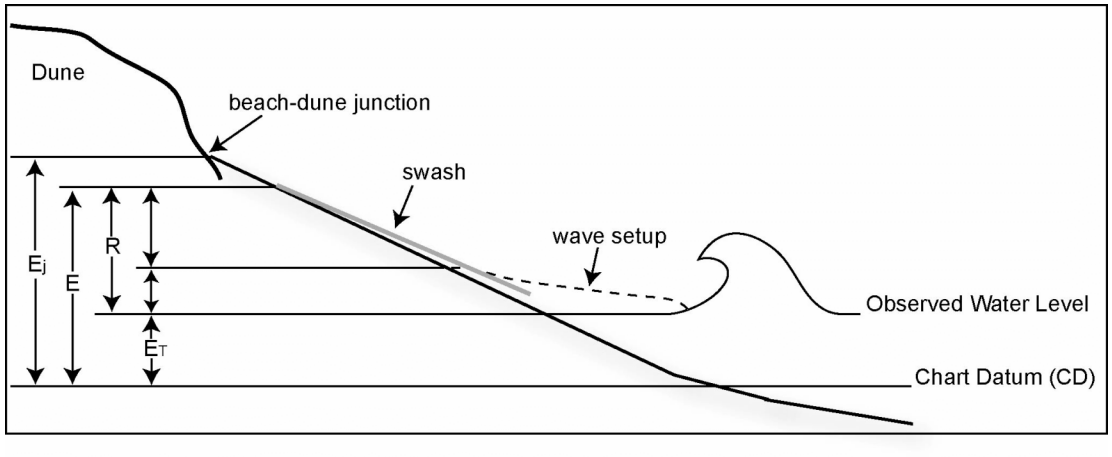

Two main components determine the total water levels on a given beach (Figure 2.1). First, the measured (i.e., observed) tidal elevation (E_T), which is made up of the predicted astronomical tide plus the effects of water temperature, winds (particularly onshore), and climate variability (e.g., oceanographic processes associated with El Niño) (Ruggiero et al., 1997, 2001). Second, the vertical component of wave runup (R) is superimposed on the measured water level. Wave runup consists of wave setup that elevates the mean shoreline and causes fluctuations in swash position along the beach profile (Ruggiero, et al., 1997, 2001). An erosive event will occur when the total elevation of the water exceeds the elevation of the beach-dune junction (i.e., $E_T + R > E_J$).

Calculating maximum wave runup and the probability of it occurring is an effective method for estimating erosive events on macrotidal beach-dune systems. On dissipative beaches in the NE Pacific, Ruggiero et al. (1997, 2001) determined that the following equation successfully describes wave runup maxima:

$$R_{2\%} = 0.27(\beta H_o L_o)^{1/2} \quad (1)$$

where $R_{2\%}$ is the two-percent exceedance elevation of wave runup maxima, β is the beach slope, H_o is the deep-water wave height, and L_o is the deep-water significant wave length ($L_o = (g/2\pi)T^2$, where T is deep-water wave period). This runup calculation has been used to estimate climate variability (e.g., ENSO) impacts on beaches in Oregon and California (Ruggiero et al., 1997, 2001; Sallenger et al., 2002). On intermediate to reflective beaches, $R_{2\%}$ is more accurately estimated using:

$$R_{2\%} = 0.75\beta(H_s L_o)^{1/2} + 0.22H_s \quad (2)$$

where H_s is the significant wave height. Details of the methods used to determine wave runup are discussed further in Chapter 3.

Cooper et al. (2004) investigated the response of high-energy, embayed, mesotidal beach-dune systems on the coast of Ireland to extreme storm events. Based on detailed wave modeling, wind analysis and observations, they concluded that embayed beaches exposed to a normally high-energy wave regime require high magnitude storm events for significant backshore erosion to occur. The authors caution that because beach-dune systems respond variably to decadal scale storm forcing, generalizing about regional-scale coastal response to climate change-induced high water level events is limited (Cooper et al., 2004).

2.2 Beach-dune morphodynamics

Wright and Thom (1977) introduced the concept of 'coastal morphodynamics' to expand on the largely descriptive objectives of previous classification work. This approach explains coastal morphology based on underlying environmental factors (e.g., wave energy, geology, and tide range). Since this, a widely accepted shift to a morphodynamic approach has occurred, and most geomorphic classifications and models for beach systems now acknowledge hydrodynamic processes as fundamental controlling forces of beach morphology (e.g., Short, 1979; Short and Hesp, 1982; Wright and Short, 1984; Masselink and Short, 1993; Anthony and Orford, 2002; Bernabeu et al., 2003a, 2003b). Wave-dominated, sandy beaches are the most responsive shorelines to variations in marine energy and atmospheric processes such as wind and aeolian sediment transport (Short and Hesp, 1982), and thus, they are the most common basis for existing morphodynamic models. Over the last few decades,

numerous models that classify and model beaches in terms of morphological variability and sediment dynamics have emerged (e.g., Aubrey, 1979; Short, 1979; Short and Hesp, 1982; Wright and Short, 1984; Masselink and Short, 1993; Anthony, 1998).

The purpose of this section is to review literature that addresses beach-dune classification and morphodynamics to provide a theoretical foundation for the morphodynamic assessment of the beaches examined in this thesis. Several key classification models are detailed including the equilibrium beach profile models of Bruun (1962, 1988), Dean (1977, 1991) and Bernabeu et al. (2003a, 2003b), the tidal range classification model introduced by Masselink and Short (1993), and the beach-dune morphodynamic classification models of Hesp (2002) and Psuty (2004). Following the discussion of the various approaches to coastal classification is an introduction to the unique morphodynamic characteristics of embayed beach-dune systems and beach rotation. This section concludes with a detailed introduction to aeolian sediment transport, including a description of Fryberger's (1979) sediment drift potential model.

2.2.1 Equilibrium beach profile

Bruun (1962, 1988) and Dean (1977, 1991) assert that a beach profile tends to maintain a characteristic slope as it uniformly balances (dissipates and reflects) incident wave energy and onshore sediment transfer with gravitational and offshore sediment transfer vectors. The shape of a beach profile, according the equilibrium beach concept, can be described by the simple function:

$$h = Ax^{2/3} \tag{3}$$

where h is the still water depth at a distance x from the shoreline, and A is a dimensional parameter related to sediment grain size (see Dean, 1991). As such, a larger grain size results in a greater value for A and thus, a steeper beach slope.

Assuming this equilibrium profile, the following beach characteristic can be expected (Dean, 1991): i) a concave shoreface; ii) a gentle slope segment with smaller grain size grading into a steeper slope section with larger grain size; iii) a planar beach face; and, iv) milder slopes resulting from steep waves. This beach model is limited by several key assumptions that are rarely met on natural beaches. For example, the model relies solely on grain size for determining beach shape, ignores the role of underlying geology in the profile shape, and fails to consider the role of multi-directional flow of sediment in the shape of the profile (i.e., assumes 2-dimensional transport). The equilibrium profile model is the foundation of the Bruun Rule (1962, 1988), a widely used model for prediction of shoreline change in response to sea-level rise.

In response to the numerous assumptions and limitations of the equilibrium beach profile models of Bruun (1962, 1988) and Dean (1977, 1991), subsequent research has attempted to improve the model by dividing the beach profile into two sections, the upper surf profile and the lower shoaling profile. From this, the reflection and dissipation of wave energy on beach profile morphology is examined (Inman et al., 1993; Bernabeu et al., 2003a, 2003b). It seems that incident energy along the profile may not be uniformly dissipated by the beach, as some is reflected to deeper water by the steeper segments of the profile (Bernabeu et al., 2003b). Further research is required to express more accurately how wave reflection modifies the

beach profile. Inman et al. (1993) found that the two-section equilibrium beach profile (2S-EBP) model suggests a surf profile and a shoaling profile that join at the breaker point. Figure 2.2 shows a conceptualized model of the 2S-EBP presented by Bernabeu et al. (2003a, 2003b), who assert that it is a significant improvement over the originally published equilibrium beach profile model. The model assumes constant sea level based on research indicating that the 2S-EBP behaves similarly for tidal and non-tidal beaches. Based on this model, beaches can be classified on a continuum from reflective to dissipative and microtidal to macrotidal (Bernabeu et al., 2003a).

Figure 2.2: General 2S-EBP Model including tidal range (TR). x_r is the horizontal distance between the surf zone and the discontinuity point; h_r is the discontinuity point depth in relation to low tide level; x_o is the horizontal distance between the surf zone and the origin of the shoaling profile over the low tide level; and h_a is the offshore depth limit of model validity [Modified from Bernabeu et al., 2003a].

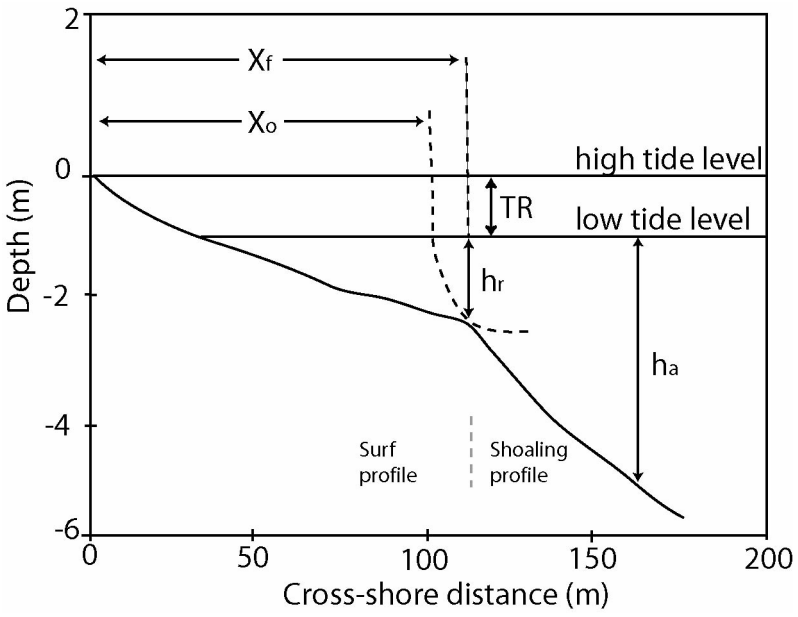

Beach profiles often show distinct seasonal variations due to changes in the onshore/offshore sediment dynamics (Figure 2.3) (Aubrey, 1979; Masselink and Pattiaratchi, 2001). A "summer beach" is typically characterized by a gradually sloping, wide beachface with numerous subaerial berms that form as a result of an accreting foreshore and an erosional offshore. Conversely, a "winter beach" is characterized by a reversal of these dynamics, with an erosional beachface and a net offshore transport of sediment resulting in a steeper, narrow beach with nearshore bar morphology and coarser sediment (Masselink and Pattiaratchi, 2001). Seasonal variations in beach morphology result from changes in wave frequency, magnitude and direction (Aubrey, 1979). The winter beach profile is steeper due to higher energy wave action transporting sediment offshore, while the summer beach profile is less steep due to lower wave action transporting sediment onshore to the beach (Figure 2.3). Aubrey (1979) used 5-years of monthly profile data on the beaches of southern California to present a model of seasonal patterns of onshore/offshore sediment movement and beach profile dynamics. Using Eigenfunction analysis, two pivotal points were identified where the eroding and accreting regions can be distinguished. The noted seasonality to the beach profile and sediment movement is due to storm-induced sand redistribution (winter) followed by return flow during calmer wave conditions (summer) (Aubrey, 1979). Aubrey (1979) notes, however, that this pattern of seasonal movement may not be valid for beaches without dominant seasonal wave climates. This seasonal beach model is also limited to systems with more complex morphodynamics such as beaches on the eastern coast of the United States and many Australian beaches (Ritter et al., 2002).

Figure 2.3: Schematic illustration of typical summer and winter beach profiles [Modified from Aubrey, 1979].

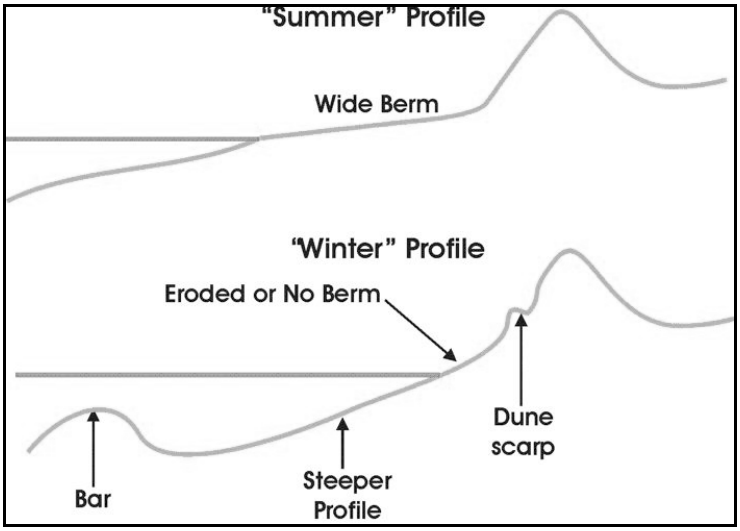

Using the equilibrium beach profile models of Dean (1977, 1991) and Bernabeu et al. (2003a, 2003b), the impacts of climate variability on beach morphology can be monitored using repeat topographic surveys. Changes in wind and wave regimes will result in an altered sediment transport pattern, which will produce localized topographic changes measurable by topographic profile surveys (Gares, 1992). For example, Houser and Greenwood (2005) used repeat topographic profiles over 14 months to assess sub-aerial and nearshore morphology response to storm events on the coast of Lake Huron. Based on analysis of these topographic profiles, they conclude that the sequence of storm events is crucial to the timing and frequency of nearshore bar movement. Larson and Kraus (1994) applied high resolution repeat topographic surveying to an Atlantic beach and noted landward transport of sediment after a storm event. This methodology of repeat topographic

surveying is a common and useful approach that may be applied to assessing the morphodynamic effects of climate-controlled processes (e.g., wind and waves).

Recently airborne lidar surveys have been used to examine beach-dune profile response to storm events (Sallenger et al., 2001; Sallenger et al., 2002). Sallenger et al. (2002) used lidar surveys to examine the relationship between sea-cliff erosion and pocket-beach changes in central California in response to the 1997-1998 El Niño event. From this analysis and wave runup calculations they identified erosional hotspots along the coast and estimated up to 14 m of cliff retreat in response to the changes in sediment transport due to the El Niño winter conditions (Sallenger et al., 2002). Lidar provides unprecedented spatial coverage, topographic survey coverage, and resolution and is an effective tool for examining coastal response to climate variability events. The greatest limitation to using lidar is the very high cost associated with data collection.

2.2.2 Tidal beach classification

One of the most widely used morphodynamic classification models is that of Masselink and Short (1993). Their model considers not only wave and sediment characteristics, but also the influence of tidal cycles on beach form. Four distinct morphodynamic variables are used to distinguish beach states: i) modal breaking wave height (H_b), ii) modal breaking wave period (T), iii) the high tide (swash zone) sediment fall velocity, and iv) the mean spring tide range (MSR) (Masselink and Short, 1993). A relative tide range (RTR), is also used to quantify tidal effects as follows:

$$\text{RTR} = MSR/H_b \tag{4}$$

The RTR parameter indicates the relative importance of swash, surf zone and shoaling wave processes in determining beach profile morphology (Masselink and Short, 1993). Morphological factors are quantified using the dimensionless fall velocity (Ω), which indicates whether reflective, intermediate or dissipative conditions prevail in the surf zone. Ω is defined as follows:

$$\Omega = H_b / w_s T \quad (5)$$

where w_s is the sediment fall velocity and T is the deep water wave period (recorded from offshore buoy). As such, the model effectively incorporates both morphological and hydrodynamic processes, making it a representative morphodynamic approach. Details on the methods used to determine these variables are discussed further in Chapter 3. Based on RTR and Ω, Masselink and Short (1993) identify 7 beach types (Figure 2.4): i) reflective, ii) low tide terrace and rip, iii) low tide terrace, iv) barred, v) low tide bar/rip, vi) barred dissipative, vii) non-barred dissipative, and viii) ultra-dissipative.

Figure 2.4: Masselink and Short (1993) conceptual beach classification model; HT and LT are high tide and low tide, respectively; beach state is a function of dimensionless fall velocity (Ω) and relative tide range (RTR). [Masselink and Short, 1993, with permission].

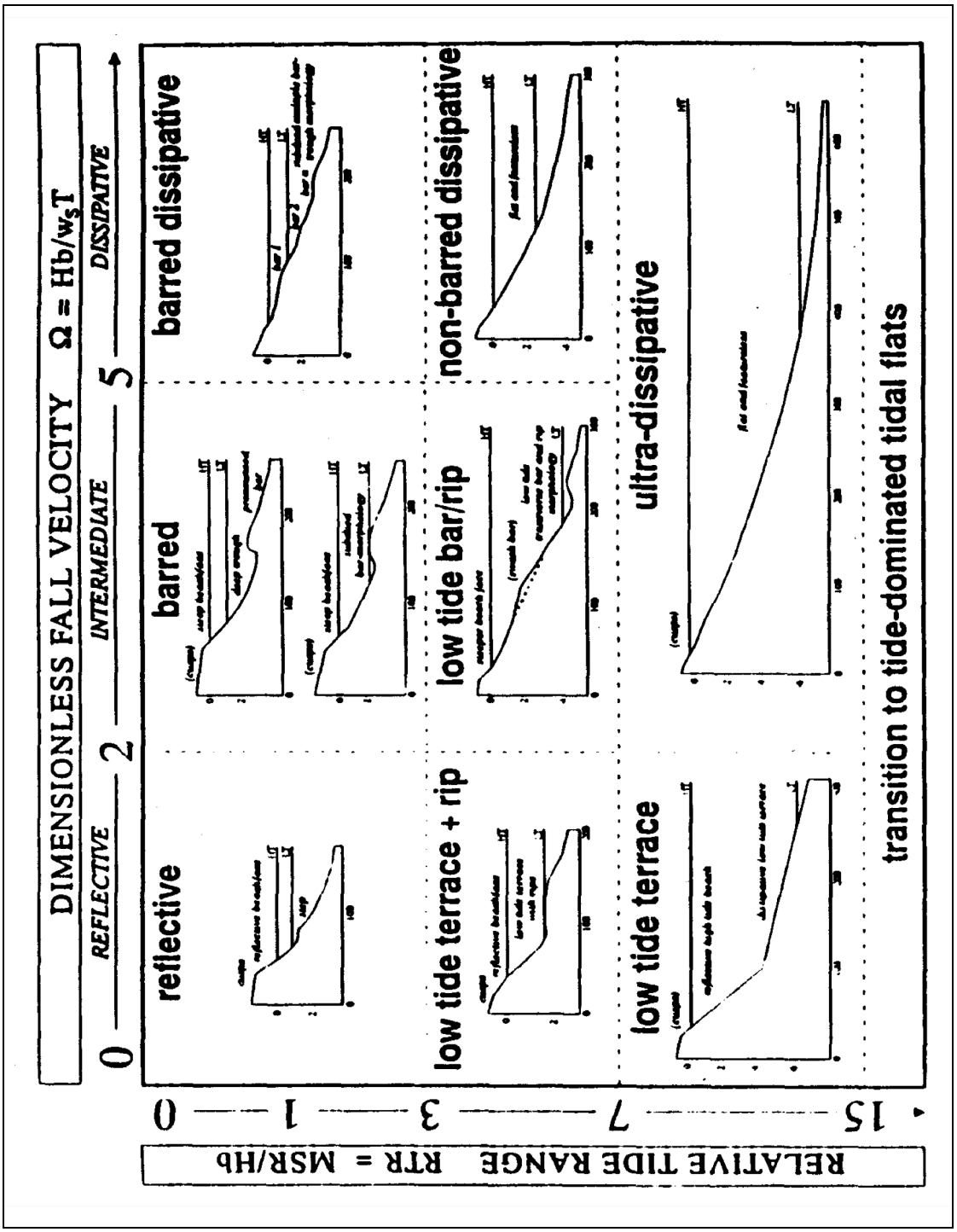

Masselink and Short (1993) explicitly state the following limitations with their model:

1. The model is primarily based on data and observations on the macrotidal coastline of Queensland, Australia and therefore should be used and tested carefully in other locations.

2. In low wave energy environments (H_b <0.25m), bar morphology may not develop due to insufficient edge wave development. Therefore the model must be carefully applied in these environments.

3. It is a conceptual model that is based on limited information about macrotidal beaches.

2.2.3 Beach-dune classification

The models discussed previously focus primarily on the beach shoreface and do not consider the morphodynamic influence and responses of the backshore (i.e., landward of the high water line). In response to this, a more integrated beach-dune approach to classifying and modelling coastal morphodynamics has emerged. Hesp (2002) presents a staged model of foredune development that involve sequences of aeolian erosion, vegetation cover, wave erosion, and dune stability based on a synthesis of several beach-dune classifications (including Hosier and Cleary, 1977; Hesp, 1988; Psuty, 1988, 1993; Saunders and Davidson-Arnott, 1990; Arens, 1994). The five main 'morpho-ecological' stages (1-5) of an established foredune represent the progression of vegetation loss resulting from increased erosion and aeolian activity (Figure 2.5). These stages represent: i) the stage that a foredune may remain in for most of its existence; and, ii) the stages through which the foredune may progress following aeolian or wave erosion, or changes in vegetation cover.

This evolutionary dune progression can change as a result of altered climate conditions and thus is important to consider in coastal morphodynamic beach-dune

research involving climate variability responses (Hesp, 2002). Change in beach-dune morphology may occur following storm events, which scarp the dune and increase its susceptibility to erosion (Saunders and Davidson-Arnott, 1990). The subsequent foredune development will depend on the degree of re-vegetation (Hesp, 2002). Reversal of this evolutionary progression is possible given changes in environmental conditions such as re-vegetation and stabilization or climate change (e.g., reduced wind). A particularly useful contribution of this conceptual model is the representation of both event-based (e.g., storm-induced wave scarp event) and long-term (e.g., accretion/progradation) coastal evolution of foredune-dominated beaches. Hesp (2002) acknowledges that this model is limited due to its insufficient representation of the five major controlling variables in beach-dune systems: wave energy/surf-zone type, wind energy, sediment supply, sea level state, and climatic region/vegetation cover. In other words, despite its usefulness in coastal classification, this model is limited due to its oversimplification of the complex foredune system.

Hesp (2002:254) calls for the explicit need for future research to "examine further the relationships between foredune development and dynamics and surf zone-beach models and sediment supply". He also notes that a common system for determining descriptive characteristics of beach-dune form, linked to formative processes, is required to allow comparison of results from different coastal settings.

Figure 2.5: Model of established foredune morphodynamic evolution for stable, accreting and eroding coasts. Erosion from waves/high water levels may take place at any time leading to erosion, which may be followed by rebuilding or removal. Boxes B and C represent longer term evolution for increasingly erosional foredune stages. [Hesp, 2002, with permission].

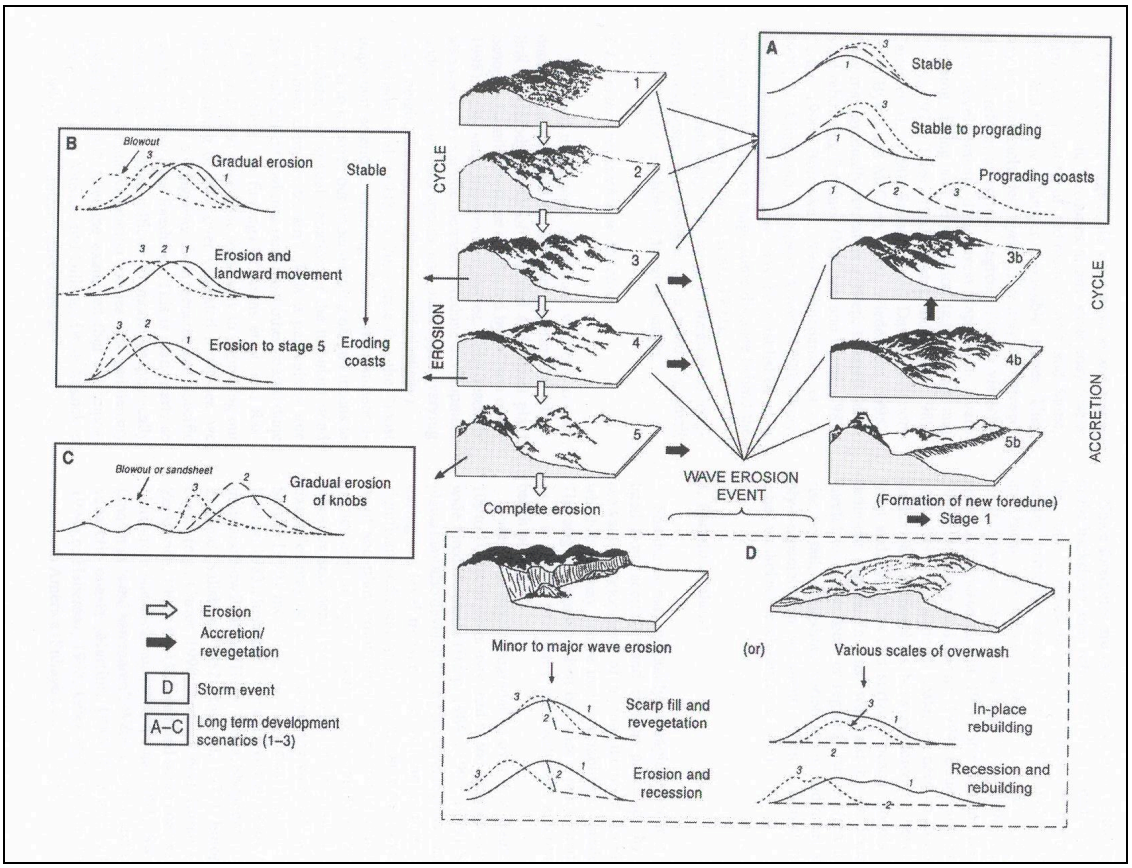

Psuty (2004) extends Hesp's (2002) beach-dune evolutionary model by describing a *beach-dune profile*, defined as a sand-sharing system composed of numerous components that respond to changes in incoming energy by episodically adjusting their sediment storing and releasing capacities (i.e., a closed system). This beach-dune model is based on a sediment budget approach to morphodynamics that emphasizes a holistic coastal system that is morphologically influenced by both time and space (Figure 2.6). This model is based on earlier work by Carter (1977) and

Psuty (1988) who stress that there is an intricate relationship between foredunes, beach dynamics (especially waves and tides), and sediment availability. The continuum model shows how the beach-dune sediment budget is integrally related to the resulting topography of both the beach and the foredune. For instance, under a positive sediment supply to the beach (i.e., shoreline progradation), the dimensions of a foredune are inversely related to the rate of beach accretion (i.e., more sediment is stored on the beach than in the foredune over that time interval) (Psuty, 2004). Once this progradation slows and sand-supply to the beach decreases, sediment transfer from the beach to the dunes will occur (provided no wave erosion occurs), resulting in growth of the foredune. This model is useful for anticipating beach-dune morphological response to erosive events and for providing a theoretical foundation for changes in observed shoreline position over time due to changes in sediment supply.

Arens (1996) and Arens et al. (2001) present alternative models of the beach-dune system incorporating the influence of vegetation and wind regime on landward aeolian sediment transport and accretion. This conceptual model, based on a sediment budget approach, which relates the landward transport of sediment towards the foredune to the erosion or accretion potential of a dune. Depending on onshore wind strength, varying amounts of sediment will be removed from the beach face via saltation and deposited on the dune crest. Incorporating this sediment budget approach and consideration for aeolian transport processes is an important, yet often overlooked, component of beach-dune conceptual modelling.

Figure 2.6: Conceptual model of beach-dune morphodynamic sediment budget. Dark line represents maximum potential foredune development, while the gray shading represents maximum potential inland sand transport. With erosion of the beach (dashed line), a negative sediment budget will result, leading to no net inland transport of sand. [Modified from Psuty, 2004].

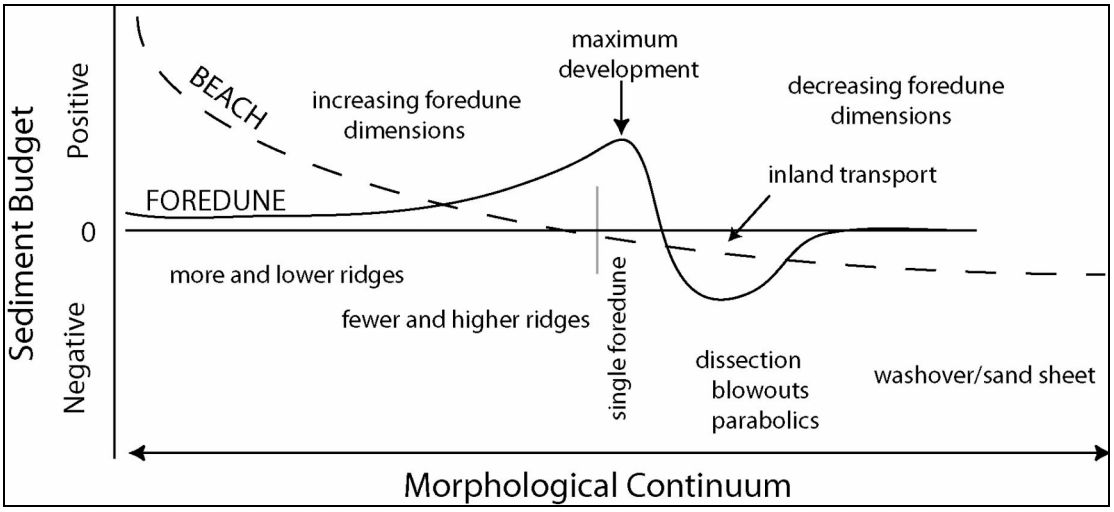

2.2.4 Embayed beach-dune systems

The size and shape of shoreline embayments is another important condition that controls beach-dune morphodynamics. The presence of rocky headlands influences the morphodynamics of sandy beach systems primarily through wave refraction and resulting alteration of sediment transport and beach planform. Embayed beach-dune systems are common on the rocky shores of BC, yet have received little attention. Globally, headland bay beaches comprise 51% of the world's coastline (Short and Masselink, 1999). Despite this prevalence, a thorough understanding of their morphodynamics is still lacking.

Embayed beaches typically have an asymmetric, curved, planform shape due to the prevailing wave refraction pattern (Figure 2.8) (Short and Masselink, 1999). Both orientation and planform of embayed beaches are determined by the refraction

pattern associated with the prevailing incident waves (direction and size) (Davies, 1958, as in Short and Masselink, 1999). The straight section of the embayment is usually parallel with the dominant wave crests. Embayment morphology and incident wave conditions control embayed beach circulation patterns. As wave height (H_b) increases and shoreline length (S_1) decreases, 'normal' beach circulation patterns (e.g., rhythmic or transverse bar formation) are increasingly modified (Martens, et al., in press, as in Short and Masselink, 1999). Once a critical threshold is reached, beach circulation becomes topographically controlled and megarip cellular circulation prevails (Short, 1985). Short (1985) introduces the non-dimensional embayment scaling parameter (δ`), where:

$$\delta' = S_1^2 / 100 C_1 H_b \quad (6)$$

and S_1 is the length of the shoreline between the headlands, C_1 is the direct length between the headlands and H_b is the modal breaking wave height (Figure 2.8). When $\delta` > 19$, normal beach circulation prevails, when $8 < \delta` < 19$, transitional circulation prevails, and when $\delta` < 8$, cellular beach circulation prevails (Short, 1985; Short and Masselink, 1999). Cellular circulation is primarily controlled by the topography of the surrounding headlands. Typically, with cellular circulation, longshore flow dominates in the embayment and strong megarips occur near the headlands. Cellular motion is also influenced by the size of the embayment. Small embayments (<2 km), for example, will shift to cellular circulation under breaking waves that are greater than 3 m, while long embayments (>5 km) only shift to cellular circulation under breaking wave conditions exceeding 6 m (Short, 1985).

Figure 2.7: Embayment scaling measurements: S_1 = shoreline length, C_1 = embayment width. [Modified from Short and Masselink, 1999].

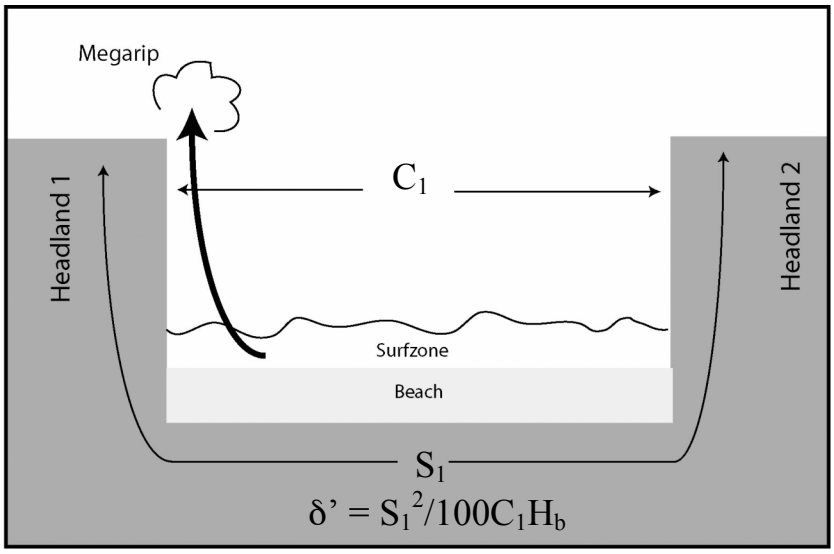

The megarips produced by cellular circulation also influence the erosion dynamics of embayed beach-dune systems (Short, 1985). Megarips can flow at high velocities for long distances (up to 1 km seaward of breaking waves). Megarips carry more sediment for a longer distance than normal circulation rips. The erosional impact of these megarips is, thus, important to consider when assessing the morphodynamics of embayed beach-dune systems.

Klein et al. (2002) examined short-term beach rotation processes and their effect on embayed beach planform morphology. Building upon the classification scheme introduced by Klein and Menezes (2001), this work suggests that embayed beaches exhibit different patterns of sediment removal as a function of the degree of curvature of the beach, the occurrence of submerged bars, rip currents and cellular circulation, the shoreline length, and the beach type (exposed vs. sheltered) (Klein et al., 2002). This research highlights the complex nature of embayed beach morphodynamics and the need for further investigation and understanding.

Recent work by Cooper et al. (2004) and Ranasinghe et al. (2004) provides a detailed re-examination of the embayed beach-dune systems of Australia's east coast. Using monthly beach profiles, daily beach video images, and daily wave direction data, Ranasinghe et al. (2004) investigated beach rotation, the periodic erosion and accretion regime of several embayed macrotidal beach-dune systems. Observations of beach and wave characteristics during the 1997-98 El Niño were analyzed in order to assess beach response to changes in wave climate induced by the ENSO climate mode. Based on this analysis, the authors present a conceptual model of beach rotation that can be used to assess the climate variability response of other embayed beach-dune systems.

2.2.5 Beach rotation

Beach rotation is a morphodynamic process characterized by periodic lateral movement of sand towards alternating ends of an embayed beach (Short and Masselink, 1999). The resulting alteration of beach planform occurs due to seasonal changes in the wave climate (e.g., wave magnitude or direction) (Figure 2.8). As the dominant wave direction induces longshore transport in one direction along the beach in a given season, the net sediment movement is in that direction. A shift in dominant wind direction that may occur with seasonal climatic changes may cause the longshore transport to switch directions and move sediment to the opposite end of the beach. As net shoreline accretion or erosion occurs on the ends of the beach, the net sediment budget may not necessarily change (i.e., no sediment is removed from the system) (Short and Masselink, 1999). Beach rotation does not require a dramatic

shift in wave climate. Particularly in long embayments, beach rotation can occur following only a slight change in wave direction.

Figure 2.8: Simplified model of beach rotation. a) Waves from one direction produce longshore sediment drift, which results in an accumulation of sediment at the downdrift headland and erosion at the updrift headland. b) Waves from another direction reverse the process. [Modified from Short and Masselink, 1999].

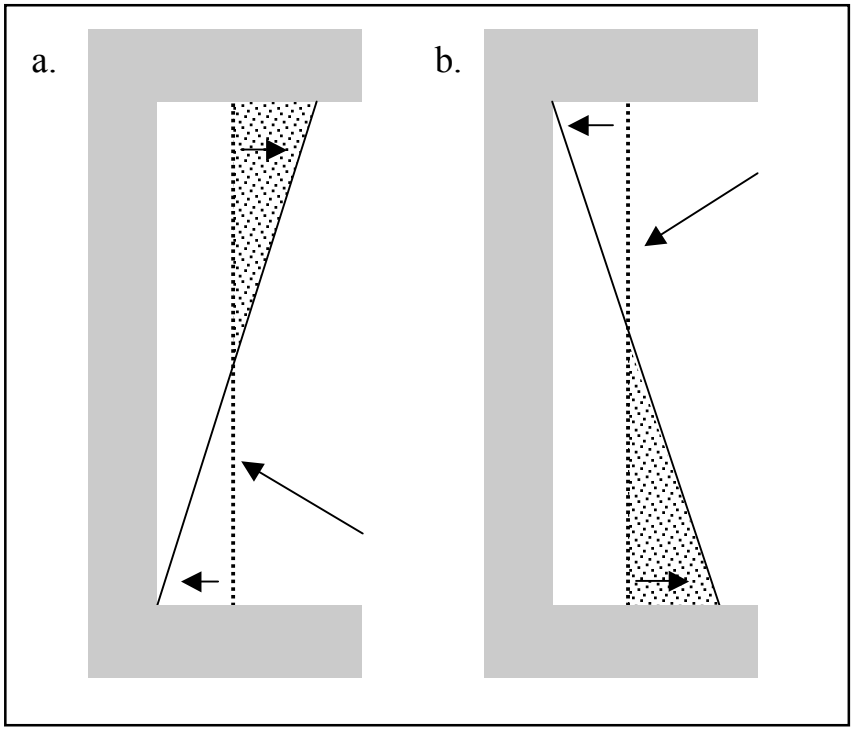

Short (1995), Ranasinghe et al. (2002), and Short and Trembanis (2004) suggest that beach rotation may occur as a result of variations in wave climate caused by shifts in the ENSO phase. From research on the east coast of Australia, Short and Trembanis (2004) found that during prolonged El Niño events, increased occurrence of oblique waves would cause the southern end of beaches to erode and northern ends to accrete. Prolonged La Niña events would result in the reverse morphodynamic response. Expanding on this, Ranasinghe et al. (2004) examined the quantitative link

between the Southern Oscillation Index, wave climate, and beach rotation, to try and identify the underlying physical processes causing beach rotation. They present a conceptual model outlining various stages of beach rotation during both an El Niño and a La Niña event on the New South Wales coast of Australia. Ranasinghe et al. (2004) conclude that there is a definitive link between ENSO phase changes and the resulting erosion/accretion cycle on the embayed beach-dune systems of eastern Australia.

2.2.6 Aeolian sediment transport

Sandy, macrotidal beaches with competent wind regimes present near-optimal conditions for coastal dune development via aeolian (wind-blown) sediment transport. Therefore, considering the aeolian transport process is an important, yet often overlooked aspect of understanding the morphodynamic response of macrotidal, high-energy beach-dune systems (Walker and Barrie, 2006).

There are several important controlling factors that influence the aeolian sand transport potential on beach-dune systems. These factors can be divided into two distinct categories:

1) supply-limiting; which limits the availability of sediment to the transport process
2) transport-limiting; which alters the ability of near-surface flow to transport available sediment (i.e., decrease near surface flow velocity)

Key *supply*-limiting variables include: i) moisture content (e.g., Sarre, 1989; Arens, 1996; Jackson and Nordstrom, 1998; McKenna Neuman and Scott, 1998; Wiggs et al., 2004; Davidson-Arnott et al., 2005); ii) precipitation (e.g., Sarre, 1989; Jackson and Nordstrom, 1998); and, iii) water level and wave climate (Regnauld and

Loubotin, 2002; Ruz and Meur-Ferec, 2004). The following *transport*-limiting variables are also identified: i) wind speed (Hsu, 1971; Wal and McManus, 1993); ii) wind direction (e.g., Svasek and Terwindt, 1974; Rasmussen, 1989; Nordstrom and Jackson, 1993; Arens et al., 1995; Davidson-Arnott and Law, 1996, Walker et al., 2006); iii) vegetation type and density (e.g., Hesp, 1988; Sarre, 1989; Arens, 1996; Arens et al., 2001; Hesp et al., 2005); iv) surface roughness (Blumberg and Greeley, 1993); and, v) secondary flow effects resulting from the interaction of dune topography, vegetation, and driftwood jam and near-surface airflow (Nickling and Davidson-Arnott, 1990; Wiggs et al., 2004; Walker and Nickling, 2003; Walker et al., 2006).

Despite the complexities introduced by these numerous variables, several quantitative models exist that estimate sediment transport rates, beginning with Bagnold's (1941) equation, expressed as follows:

$$q = C(d/D)^{1/2} * u_*^{3} * \rho/g \qquad (7)$$

where q is the sediment transport rate in kg m^{-1} s^{-1}, C is a dimensionless grain size distribution coefficient, d is grain diameter, D is a standard grain size diameter (0.025 cm), u_* is shear velocity, ρ is the density of air (1.22 kg m^{-3}), and g is the force of gravity (9.8 m s^{-2}).

Bagnold's (1941) equation laid the foundation for further aeolian sediment transport research, but is limited in its effectiveness for accurately estimating sediment transport in beach-dune (i.e., coastal) settings (Psuty, 2004). The equation does not include a threshold term or consideration of moisture effects, and, as such, sediment transport is predicted at shear velocities lower than what is required for

entrainment. Since Bagnold's (1941) initial work, a variety of sediment transport prediction equations have been developed, though none accurately predict coastal sediment flux due to their primary assumption of transport-limited conditions (see reviews in Sarre, 1989 and Sherman et al., 1998). Models based on Bagnold's (1941) work use a measure of shear velocity (u_*) at the surface, which is hard to determine over complex surfaces due to roughness and topographic effects. Therefore, aeolian transport over complex surfaces, such as beach-dune environments, requires the use of above surface shear velocity measurements (i.e., 10 m above the surface) to eliminate the influence of surface roughness on the estimated flux value.

In a coastal setting, aeolian transport is not only influenced by the characteristics of the wind regime, but also by numerous other factors such as nearshore processes, littoral sediment, water level (e.g. tidal range, runup), beach slope, presence of a driftwood jam, beach-dune topography, and fetch distance. As such, assessing aeolian activity and foredune development at a regional scale is somewhat limited in coastal settings. Regional sediment transport and beach-dune rebuilding potential can be approximated using Fryberger's (1979) sediment drift potential model and readily available meteorological data.

Fryberger's (1979) sediment drift potential

Fryberger (1979) developed a drift potential model to relate observed desert dune morphology from Landsat satellite images to regional wind regime using standard meteorological data. The Fryberger (1979) model calculates maximum regional sediment drift potential (DP) using wind data recorded at 10 m above the

surface. Based on the Lettau and Lettau (1978) sediment transport equation, the model estimates the sediment DP for each directional mode in the wind regime using:

$$DP = \frac{V^2(V - V_t)}{100} * t \quad (8)$$

where V is mean wind speed at 10 m (in knots), V_t is the threshold of sediment transport (i.e., 12 knots or 6 m s^{-1}) measured at 10 m, and t is the time wind blew expressed as a percentage of the analysis period. DP values for each direction mode are then summed using vector analysis to produce a resultant drift potential (RDP) vector with a resultant drift direction (RDD) for the region. Plotted graphically, DP vector produces a drift rose showing potential sediment transport from different directional classes, with a net RDP vector (e.g., Figure 5.5).

According to Fryberger (1979), the directional variability of a regional wind regime can be characterized using total DP values and the ratio of RDP/DP (Table 2.1). This ratio ranges from zero (multi-directional) to one (unimodal). In coastal settings, the Fryberger (1979) model provides an adequate relative measure of regional sediment drift potential (Pearce, 2005). Measures of dune mobility such as the Lancaster (1988) Index or the Tsoar and Illenberger (1998) dune mobility model are not applicable to coastal settings.

The Fryberger (1979) model has been used in a variety of environments to examine wind energy and sand transport potential. When using the model it is important to understand that it is based on two key assumptions: that the sediment surface consists of dry, quartz sand, and that there is sparse vegetation cover and no bedform roughness more than ripples (Pearce and Walker, 2005).

Table 2.1: Fryberger's (1979) classification of wind energy environments.

Drift Potential Ranges (VU)	Energy of wind environment	Directional Variability (RDP/DP)
<200	Low	< 0.3 Complex to obtuse bimodal
200-400	Intermediate	0.3 to < 0.8 Obtuse to acute bimodal
>400	High	> 0.8 Wide to narrow unimodal

2.2.7 Foredune types and dynamics

According to Hesp (2002), foredunes are defined as alongshore dune ridges that are formed at the back of the beach by aeolian sediment deposition within vegetation. Foredunes that are actively being formed are at the most seaward position in the backshore, while relict foredunes may occupy more landward areas of the backshore. Foredunes are classified as either incipient or established (Hesp, 2002). Incipient foredunes are developing foredunes located in backshore areas characterized by the presence of pioneering plant clusters or driftwood jams. The morphological development of incipient foredunes is influenced primarily by plant density, distribution, height and cover in the backshore, wind speed and direction, sediment transport rate, frequency and magnitude of swash inundation, and rates of storm wave erosion (Hesp, 2002). Incipient foredunes eventually develop into established foredunes, which are distinguished by their greater morphological height, width and age and commonly by the presence of large woody plant species. On sedimentary coasts, foredunes are an integral part of beach-dune evolution and morphodynamic

response to storms. Incipient and established foredunes buffer the beach against storm wave inundation by storing and redistributing sediment to the nearshore.

2.3 Beach-dune response to sea level rise

Based on the equilibrium beach profile model (presented above in Section 3.1.1), Bruun (1962) proposed a model of how shorelines retreat in response to rising sea-level (Figure 2.11)(commonly referred to as the 'Bruun Rule'). This simple, two dimensional model is based on the assumption that sediment is eroded from the upper shoreface and deposited on the lower shoreface in order to maintain the equilibrium profile with rising sea level. The thickness of sand transferred is said to be equal to the vertical rise in sea-level. The basic relation for predicting horizontal recession of shoreline (R) from an increase in sea level (S) is defined as (Bruun, 1962):

$$R = \frac{L_*}{B + h_*} S \tag{9}$$

where L_* is the cross-shore distance to depth h_* (depth of closure), and B is the height of the berm or other sediment formed on the land that is eroded. This can also be represented as Davidson-Arnott (2005) did by:

$$R = \frac{1}{\tan\theta} S \tag{10}$$

where θ is the average slope of the nearshore along the cross-shore width L_*.

The Bruun Rule has been applied widely in engineering and coastal management projects across the globe since its formulation in 1954 (Cooper and Pilkey, 2004). More recent findings, however, have invalidated the Bruun Rule, primarily due to common violations of key assumptions (e.g., Cooper and Pilkey,

2004a). Cooper and Pilkey (2004a), who insist that the Bruun Rule be completely abandoned, assert that the pervasive use of this model is due to its simplicity, ease of use, lack of critical scientific appraisal of the model, and lack of useful alternatives.

Similarly, Davidson-Arnott (2005) challenges the Bruun Rule saying that the assumption of net transfer to the nearshore is not justifiable. Based on the beach-dune concept of morphodynamics, Davidson-Arnott (2005) presents an alternative conceptual shoreline response model (herein referred to as the RD-A model) (Figure 2.12) that takes into consideration the dune sediment budget and beach/dune interactions. In modelling for sea-level rise, this theoretical model predicts foredune preservation via landward migration, as well as no net transfer of sediment to the nearshore profile. The RD-A model predicts landward migration of the beach-dune profile by a distance R, based on the beach slope and Equation 10 (above). The RD-A model has yet to be tested in a real-world modelling application, though it is important to consider that future applications will require consideration of volumetric changes of beach-dune morphology in response to sea-level rise. The RD-A model provides a possible foundation upon which future shoreline change models may be based.

Figure 2.9: Illustration of the Bruun (1954) model of beach profile response to sea level rise via coastal retreat and dune loss. [Modified from Davidson-Arnott, 2005].

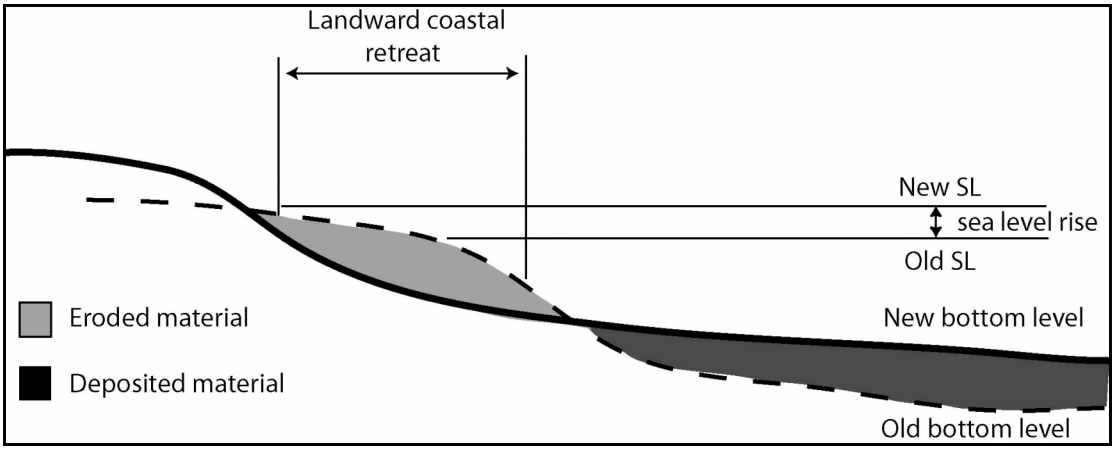

Figure 2.10: Conceptual RD-A model of beach dune response to sea level rise via landward dune migration. [Modified from Davidson-Arnott, 2005].

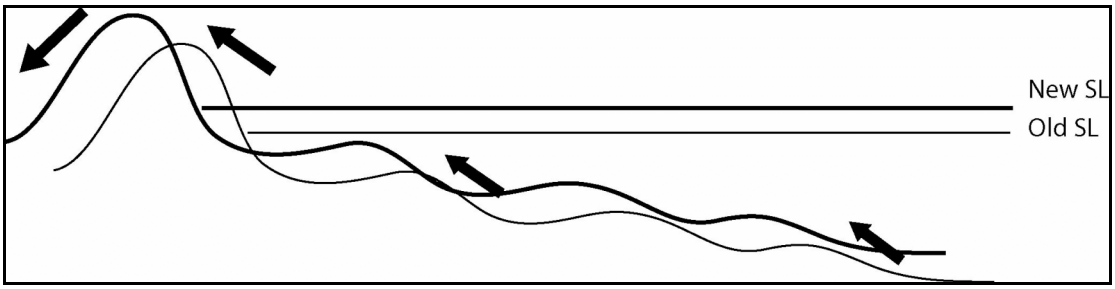

2.4 Climate variability modes and impacts

Climate is a general description of long-term weather conditions for a given region including temperatures of surface air, water, land, wind and ocean currents, and pressure and density of the atmosphere and ocean. *Climate change* represents longer-term trends (i.e., decades to centuries) in these, and other, climate properties. According to the BC Ministry of Water, Land and Air Protection's (BC-MWLAP) *Indicators of Climate Change* report (2002), several properties of BC's climate have changed in the 20th Century. On the coast of BC, for example, average annual air

temperatures increased by 0.6°C, sea surface temperatures increased by 0.9°C to 1.8°C, and sea level rose by 4 to 12 cm. In the same report, future predictions for climate change in the 21st Century suggest an average air temperature increase by 1°C to 4°C, sea level rise of up to 88 cm, and average annual precipitation increase by 10 to 20 percent. These trends reflect climate change, which occurs simultaneously with, and has an influence on, climate variability.

Climate variability represents relatively short-term (i.e., seasonal to inter-annual) changes in climate usually resulting from natural alterations in the climate system or complex interactions between the atmosphere and the ocean (BC-MWLAP, 2002). The climate of Haida Gwaii (HG) is strongly influenced by two distinct climate variability patterns, the El Niño Southern Oscillation (ENSO) and the Pacific Decadal Oscillation (PDO). These climate variability patterns are natural phenomena of the global climate system and are super-imposed on longer-term climate change. The next sections discuss these two phenomena and their impacts on coastal systems in the NE Pacific.

Parks Canada suggests monitoring for climate variability impacts using *geoindicators* (Welch, 2002), which are defined as measures of Earth surface processes and phenomena that are important in understanding environmental change over periods of <100 years. These indicators relate to geology, geomorphology or soil properties and include the following components: dunes, extreme events, lake and ocean sediment, marine nearshore environments, mass movements, proxy record, sea level, shorelines, soil erosion, and wind erosion (Table 1.1).

2.4.1 ENSO

The most well-known, large-scale climate variability phenomenon that influences global atmospheric circulation patterns is the ENSO. ENSO is a warming of the tropical Pacific that occurs on a cycle of approximately 3-7 years and lasts for 6-18 months. This phenomenon occurs following a disruption in the trade wind pattern across the equator as atmospheric pressure rises in the western Pacific and falls in the eastern Pacific. As trade winds weaken during an El Niño, warm ocean waters shift eastward, resulting in reduced upwelling of cold water along the equator and the west coast of South America. This reduced upwelling causes sea surface temperatures to rise and sea levels to increase due to thermal expansion of coastal water and, to a lesser degree, increased freshwater discharge. The La Niña phenomenon, the other portion of the ENSO cycle, displays global climate conditions that are opposite to those during El Niño. That is, La Niña is characterized by stronger trade winds and colder equatorial Pacific sea surface temperatures and thus, results in increased biological productivity, fewer storms, and generally more stable weather patterns.

Since the 1950s there have been 10 notable El Niño events and 8 La Niña events (Figure 2.13). The Intergovernmental Panel on Climate Change (IPCC) documents that since the mid-1970s, El Niños have been more frequent, persistent, and intense (IPCC, 2001). As a result, there is an increasing awareness of the global and regional atmospheric, oceanographic, and terrestrial impacts of this phenomenon.

Globally, the ENSO regime can be characterized by the Southern Oscillation Index (SOI) and the Multivariate ENSO Index (MEI) (Wolter and Timlin, 1993, 1998). The SOI describes the pressure difference between the southeast tropical

Pacific (at Tahiti) and the Australian-Indonesian region (at Darwin, Australia). The full regime of ENSO is represented by the MEI, which is the weighted average of numerous environmental variables specific to the tropical Pacific, including: sea surface temperature (SST), the east-west and north-south components of surface winds, sea level pressure, sea level temperature, and cloudiness. El Niño (warm) phases of ENSO are represented as positive SOI and MEI values, while La Niña (cool) phases are represented as negative values.

The remote, extra-tropical effects of El Niño and other phenomena that affect surface conditions and anomalous weather events over landmasses and the ocean are termed *"teleconnections"* and result from interactions between different latitudes of the atmosphere-ocean system (McPhaden, 2002). NE Pacific regional teleconnected responses to ENSO are described by the Northern Oscillation Index (NOI) (Schwing et al., 2002). The NOI is a climate variability index related to the ENSO signal and regionally specific to the NE Pacific (Figure 2.13). NOI is based on the difference in sea level pressure between the North Pacific High in the NE Pacific and an area of low pressure near Darwin, Australia (Schwing et al., 2002). As such, NOI describes a direct, physical link between extra-tropical climate variations in the NE Pacific to those in the tropics. Schwing et al. (2002) propose that the NOI may provide a direct means for categorizing the underlying processes of climate change specific to the NE Pacific. Large positive NOI values correspond with La Niña years, while large negative NOI values are associated with El Niño years. The NOI is strongly correlated ($r = 0.77$) with the Southern Oscillation Index (SOI), but it represents

distinct regional differences in climate patterns and individual events that are not captured in the tropically-based SOI (Schwing et al., 2002).

Figure 2.11: Climate variability indices: Multivariate ENSO index (MEI), Northern Oscillation Index (NOI), and Pacific Decadal Oscillation (PDO). [Modified from Walker, 2006].

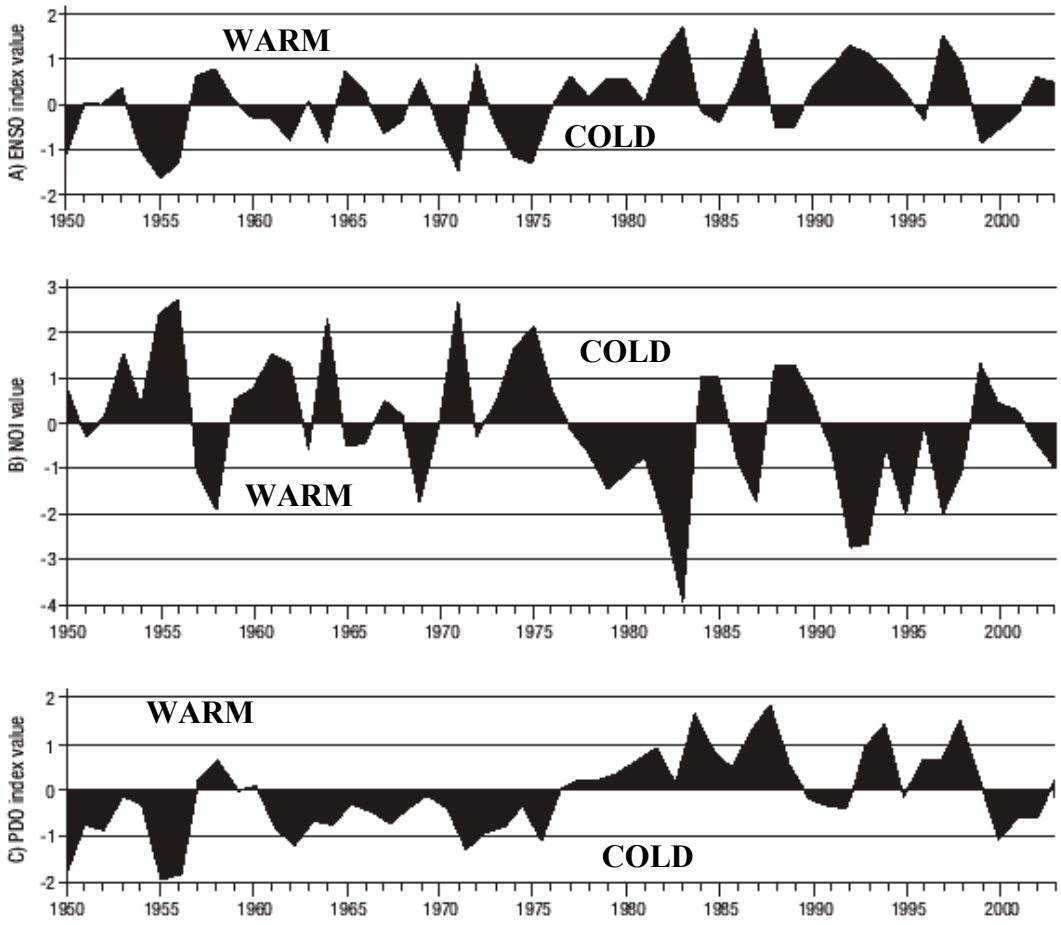

2.4.2 ENSO responses

Coastal zones of the NE Pacific experience ENSO teleconnected impacts primarily due to the unusually thick layer of warm surface water along the coast causing thermal expansion of coastal waters, and the offshore winter storms associated with the altered jet streams. In the NE Pacific, El Niño conditions divert

the jet stream causing a stronger than normal Aleutian Low pressure system in the winter months (December – February) (Shabbar at al., 1997). This results in a greater number of storms reaching the north coast of BC, meaning wetter and stormier weather in HG and a milder, drier winter in southern Canada (Walker, 2006).

Recent research efforts focus on identifying the teleconnections between ENSO and coastal morphological response (Storlazzi and Griggs, 2000; Storlazzi et al., 2000; Allan and Komar, 2002, 2006; Barrie and Conway, 2002; Dingler and Reiss, 2002; Sallenger et al., 2002; Maia et al., 2005). To date, however, little research exists on the specific teleconnections between regional ENSO climate modes and local hydrologic and morphologic impacts on the west coast of Canada (Walker, 2006). Abeysirigunawardena and Walker (unpublished data, 2007) found statistically significant evidence that mean sea level variations recorded at Prince Rupert (PR) (on the west coast of BC) respond to climate variability driven by ENSO. More specifically, based on statistical analysis, they conclude that mean sea level in this region, which is rising at a rate of 1.6 mm yr^{-1}, responds to ENSO-related climate forcing during the winter months.

Subbotina et al. (2001) identified that during strong El Niño events (1982-83, 1997-98) coastal water levels on the west coast of North America rose by as much as 100 cm. On the Pacific coast of Canada, sea levels typically rise about 10 to 20 cm above seasonal heights during strong El Niño events (Crawford et al., 1999). Sea level rise in response to climate variability events occurs primarily due to thermal expansion from elevated sea surface temperature and to a lesser degree increased terrestrial freshwater (Walker, 2006). Higher than normal sea-surface elevations

combined with storm-generated surface waves, ocean swells and high tides often result in increased erosion along the coast of North America during El Niño years (Storlazzi and Griggs, 2000; Allan and Komar, 2002, 2006). In HG, Barrie and Conway (2002) estimated a rise of 40 cm above mean sea level and as much as 12 m of coastal retreat in response to the 1997-98 El Niño.

2.4.3 PDO

The PDO another ocean-atmosphere variability phenomenon affecting climate and erosive events in HG, characterizes the inter-annual variability of the mean sea surface temperature in the North Pacific (Figure 2.13) (BC-MWLAP, 2002). With a periodicity of ~20-30 years, it is a longer cycle than ENSO but has similar warm and cool phases (Mantua et al., 1997). Although the mechanisms of the PDO remain unknown, the climate conditions for positive and negative phases are well understood. The El Niño-like warm phase of the PDO corresponds with an enhanced Aleutian Low pressure system in the winter and warmer waters along the west coast of North America, while the cool phase corresponds to La Niña-like conditions (Mantua and Battisti, 1995; Zhang et al., 1997). Abrupt transitions between the warm and cool phases occur approximately every 25 years (Gedalof and Smith, 2001). There have been two full PDO cycles during the 20th century (Figure 2.13): 1890-1924 (-; cool), 1925-1946 (+; warm), 1947-1976 (-; cool), and 1977-mid-1990s (+; warm). Currently we are in a cool (-) PDO phase following the phase shift in the mid-1990s. PDO regime shifts affect the NE Pacific climate by either enhancing or suppressing the strength of the ENSO signal (Gershunov and Barnett, 1998).

Extreme El Niño events that are enhanced by PDO phases (e.g., 1982-1983 and 1997-1998) may be related to longer-term climate change (Timmerman et al., 1999).

Abeysirigunawardena and Walker (unpublished data, 2007) examine the effects of PDO climate variability on oceanographic conditions of the BC coast. Using statistical analysis of annual mean sea level and maximum sea level at PR and PDO climate index values, they identified a statistically significant linear relation between mean annual sea level on the north coast of BC and PDO index values (Abeysirigunawardena and Walker, unpublished data, 2007). Additionally, they identified that mean sea level responses were related to sea surface temperature effects (via thermal expansion) and are related to longer-term PDO signals, particularly in the summer months (Abeysirigunawardena and Walker, unpublished data, 2007).

2.4.4 ALPI

The Aleutian Low Pressure Index (ALPI) provides a measure of the intensity of the December to March (winter) Aleutian low-pressure system in the north Pacific (Beamish and Bouillon, 1993; Beamish et al., 1997) and thus describes regional climate variability for the greater north Pacific. The ALPI is calculated as the mean area with sea level pressure ≤ 100.5 kPa from December to March and is expressed as an anomaly from the 1950-1997 mean (Beamish et al., 1997). Positive phases of the ALPI are associated with an intensification of the Aleutian Low, warmer sea surface temperatures, and increased westerly storms and wind stress in the NE Pacific (King et al., 2000; Brown, 2002). This index has primarily been used as an ecological indicator for climate variability responses, but has strong potential as a climate

variability indicator for coastal geomorphic change in the NE Pacific due to its association with high south-westerly winds (King et al., 2000), which may increase rates of erosion by enhancing storm surges on the NW Pacific coast. ALPI has been significantly correlated (r = 0.483) to the mean sea level response at PR (Abeysirigunawardena and Walker, unpublished data, 2007).

2.5 Summary and research gaps

This broad survey of literature on beach-dune morphodynamics and climate variability events allows identification of several key research gaps as follows:

1. Embayed, high-energy, macrotidal beach-dune morphodynamics are understudied. The models commonly used to understand and describe macrotidal beach-dune morphodynamics provide a useful foundation upon which future research may expand. There is, also, a clear need to develop a common system for determining the descriptive characteristics of beach form and process so that the results from different coastal studies may be more reasonably compared (Hesp, 2002). Expanding the spatial application of beach classification models is necessary to achieve this disciplinary goal.

2. Fryberger's (1979) model of sediment drift potential is limited and requires additional application and testing in order to improve its robustness, particularly in coastal environments. Statistical analysis of the recurrence of extreme total water levels and wave runup is rare. Combining these types of analysis may improve current understanding of the role that wind and total water levels play in the erosion and rebuilding regimes of high-energy beach-dune systems.

3. Despite known relationships between climatic variability and regional oceanographic responses elsewhere (e.g., Oregon, Washington, California), local- and regional-scale hydrodynamic and morphodynamic impacts of climate

variability and change remain poorly documented and understood in British Columbia, particularly for the Haida Gwaii region. Further research is required to assess whether relationships between climate indices and coastal impacts are similar regionally and globally. There is little research to date that establishes a method for monitoring coastal geoindicators (e.g., coastal erosion, sea level rise, and extreme events) in Canada's National Parks. Improving this area of research within Gwaii Haanas National Park Reserve and Haida Heritage Site has potential applications in Parks management and planning for future climate change scenarios.

3.0 Research Methods

This chapter outlines the methods used to achieve the three objectives described in Chapter 1. First, to assess the geomorphology and morphodynamics of two embayed, high-energy beaches of Gwaii Haanas National Park Reserve and Haida Heritage Site (GH-NPR), a detailed qualitative description and parametric classification of two representative beach sites was conducted. Second, using Fryberger's (1979) model of regional aeolian sand drift potential, as well as statistical analysis of total water levels and wave runup, the erosion and rebuilding regimes of these two beaches were examined. Third, to identify regional climatic variability and climate change-induced signals, statistical analyses of annual mean and maximum water levels and climate indices were conducted. These research methods expand on surveys and observations from a reconnaissance field season in June 2005 and a more thorough field season in June 2006.

3.1 Geomorphic assessment of Woodruff Bay and Gilbert Bay beaches

The geomorphic features of Gilbert Bay and Woodruff Bay beaches were assessed using both qualitative and quantitative description and classification. Qualitative analysis was based on site visits, site photographs, topographic and bathymetric maps, and aerial photographs, while the quantitative analysis was based on sediment grain size analysis, topographic and bathymetric surveys, and digital aerial photograph analysis. Historical aerial photograph analysis (e.g., retreat rate estimation) was attempted, but was not possible due to limitations in photograph resolution and temporal availability.

3.1.1 Topographic profiles

Topographic beach-dune profiles were established on both beaches as part of a coastal erosion monitoring project in GH-NPR. In June 2005, three benchmarks were established in the mature forest on the relict dunes of Woodruff Bay beach and marked with rock cairns. Shore-normal topographic profiles were established at each of the benchmarks in June 2005 using a compass, measuring tape and abney level. In June 2006, these profiles were resurveyed in detail using a digital Topcon™ total station. On Gilbert Bay beach, one benchmark was established and a detailed shore-normal profile was conducted in June 2006 using the digital total station. Details of the four benchmarks and profiles are outlined in Table 3.1.

For each profile, the water line and time of survey were used to tie the profiles into mean sea level using predicted water levels from the Canadian Hydrographic Service (CHS). This method was used because there are no vertical control markers in the survey area. To adjust the profiles relative to mean sea level, the water line was tagged during each survey and the time (to the nearest minute) was recorded. The corresponding predicted (tidal) water level for Cape St. James (CSJ) (in metres above mean sea level, MSL) was then obtained from CHS data. On each topographic survey, the profile elevations were adjusted to this elevation. Storm surge, pressure, and fetch effects were assumed negligible because the surveys were conducted on calm, high pressure days with no noticeable change in total water level. Therefore, the predicted water levels were assumed to represent the total water levels at the time of survey.

Table 3.1: Details of the shore-normal topographic profiles from Gilbert Bay and Woodruff Bay beaches.

Profile	Benchmark 1 location UTM (m)	Benchmark 2 location UTM (m)	Length of survey (m)	Profile azimuth (°)	Sample density (points/m)
Woodruff 1	360149E 5760155N	360132E 5760162N	198	130	0.389
Woodruff 2	359944E 5759969N	359938E 5759982N	172	140	0.401
Woodruff 3	359794E 5759815N	359778E 5759812N	143	123	0.385
Gilbert	357062E 5767619N	357078E 5767645N	260	195	0.565

Each topographic profile transect was extended offshore to document the bathymetric characteristics of each site. This was completed on a Parks Canada vessel (Yo-Dang) using an on-board Global Positioning Unit that recorded data points in UTM (Easting and Northing values), and an electric depth sounder to record water depth in metres. The topographic and bathymetric profiles were joined by plotting both sets of survey data (UTM Eastings and Northings) on a single plan-view plot (e.g., Figure 3.1). The gap between the topographic and bathymetric portions of the combined plot (e.g., circled on Figure 3.1) occurs because the bathymetric survey was conducted using a boat that was effected by the waves and currents which made lining up precisely with the land survey difficult. The Woodruff 3 bathymetric survey was not extended very far into the bay because large rocky outcrops prevented the boat from traveling along the appropriate azimuth. The bathymetric profile at Gilbert Bay beach has a different azimuth than the topographic profile (see Figure 3.2) because, when extended into the headland-confined bay, the shore-normal azimuth on

the beach backshore and foredunes (195°) did not correspond to the middle of the bay. While collecting the bathymetric data from the boat, the azimuth was adjusted to 174° to better capture the bathymetric characteristics of the centre of the bay.

The topographic and bathymetric profiles for each site were used to characterize and classify the beach based on a sediment budget approach and the equilibrium beach profile concept (Bruun, 1962, 1988; Dean, 1977, 1991; Bernabeu et al., 2003a, 2003b). Using the profiles, on-site observations and site photos, geomorphic features present at each site were described.

Figure 3.1: Woodruff Bay beach and bathymetric survey plan view.

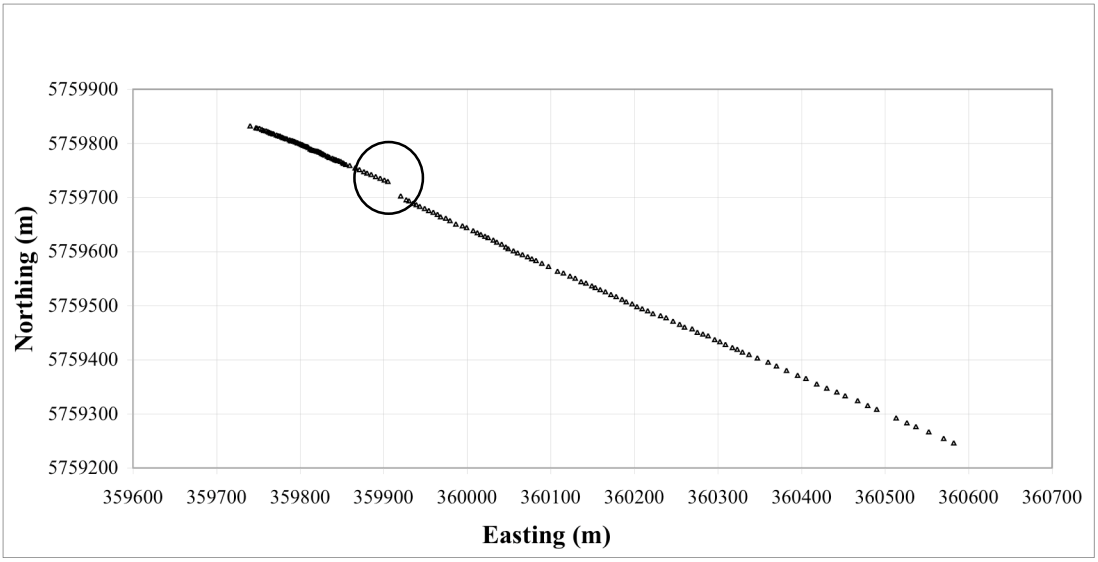

Figure 3.2: Gilbert Bay bathymetric survey plan view, alteration in azimuth evident at ~357000 m E.

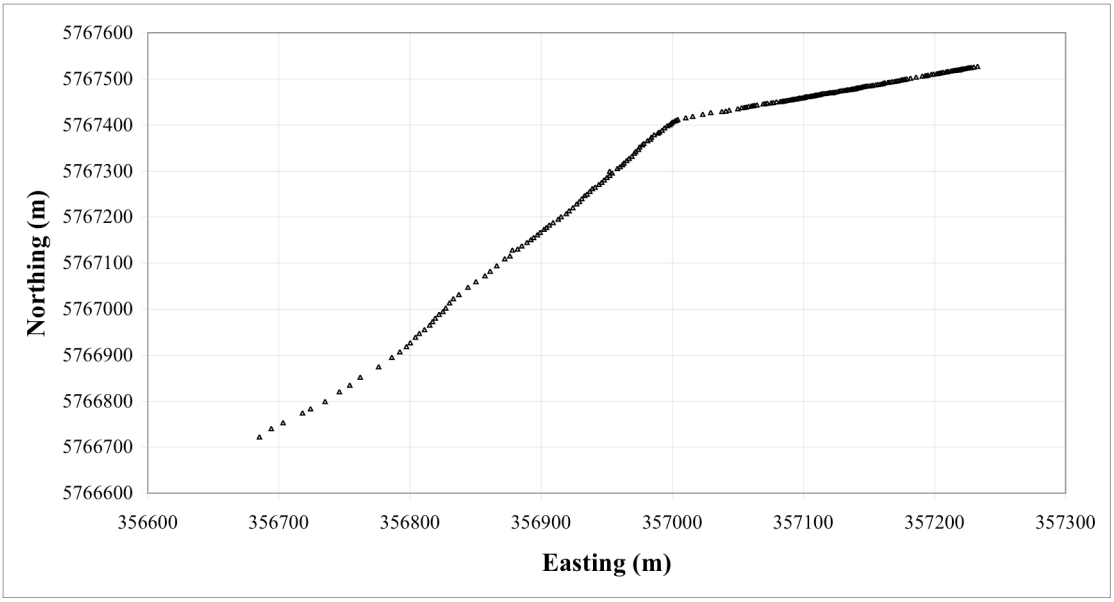

3.1.2 Sediment transport pathways

Using the McLaren and Bowles (1985) approach, high-tide swash line sediment samples were collected linearly along each beach at 10 m intervals. A metal soup can was pressed in the beach to a depth of ~10 cm to collect the top layer of sediment. The sediment samples were dried and sieved using half phi intervals. Sediment grai nsize statistics were calculated using GRADISTAT[1].

3.1.3 Wave height and embayment characteristics

To characterize the modal breaker wave height (H_b) of the two beaches, the following formula presented by Short and Masselink (1999) was used:

$$H_b = \sqrt{H_o^{\,2}(C_l / S_l)} \tag{11}$$

[1] Available online at http://www.kpal.co.uk/gradistat_abstract.htm

where H_o is offshore significant wave height, C_l is the distance between the embayment headlands, and S_l is the shoreline length of the embayment (Figure 2.8). It is noted that this calculated H_b value is only an approximation because it ignores shoaling and bed friction and simply represents the square root of the energy reaching the shoreline from the incident waves. In addition to the equilibrium beach profile model, this H_b value is used to classify the beach according to the Masselink and Short (1993) model (Equations 4, 5) and in calculating the non-dimensional embayment scaling parameter (δ`) (Short, 1995). This parameter (Equation 8) is used to examine the degree of embayment size and shape at each site.

H_o was determined by averaging the available significant wave height observations (1993-present) from Environment Canada's (EC) 'South Moresby' stationary wave buoy (C46147, 51°49'59", 131°13'59"), which is located approximately 18 km WSW of CSJ. The average significant wave height represents the highest 1/3 of the waves for the given time interval (e.g., hourly). To capture extreme wave conditions, an average winter (September through February) maximum significant wave height was also calculated.

3.1.4 Beach classification

To classify the beach form and morphodynamic relations to wave and tide range, the Masselink and Short (1993) model (see Figure 2.4, Equations 4 and 5), mean spring tide range (MSR), H_b, modal wave period (T), and sediment fall velocity are required. MSR was calculated from CHS modal large (spring) tide water levels. Highest High Water Large Tide (HHWLT) is defined as the average of the annual highest high waters for 19 years of tidal predictions, Lowest Low Water Large Tide

(LLWLT) is defined as the average of the lowest low water levels for 19 years of tidal predictions, and MSR is the difference between HHWLT and LLWLT (CHS, 2006). H_b was calculated using Equation 13 (above). T was derived from buoy C46147 by averaging the observed wave period for the available record (1993-2006). Sediment fall velocity was measured from surface sediment samples collected from the high-tide swash zone along each topographic profile transect. Stokes' law was used to determine sediment fall velocity (w, m s^{-1}) (Ferguson and Church, 2004):

$$w = \frac{RgD^2}{C_1 v} \tag{12}$$

where, R is the particle's submerged specific gravity (1.65 for quartz in water), D is the particle's diameter (m), C_1 is a constant with a theoretical value of 18, and v is the kinematic viscosity of the fluid (1.0 X 10^{-6} kg m^{-1} s^{-1} for water at 20°). w was calculated for each beach based on the respective high tide mean sediment grain size.

To classify the beaches, the relative tide range (RTR) and dimensionless fall velocity (Ω) were calculated according to Equations 4 and 5. Using the Masselink and Short (1993) conceptual classification model (Figure 2.4), the beaches were then classified along a continuum of dissipative to reflective, and barred to terraced. Results from this classification model were validated using measured cross-shore profiles and site photos. The beach-dune systems were also classified according to qualitative models (e.g., Hesp, 2002; Psuty, 2004; Arens, 1994) based on site observations, sediment characteristics, aerial photographs, and topographic profiles.

3.2 Assessing regional aeolian activity and wind regime

3.2.1 Meteorological data

Wind data from the EC station at CSJ (ID-1051350; 51°55'N, 131°1'W; 93 m above mean sea level) were used to assess the regional wind regime and aeolian sediment transport potential. The station records wind speed and direction at a standard height of 10 m above the surface. Wind data are recorded hourly as 1-minute, or since 1985, 2-minute averages recorded on the hour to the nearest kilometre per hour (km hr^{-1}). Due to the extreme conditions and remote nature of the station there are some gaps in the data, primarily due to instrument failure and delayed maintenance. To facilitate comparison with previous work in northern HG (Pearce, 2005), the wind analysis was conducted using the complete 5-year period from 1995 to 1999.

The wind record available from CSJ has a significant limitation because the meteorological station is situated at an elevation of 93 m above mean sea level where the steep topography of St. James Island may cause wind acceleration. Therefore the average wind speed recorded at CSJ may be an overestimate. Also, this research assumes that the wind conditions at CSJ are representative of the conditions at Woodruff and Gilbert Bay beaches without accounting for site-specific topographic effects such as shadowing. Each of the beaches is backed by steep forested terrain that may block winds from certain directions (NE at Gilbert and NW at Woodruff) (Figure 1.4). Site specific selection of the wind record may have addressed this limitation, but was not conducted for this thesis.

Using the 1995-1999 hourly wind record from CSJ, one annual and twelve monthly average wind roses were produced using Lake Environmental's WRPLOT View[2]. Wind speed was classified into four classes: <6 m s^{-1} (non-transporting winds), 6-12 m s^{-1}, 12-18 m s^{-1}, and >18 m s^{-1}. Wind direction was classified in 36 directional classes according to the cardinal directions (north, east, south, west), where each class contains 10 degrees of the compass rose. These wind speed and direction classes were chosen to facilitate comparison between the wind and drift roses from the Rose Spit (RS) and CSJ stations (Pearce, 2005). The regional wind regime was characterized based on the frequency and magnitude of winds, their directional variability, and the percentage of winds above the threshold for sediment transport (i.e., 6 m s^{-1}). This regime was then compared to that from RS in order to assess the greater regional wind regime of Haida Gwaii (HG).

3.2.2 Sediment drift potential

Using the same wind data as above, Fryberger's (1979) drift potential (DP) model (Equation 10) was used to assess aeolian sand transport potential, as a means to quantify aeolian activity within regional beach-dune systems. Wind data were processed into frequency tables with six wind speed classes and 36 direction classes centred on north (0°), similar to Pearce (2005) for the northern region of HG (i.e., 12-16.99, 17-21.99, 22-26.99, 27-31.99, 32-36.99, and >37 knots). The Fryberger transport equation (10) was applied to each wind speed and direction class. The wind speed class mid-point was used for V, 12 knots was the threshold of transport (V_t), and t was considered the percentage of time that wind blew in that wind speed class.

[2] available from http://www.lakes-environmental.com/lakewrpl.html

Wind speed was analyzed in knots rather than m s^{-1} as DPs can only be applied to Fryberger's (1979) wind-energy classification scheme accurately if the units are in knots (Bullard, 1997).

To determine directional DP values for each of the 36 direction classes, the six DPs in each direction bin were summed. The summed value of all directional DPs produced a total DP for the dataset. Using vector analysis, the RDP and RDD were calculated using the midpoint of each direction class. Based on these vectors sediment drift roses were created manually using Adobe™ Illustrator.

3.3 Water levels

The CHS maintains a network of 13 water level observation stations along the Pacific Coast of Canada. These stations record water levels relative to chart datum (lowest normal tide) every 5 minutes. There is no observation station at CSJ and, due to the behaviour of the tidal wave in this region, water levels from the nearest station (Queen Charlotte City) do not accurately reflect water levels at CSJ. Rather, total water level values at Winter Harbour (NW Vancouver Island) are more representative when adjusted by +45 minutes and +4% in elevation (Ballantyne, 2006). Resulting hourly "pseudotides" (i.e., translated total water level) for CSJ were derived from the longest available record from Winter Harbour (1989-2006) and provided by CHS (Sinnott, 2006). Time series of monthly, seasonal, and annual mean total water level were compiled using these pseudotide calculations.

Total water level values were compared to hourly, predicted tides from CHS to assess the influence of meteorological conditions (e.g., wind, pressure, sea surface temperature) on the water level. Predicted water level values are computed based on

the lunar cycle and can be predicted years into the future. These values do not consider such effects as atmospheric pressure, fetch and wind strength, or sea surface temperature. The difference between the predicted tide and pseudotide (total water level) values indicates the combined effect of these environmental conditions, commonly termed *surge*. Surge commonly increases during low-pressure storm events with strong onshore winds.

Using the intermediate beach runup model presented by Ruggiero et al. (1997, 2001), extreme runup events were identified using beach slope and the deep-water significant wave heights associated with extreme total water level values (Equation 2). By plotting these runup values onto the cross-sectional beach profiles, erosive events were defined as those reaching or exceeding the elevation of the beach-dune junction (Figure 2.1).

3.4 Climate indices

Several readily available climate variability indices were used in this research to characterize regional climate variability. To characterize ENSO, the Multivariate ENSO Index (MEI) was used (Wolter and Timlin, 1998)[3]. The MEI represents the weighted average of several tropical Pacific variables such as sea-surface temperature, surface winds, sea level pressure, sea level temperature, and cloudiness. The NOI, as described by Schwing et al. (2002), represents the regional inter-annual variations in the ENSO regime, specific to the NE Pacific[4]. The PDO index

[3] retrieved 02/04/07 at http://www.cdc.noaa.gov/people/klaus.wolter/MEI/table.html
[4] retrieved 02/04/07 at http://www.pfeg.noaa.gov/products/PFEL/modeled/indices/NOIx/noix

characterizes the inter-annual climate variability in the north Pacific[5]. Finally, the ALPI characterizes the strength of the Aleutian Low in the north Pacific.[6] For details of these indices and their regional impacts, see section 2.4.

3.5 Statistical analysis

3.5.1 Water level trends

Using the adjusted water level record for CSJ (1989-2006), simple linear regression analysis was applied to the annual average water levels (AAWL) and annual maximum water levels (MaxWL). The resulting linear regression models were used to identify statistically significant long-term linear trends. In order to assess the reliability of these models, the trends were tested for statistical significance using the t-test statistic and a 95% confidence interval. Linear regression models were also applied to the Prince Rupert (PR) water level record for the same time interval (1989-2006). The results were compared to longer-term regional water level trends from PR (Abeysirigunawardena and Walker, unpublished data, 2007).

3.5.2 Recurrence curves

To establish a recurrence curve for annual maximum water levels, the data were fit to a non-linear Generalized Extreme Value (GEV) distribution using the Extreme Values Toolkit.[7] Because the water level record for CSJ is only 17 years long, this recurrence curve allows extrapolation of return periods for only 10 years.

[5] retrieved 02/04/07 at http://jisao.washington.edu/pdo/PDO.latest
[6] retrieved 02/04/07 at http://http://www.pac.dfo-mpo.gc.ca/sci/sa-mfpd/climate/clm_indx_alpi.htm
[7] National Center for Atmospheric Research, available at http://www.isse.ucar.edu/extreme values/evtk.html

Extrapolation for longer return periods requires that the dataset have more than 50 observations (Gumbel, 1958).

3.5.3 Climate variability and water level impacts

Simple correlation analysis and linear regression models were applied to various climate variability indices and AAWL and MaxWL from CSJ. These exploratory statistical techniques were used as a scoping tool to identify possible relationships between climate variability in the NE Pacific and regional water levels. Annual and seasonal (winter: September to February; summer: March-August) AWL and MaxWL were compared to annual and seasonal averages for MEI, NOI, and PDO. Averaged mean and maximum water levels for December to March were used in the regression model applied to the annual ALPI values because this index represents the winter (December to March) intensity of the Aleutian Low pressure system. These regression models were run and the statistical significance of the relationship was assessed based on 95% confidence intervals and the student's t-test.

4.0 Geomorphology of Gilbert Bay and Woodruff Bay Beaches

The first objective of this thesis was to describe and classify the geomorphic features and processes of Gilbert and Woodruff Bay beaches in Gwaii Haanas National Park Reserve and Haida Heritage Site (GH-NPR). This chapter describes the environmental setting of Gilbert Bay and Woodruff Bay beaches, including a discussion of their Quaternary history, modern climate, wind, tide and wave regimes, sediment characteristics, vegetation cover, and the role of driftwood in beach-dune morphodynamics. Following this, detailed qualitative and quantitative descriptions and classifications of the geomorphology of these two beach-dune systems are provided. This chapter sets the geomorphic context for Chapters 5 and 6, which address the morphodynamic regime of these beach-dune systems and the regional climate variability signals in the water level record.

4.1 Environmental Setting

4.1.1 Quaternary History

The continental margin of Canada was glaciated several times during the Pleistocene Epoch, with the most recent glaciation (during the Late Wisconsonian) ending ~16,000 to 13,000 years ago (Barrie et al., 2005). The extent of this Late Wisconsonian glaciation on Haida Gwaii (HG) remains uncertain. Clague (1991) estimates that the ice sheet extended to the edge of the continental shelf, while Barrie et al. (2005) estimate that it may have extended part way across Dixon Entrance, Hecate Strait, and Queen Charlotte Sound. The ice sheet reached its maximum

between ~21,000 and 15,000 years ago (Blaise et al., 1990). HG was mostly ice-free by ~13,000 years ago following rapid glacial retreat that began ~15,000 years ago (Barrie and Conway, 1999). These Quaternary glaciations produced a variety of geomorphic features including large river valleys on Moresby Island, extensive glacial till deposits in Hecate Strait, and subaerial and drowned coastal landforms across HG (Harper and Bartier, 2006). On NE Graham Island, large amounts of glacial outwash sediments were deposited during this time. In the modern setting these sediments, such as those stored in the large eroding bluff deposits at Cape Ball, provide a continuous supply of sediment to the littoral systems of East Beach. This contrasts the sedimentary setting of Moresby and Kunghit Islands, in southern HG, where former glacial/river valleys, now submerged, provided coastal sediments that are more limited in their availability.

Following deglaciation of HG, sea level rise and isostatic rebound of the crust resulted in dramatic changes to the coastal landscape (Fedje and Christensen, 1999). In Hecate Strait and along the east coast of Graham Island, for example, sea levels were ~150 m lower than present day sea level ~13,000 to 10,500 years ago (Figure 4.1)(Fedje, 1993; Josenhans et al., 1995, 1997; Fedje and Christensen, 1999). Subsequent sea level transgression in this region was varied due to the effects of the glacial forebulge (i.e., the elevated land in front of an advancing glacier). When a glacier melts, the land that makes up the peripheral forebulge subsides, while the land under the glacier uplifts. Generally, sea level rose to a highstand of ~14 to 16 m above the current level between ~11,000 and 9,000 years ago, in response to the collapse of the glacial forebulge (Fedje, 1993; Josenhans et al., 1995, 1997; Fedje and

Christensen, 1999). The coasts of northern and southern HG host evidence of these higher sea level stands in relict, stabilized dune ridges landward of the modern dune systems. Relative sea level in southern HG has been falling since ~5,000 years ago due to tectonic uplift (Fedje and Christensen, 1999). During the 20th century sea levels have risen in response to thermal expansion of warmer ocean waters, increased melting of floating ocean ice, and changes to ocean salinity (Noerdlinger and Brower, 2007).

Figure 4.1: Generalized sea level curve for Gwaii Haanas [modified from Fedje and Christensen, 1999].

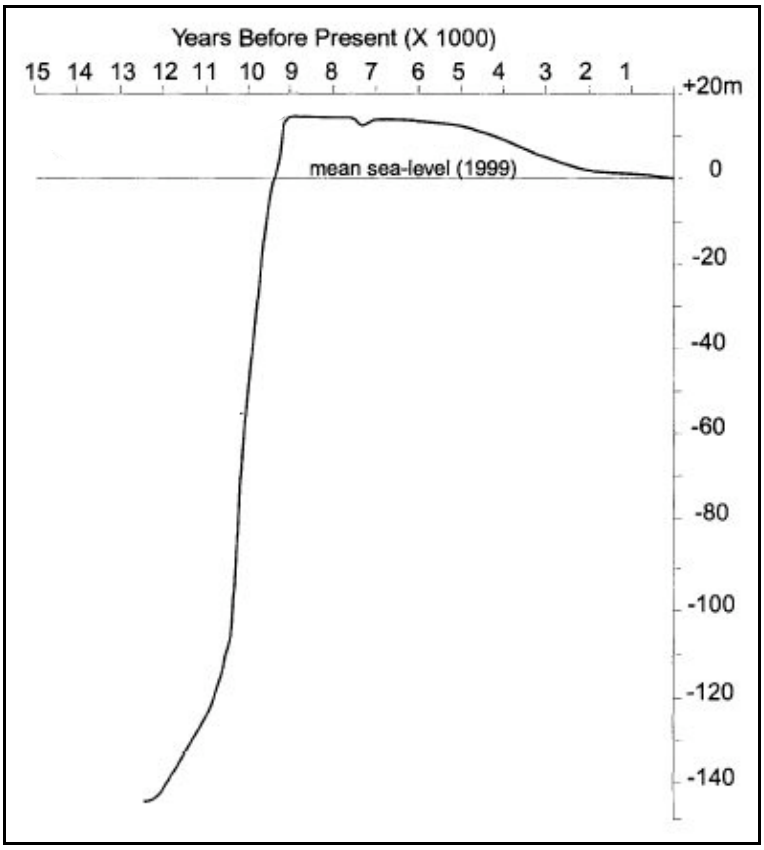

Holocene climate in HG is described in three intervals (Mathewes and Heusser, 1981; Hebda, 1995; Pellatt and Mathewes, 1997): i) the early to mid-Holocene xerothermic period (~9500 to 7000 ^{14}C yr BP): warmer and drier conditions than present, ii) the mid-Holocene mesothermic period (7000 to 3500 ^{14}C yr BP): cooler temperatures and increasing moisture, and iii) the late-Holocene neoglacial period: further cooling and the establishment of modern climate and vegetation conditions. The dry and warm early-Holocene conditions in HG would have increased the sediment availability on sandy beach systems due to decreased moisture content enabling enhanced sediment transport. This increased sediment availability and lack of vegetation resulted in the formation of large Holocene dunes that back the sandy beach systems.

4.1.2 Modern climate

The climate of HG is defined by the Köppen classification as C_{fb} (*marine West Coast cool*), where C is a moist, subtropical, mid-latitude climate, f indicates no period of precipitation deficiency, and b indicates a median range of temperatures where summers are cool and winters mild. Within GH-NPR, the longest climate record from Environment Canada (EC) (1953-2006) is from the Cape St. James (CSJ) meteorological station (EC-ID 1051350). The climate information presented here is based on the Canadian Climate Normals (1971-2000) period for CSJ. The annual average air temperature in this region is 8.9°C, with an average daily maximum of 11.2°C, and an average daily minimum of 6.6°C. Monthly mean air temperatures vary from a low of 4.9°C in January to a high of 14.2°C in August (EC-CMC, 2002) (Figure 4.2). On average, air temperatures fall below freezing only 2.2 days per year

(for 1971-2000). Recorded extreme air temperatures range from 28.3°C (June 6, 1958) to -13.7°C (February 1, 1989).

The region experiences high year-round precipitation with rainfall (> 0.2 mm) occurring 235 days of the year (EC-CMC, 2002). Between 1971-2000, the average total annual precipitation at CSJ was 1610.3 mm, with 48% falling from October through January and only 20% falling during the summer months (May through August). The least monthly mean precipitation occurs in July (62.3 mm), while the greatest occurs in November (206.8 mm). Snowfall occurs in the winter (November through March), but contributes only 3% to the total precipitation of the region.

Figure 4.2: Monthly 30-year climate normals from CSJ (1971-2000) show the seasonal pattern in both precipitation and air temperature. Precipitation values represent monthly average values of rain and snow while temperature values represent average monthly temperatures based on the difference between the monthly high and monthly low. [Data from Environment Canada; retrieved December, 2, 2006 from http://www.climate.weatheroffice.ec.gc.ca/climate_normals/index_e.html].

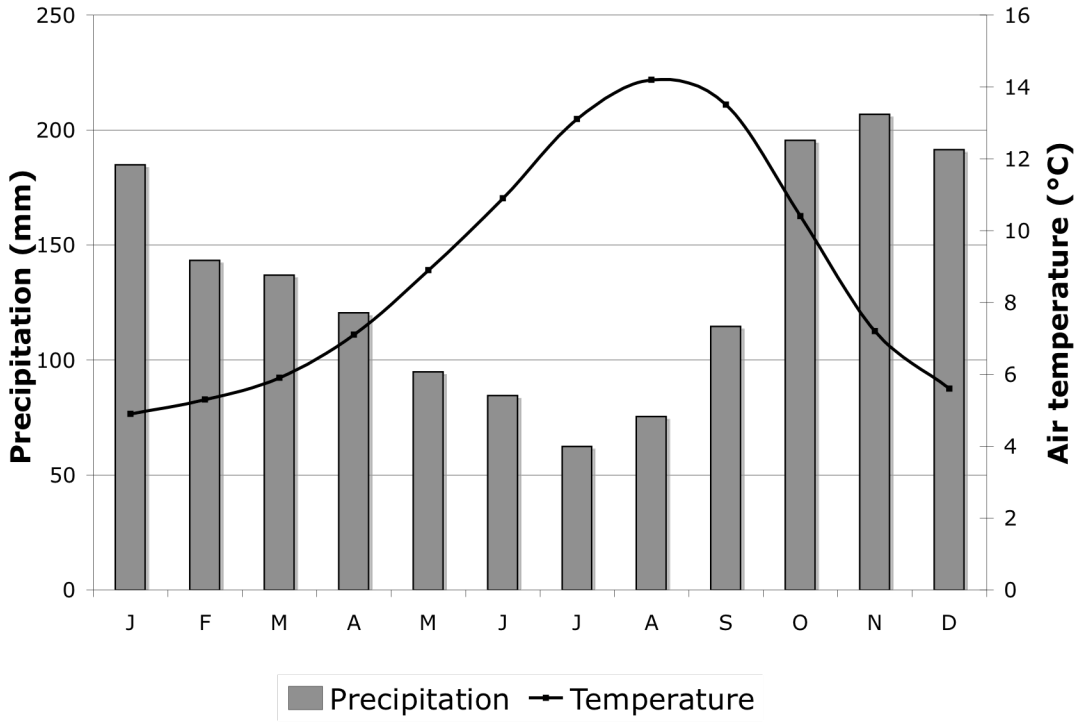

4.1.3 Wind regime

The regional wind regime of HG is determined by pressure gradients and storms associated with the seasonally dominant Aleutian Low and the North Pacific High pressure systems. These two systems affect the climate of HG via seasonal changes in circulation that cause changes in surface winds. In the fall, when the Aleutian Low cyclonic system intensifies, it causes counter clockwise circulation of surface winds that brings strong and frequent SW through SE winds up Queen Charlotte Sound and Hecate Strait in the winter months (October – April). By May, the system diminishes and moves to the NW. As this occurs, the North Pacific High intensifies and moves over HG. Accordingly, the summer months in HG are characterized by higher atmospheric pressure, clearer skies, less frequent rainfall and W through NW winds.

The wind at CSJ averages 8.87 m s^{-1} (31.9 km hr^{-1} or 17.2 knots) annually (1953-2006), most frequently from the WNW due to the exposure of the station to the open Northeast Pacific. Winds in the region are some of the strongest and most persistent in Canada (Walker, 2006). Extreme winds are common at CSJ, as indicated by an annual average of 122 days with winds exceeding 17.5 m s^{-1} (63 km hr^{-1} or 34 knots; gale force according to EC). The maximum hourly wind speed recorded at CSJ was 49.2 m s^{-1} (177 km hr^{-1} or 95.6 knots; hurricane force), recorded on October 31, 1963 (EC-CMC, 2002).

The average annual wind regime at CSJ (Figure 5.1a) is seasonally opposed with the strongest and most frequent winds occurring from two dominant modes, WNW and S. Implications of this wind regime for sand transport and dune maintenance are discussed further in section 5.1.1.

4.1.4 Tides, Currents and Waves

The tidal regime in southern HG is mixed semi-diurnal and has a mean spring tidal range of ~5 m (meso-macrotidal). The mean water level (MWL)[8] is 2.33 m above Chart Datum (aCD), the Higher High Water Large Tide (HHWLT) [9] is 4.52 m aCD, and the Lower Low Water Large Tide (LLWLT)[10] is -0.14 m aCD (CHS, 2006). To provide regional context, Table 4.1 compares these values to PR, RS and Queen Charlotte City.

The swell-dominated wave climate of HG is among the most energetic in Canada due to the extensive open fetch of the North Pacific Ocean and the frequent storms generated by the Aleutian Low pressure system (Harper, 2006). The CSJ region experiences an average annual offshore significant wave height (H_s) of 2.63 m (from EC #46147, South Moresby Buoy, 51˚50'N, 131˚14'W, 1993-2006, see Figure 1.2). Between 1993 and 2006, the maximum observed H_s was 12.5 m on February 10, 1998. James (1969) reports that in October 1968 an oil-drilling rig anchored near CSJ was hit by a 29 m wave that was propagated against a strong local ebb current. This anecdotal account illustrates the extreme wave conditions that characterize CSJ.

[8] MWL is the average of all hourly measured water levels over the available period of record (1989-2006)
[9] HHWLT is defined as the average of the highest high waters, one from each of the 19 years of predicted water levels (CHS).
[10] LLWLT is the average of the lowest low water, one from each of the 19 years of predicted water levels (CHS).

Table 4.1: Tidal characteristics for regional tidal gauge stations on the coast of BC.

Station	MWL (m aCD)	HHWLT (m aCD)	LLWLT (m aCD)
Prince Rupert	3.8	7.5	-0.1
Rose Spit	3.3	6.4	-0.1
Queen Charlotte City	4.0	7.8	0.1
Cape St. James	2.3	4.5	-0.14

4.1.5 Sedimentary setting

Non-rocky systems comprise ~31% of the HG shoreline, with ~26% of these comprised of sand and or sand/gravel (Harper, et al., 1994). Although most of these sedimentary systems in HG are on the north and east coast of Graham Island, there are several large beach-dune systems on Moresby and Kunghit Islands within GH-NPR. The sedimentary systems in southern HG consist of re-worked glacial and river valley sediments that were deposited as glacial till or outwash following the last glaciation. In the modern setting, these sediments are reworked by aeolian, tidal, and wave action within mostly embayed settings. The sediment supply for the dune systems at Gilbert and Woodruff Bay beaches is from the nearshore where glacio-fluvial and Holocene aeolian sands are deposited and reworked. The sediment is transported into the nearshore via fluvial erosion of the relict dunes that back the modern beach-dune systems (Figure 4.3).

At Gilbert and Woodruff Bay beaches, sediments are well-sorted, medium-grained sand (Gilbert: mean grain size = 0.360 mm, SD = 0.00125 mm, skewness = -0.21; Woodruff: mean grain size = 0.490 mm, SD = 0.0012 mm, and skewness = -

0.06). Analysis of alongshore variations in grain size statistics (e.g., mean grain size, skewness, and sorting per McLaren and Bowles, 1985) yields no statistically significant net sediment pathways (e.g., courser, better sorted, more positively skewed or finer, better sorted, more negatively skewed). Oscillatory flow in these embayed systems causes large-scale mixing of sediment in the nearshore, which appears to overshadow any longshore transport patterns.

Figure 4.3: Fluvial erosion of relict dunes backing Gilbert Bay beach. River is flowing away from the foreground and enters the east side of Gilbert Bay at a large sandy estuary (See aerial photograph in Fig. 4.6 and site photo in Fig. 4.8).

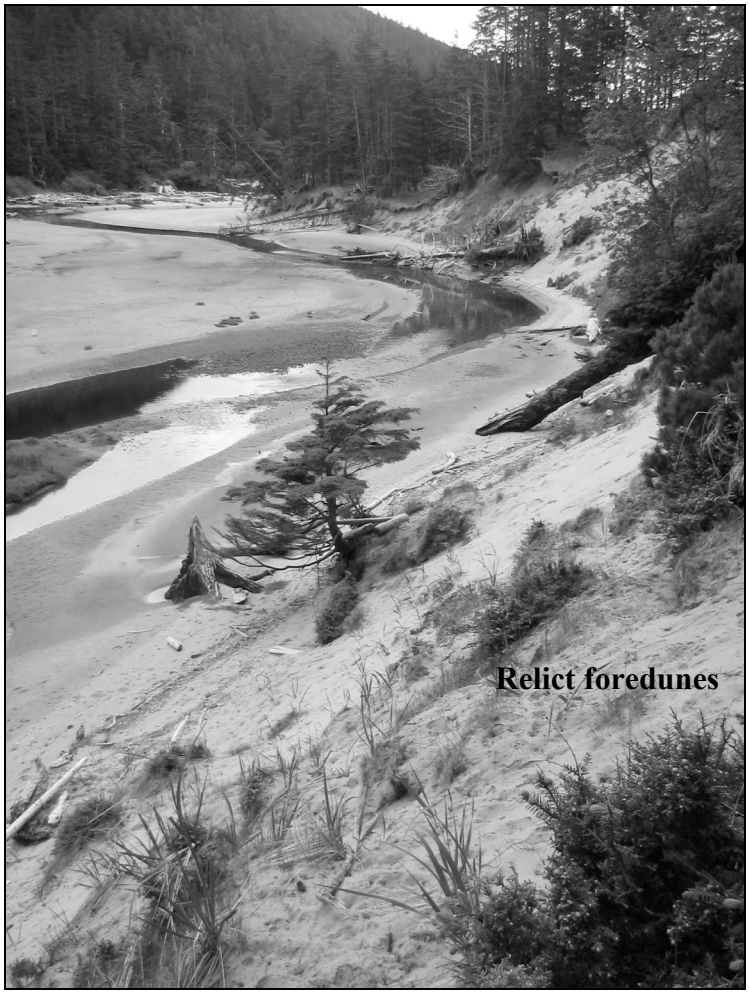

4.1.6 Vegetation

The beach-dune systems of southern HG are dominated by several perennial plant species that thrive in salty, windy, and sandy conditions. Vegetation on the backshore of beaches in this region includes (Wiedemann et al., 1999): American dune grass (*Leymus*[11] *mollis*) (Figures 4.4 and 4.5), species of rush (genus *Juncus*), and large-head sedge (*Carex macrocephala*). Sitka spruce (Figures 4.4 and 4.5) is the dominant tree species on the coast of this region, while other species present include Western hemlock (*Tsuga heterophylla*), Red cedar (*Thuja plicata*) and Red alder (*Alnus rubra*) (Pojar and MacKinnon, 1994).

[11] Formerly *Elymus*

Figure 4.4: Shore normal view of the vegetated backshore at Gilbert Bay beach. Dune grass and Sitka spruce seedlings present on dune ridges.

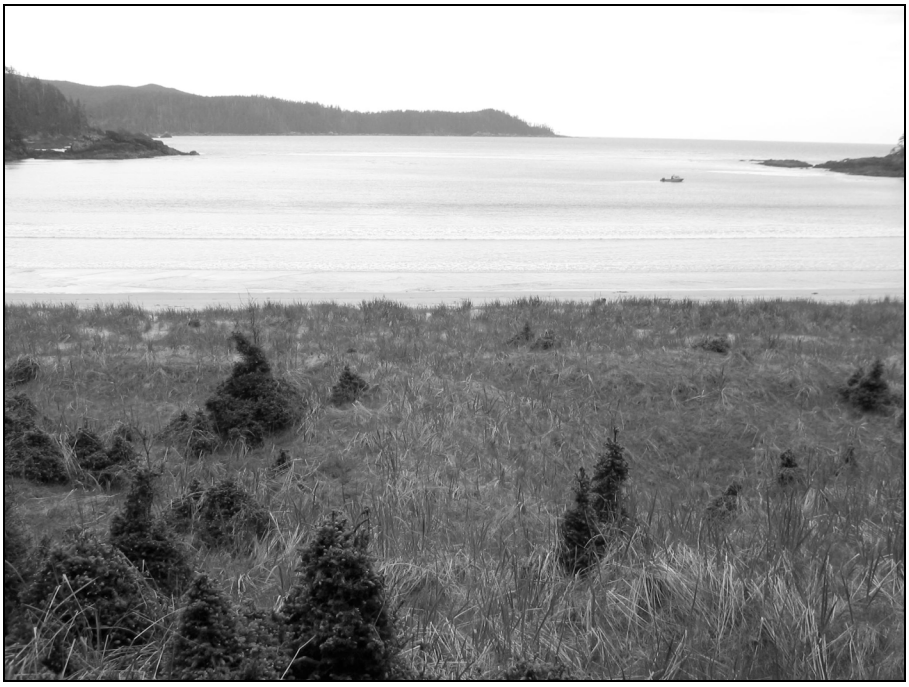

Figure 4.5: Driftwood jam, active foredune, and established foredune at Woodruff Bay beach; dune grass and Sitka spruce colonization of the dunes is apparent.

4.1.7 Driftwood

Driftwood is pervasive along the coast of HG and may play an important role in the geomorphology of Gilbert and Woodruff Bay beaches (Figures 4.4 and 4.5). Driftwood logs accumulate in the backshore forming driftwood jams that range from a few scattered logs to dense jams more than 200 m wide and several metres deep. Driftwood influences sandy beach-dune systems in three ways (Walker and Barrie, 2006). First, the roughness caused by the driftwood jam interrupts airflow causes localized turbulence and sediment accretion causing the driftwood jam to act as an 'accretion anchor' in the backshore (Walker and Barrie, 2006). In doing so, the second important function of driftwood jam, provided the system is not eroded, is to provide a nucleus for incipient dune formation. Aeolian sediments may accumulate within the driftwood jam and form shadow dunes around logs (Walker and Barrie, 2006). As aeolian transport continues and, in the absence of wave attack, the driftwood jam may continue to infill and may develop into an incipient foredune (Walker and Barrie, 2006). The third geomorphic function of driftwood is to dam wetland and stream discharge. For example on East Beach, NE Graham Island, this results in the formation of backshore swales and lakes fronting established foredunes. When the driftwood jams are breached by wave attack, these lakes drain rapidly and are infilled by aeolian sediments (Walker and Barrie, 2006). On Gilbert and Woodruff Bay beaches the driftwood jams do not create dammed lakes, but they do seasonally influence the position of the fluvial systems (e.g., Gilbert Bay beach, Figure 4.8).

Sediment-laden driftwood jams act as buffers to dune erosion during wave attack. Instead of enabling erosion to the base of the established foredune, the driftwood jams release stored sediment and logs during erosive high water levels and

wave events. If completely inundated during a high water event, however, rafted driftwood logs may act as 'battering rams' that enhance erosion by thrusting up against the foredunes during wave attack (Pearce, 2005). Thus, rates of foredune erosion will increase if a high water storm event occurs following a previous high water level event that has removed the driftwood. Detailed understanding of the role of driftwood on the erosional and rebuilding regime of sandy beach-dune systems is lacking. Additionally, the role of historical logging on the amount of driftwood accumulating on coastal beaches has not been investigated. It is highly likely, however, that the amount of driftwood on the beaches of HG has increased with increased logging in the past century (Pearce, 2005).

Figure 4.6: Gilbert Bay beach DWJ acting as an accretion anchor for aeolian sands and initiating formation of an incipient dune ridge seaward of the active foredune (note: person for scale).

4.2 Geomorphology of Gilbert and Woodruff Bay Beaches

The shoreline of GH-NPR is host to numerous types of coastal systems, including low gradient sandy beach-dune systems, coarse gravel beaches, and cobble-dominated reflective beaches. Despite the important biophysical habitat that beach systems provide, the coastal geomorphology of this area is not well documented. Initial baseline assessments of several distinct and important coastal sites have been conducted and are presented in an unpublished Parks Canada report (Walker, 2007). The following sections document and describe the geomorphic features of Gilbert and Woodruff Bay beaches. These two systems share the following key characteristics common to sandy, high-energy, embayed systems (Cooper et al., 2004):

i) There is very little to no contemporary sediment supply, only reworking of relict dune sediments and nearshore bars.

ii) The systems are constrained by rocky outcrop headlands.

iii) Refracted swell waves influence the shape of the beach systems.

iv) Littoral sediment is moved onshore via aeolian action from frequent transporting winds that maintain active foredune systems.

v) The active dunes front large, vegetated, Holocene dune ridges.

Despite these similarities, two key controlling conditions, embayment aspect and size, differ at these two sites and, hence, their response to the regional morphodynamic regime (i.e., interactions between the regional wind, waves, and water levels) differs significantly. The smaller, SW facing Gilbert Bay beach (see section 4.2.1) is characterized by distinct prograding foredune ridges, while Woodruff Bay beach (see section 4.2.2) is characterized by a larger, eroded foredune complex with recent backshore DWJ infilling. The following sections describe the geomorphic features and classifications of these two systems.

4.2.1 Gilbert Bay Beach

Gilbert Bay beach is a small, embayed, sandy beach-dune system on the southwest coast of Kunghit Island (Figure 4.7). The beach is located on the north side of Gilbert Bay and, with an average orientation of ~195° to true north, is exposed to the open Pacific Ocean. The beach is ~450 m long and ~150 m wide at low tide and is bounded on both ends by large rocky basalt outcrops of the Karmutsen Formation (formed ~228-200 millions years ago) (Haggart, 2004).

The embayment at Gilbert Bay is characterized by two headlands that are ~325 m apart (C_1), while the entire embayment is ~1300 m long (S_1) (see Figure 4.7). Incident waves refract around these headlands and the wave energy dissipates across the entire embayment. The embayment scaling parameter (δ‘) for Gilbert Bay is ~42, which classifies the system as having a normal circulation pattern (per Short and Masselink, 1999).

The cross-sectional topographic profile in Figure 4.9 shows the large, relict dune ridges that back the modern beach-dune system. These forested, lobate dune ridges reach heights of ~25 m aCD, occupy a width of ~700-800 m, and extend ~500 m inland. The sinuous morphology of these relict dunes is indicative of either a highly energetic prehistoric wind regime that was capable of forming parabolic and/or blowout dunes, lesser dune vegetation cover, or a higher sediment supply to the system. These stable secondary dunes have been stranded due to coastal progradation during the regression of the sea level high stand and since stabilized by vegetation (e.g., Sitka spruce trees ~200-300 years old). Optical dating of these relict features is required to determine a specific date of formation/stabilization. These techniques are

beyond the scope of this thesis, but are recommended for future research in this region.

Figure 4.7: Aerial photograph of Gilbert Bay beach (#BCC04002, 2004, with permission). S_1 is measured along the approximate position of mean water level.

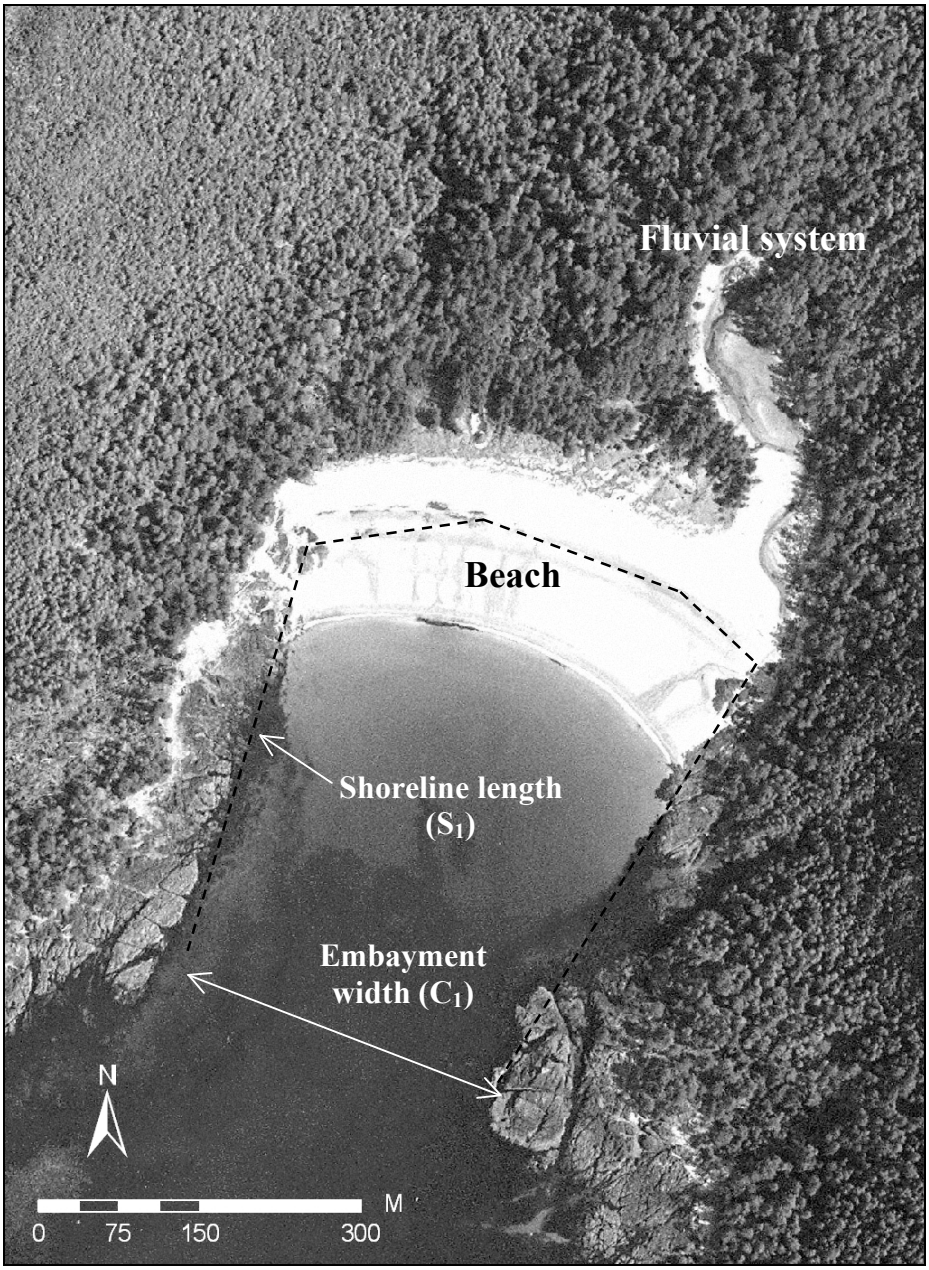

Behind the active beach-dune system, the river system has migrated into the relict dune complex. Fluvial processes are actively eroding the relict dunes and transporting the sediment back to the modern beach-dune system (Figure 4.3). This delivery of sediment to the beach plays an important role in the modern sediment dynamics of this system.

The stabilized dune complex is fronted by well-developed, actively accreting, and prograding foredune ridge that is fully colonized by dune grass and colonizing Sitka spruce saplings (Figures 4.4 and 4.8). Unlike neighbouring Woodruff Bay beach, these active dune ridges show no evidence of erosional dune scarps. Approximately 2-3 active dune ridges are visible on the cross-sectional profile of the beach (Figure 4.9). The seaward-most aeolian feature is an unvegetated, actively accreting, incipient dune with a driftwood core. The Psuty (2004) classification scheme (Figure 2.6) suggests that these active seaward most, or "primary" dunes would have a positive sediment budget due to active sediment exchange with the beach. From the forest to the beach the elevation of the dune ridge crests decreases gradually by ~5 m in elevation over a ~30 m distance (see Figure 4.8). This morphology and absence of erosive features (e.g., dune scarps) suggests that the modern beach-dune system is experiencing either enhanced onshore sediment supply or relative sea-level regression due to tectonic forces. This speculation on tectonic uplift in southern GH-NPR is difficult to verify due to the lack of vertical control markers in the region (Bartier and Sloan, 2007).

Moving seaward, the active dune is fronted by a large driftwood jam (~5-10 m wide) that provides a roughness matrix for sediment accretion (Figures 4.6 and 4.8).

At the NE end of the beach, where the river outflow truncates the dune system (Figure 4.11), the driftwood jam is expansive (~50 m wide) and extends up river to a large dense driftwood log jam behind the relict dunes. This up-river jam was likely deposited during an extreme high water event and is decades old, evidenced by the growth of tree saplings on the drift logs. To the east of the river outflow large, exposed, basalt outcrops, with caves and supra-tidal sea stacks dominate the beach. These features are indicative of high wave energy conditions at a higher former sea level stand.

The offshore bathymetric profile for Gilbert Bay (Figure 4.10) shows distinct bars, ~3 m tall and positioned ~200 m offshore from the LLWLT, that may store sediment in the embayment. It is not clear, however, if these features are composed of sand, gravel, or cobbles. If sandy, the bars may deliver sediment onshore during high-energy winter storm events (Houser and Greenwood, 2005, Walker and Barrie, 2006). Further repeat (interannual to seasonal) bathymetric profiles are required to explore seasonal changes in these bar features and the possibility of beach rotation (see section 2.2.5) in response to winter storm events. Additionally, swath bathymetry data and/or sediment grab sampling would assist in determining the sedimentary composition of the bars and allow more accurate assessment of the morphodynamic role that they serve.

Sediment Budget

Though speculative, the beach-dune sediment budget at Gilbert Bay appears to be supplied primarily by fluvial erosion of sediments stored in the relict dunes that back the modern beach-dune system that feed the local littoral cell at the SE end of

the beach. Subsequent tidal currents, wave swash, and aeolian action then transport the sands onshore to the beach and into active established foredune ridges, which act as sediment sinks. During high-energy storm events some sediment may be seasonally eroded from backshore incipient dune and established foredune systems, although there was no evidence of dune erosion on Gilbert Bay.

The foredune ridges at Gilbert Bay beach exhibit a positive sediment budget, exemplified by active accretion and incipient dune formation (Psuty, 2004). The beach may be in a state of mass balance, with the amount of sediment being transported into the system by fluvial action equaling the amount transported into the dunes by aeolian action. Continued monitoring of the beach-dune profile into the future will provide evidence for the mass balance state of this system over time.

Figure 4.8: Prograding dune ridges and actively accreting driftwood jam at Gilbert Bay beach.

Figure 4.9: Cross-sectional profile of Gilbert Bay beach including the beach, modern prograding foredunes, and large relict foredune ridges. (Vertical exaggeration = 5.6X).

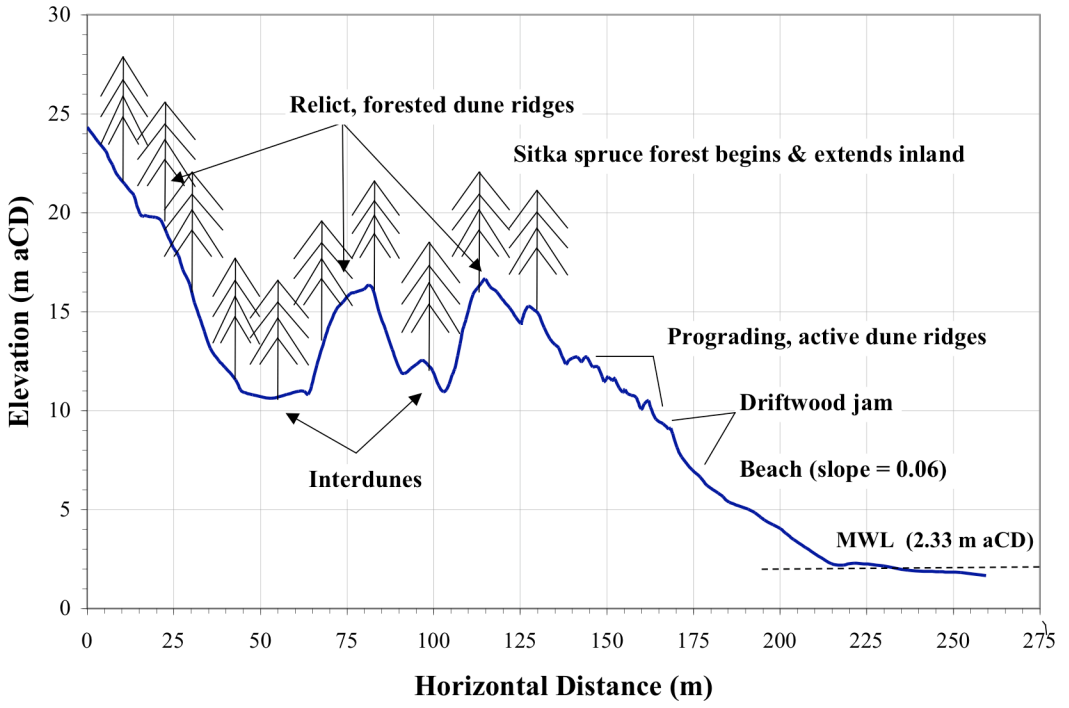

Figure 4.10: Cross-sectional topographic and bathymetric profile of Gilbert Bay. (Vertical exaggeration = 16.7X).

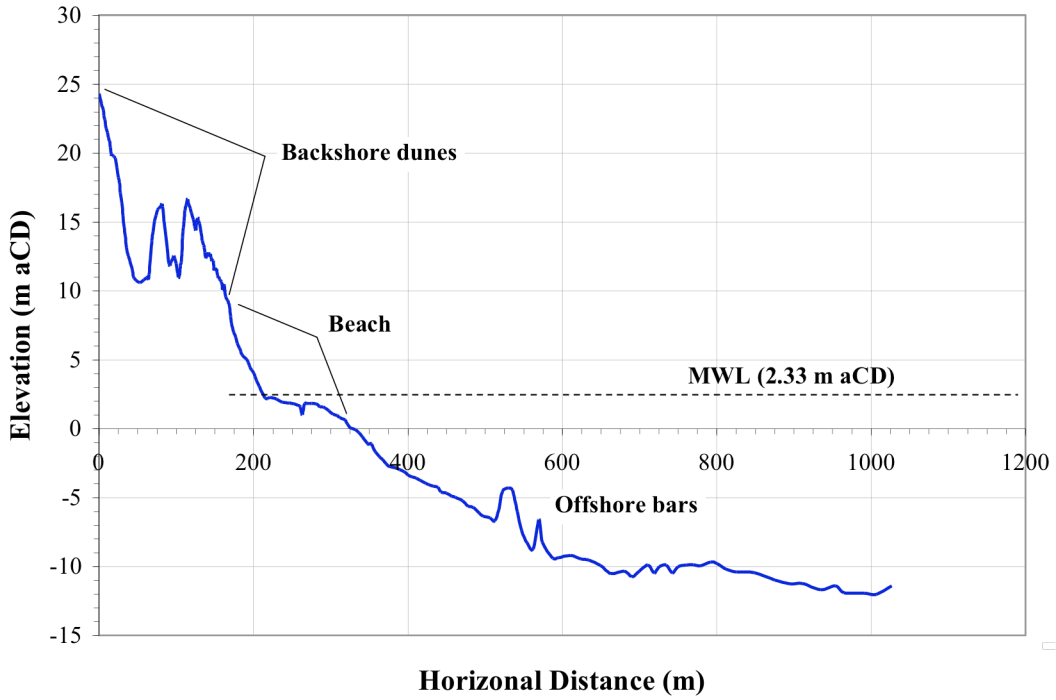

Figure 4.11: River outflow at north end of Gilbert Bay beach truncates the foredune system and erodes the dense driftwood jam and stored beach sediments.

4.2.1.1 Classification

The prograding beach-dune system at Gilbert Bay could be categorized as Stage 1 of Hesp's (2002) evolutionary foredune morphology model (Figure 2.5). Under the current morphodynamic regime (winds and water levels), the active foredune ridges are accreting and the system is prograding seaward. Under higher, erosive water levels, however, the system could easily progress to a more erosive stage (3b-4b) following a wave erosion event (see D in Figure 2.5).

Using the Short and Masselink (1999) breaker wave height calculation based on the average annual offshore significant wave height (H_b=1.24 m), Gilbert Bay beach is classified as a reflective, low tide terraced beach with rip currents. The topographic beach profile (Figure 4.9), however, shows a more intermediate morphology with a steep upper beach face and subdued bars in the nearshore. It is possible then that the Masselink and Short (1993) conceptual model does not accurately classify this system due to the inherent complexities of classifying dynamic coastal systems. Alternatively, this misclassification occurred because the model is highly sensitive to breaker wave height because it is used in calculating both the relative tide range and the dimensionless fall velocity (See Equations 4 and 5). As a high-energy, macrotidal beach-dune system, Gilbert Bay beach may be dominated by extreme wave and water level events. Considering this, it follows that the beach would be better classified using an average of the extreme winter significant wave heights. Using average winter (September through February) significant wave height (3.9 m), the Masselink and Short (1993) model more accurately classifies this beach as barred intermediate (RTR = 2.4, Ω = 1.5). Masselink (pers. comm., 2007)

acknowledges the sensitivity of this model to H_b and reiterates that it is conceptual and is intended to illustrate that there are different types of beach-dune morphodynamic states that occur under variable wave and tidal conditions.

4.2.2 Woodruff Bay Beach

Woodruff Bay beach is a larger, embayed, medium-coarse sandy beach located on the southeast coast of Kunghit Island (Figure 4.12). This beach has an average orientation of ~140° towards Queen Charlotte Sound, is ~900 m long and ~100 m wide at low tide. Like Gilbert Bay beach, Woodruff Bay beach is bounded on both ends by large rocky basalt outcrops of the Karmutsen Formation (Haggart, 2004).

The embayment at Woodruff Bay is much larger and wider than the embayment at Gilbert Bay (~2 km apart (C_1), with entire embayment (S_1) is ~4 km long) (see Figure 4.12). The embayment scaling parameter (δ') for Woodruff Bay is ~70, indicating that normal circulation patterns prevail in this system and that strong rips probably do not occur in the nearshore (per Short and Masselink, 1999).

The large, meso-macrotidal beach is backed by a dense Sitka Spruce forest (trees avg. ~5-7 m in circumference) that has colonized several large relict foredune ridges (~13 to 18.5 m aCD) (Figure 4.13). The sinuous and lobate form of these stabilized dunes suggests prehistoric blowout formation as a result of increased aeolian activity, enhanced sediment supply, or a decrease in vegetation cover. Like Gilbert Bay, the dune ridges have migrated into a river ~500 m inland where modern river migration actively erodes the northern end of the dune field. The morphology of

this dune field suggests that, prehistorically, the large dunes at Woodruff Bay were possibly prograding seaward.

The stabilized dune field at Woodruff Bay is fronted by an established primary foredune (Psuty, 2004) with a large erosional scarp (Figures 4.15 and 4.16). Driftwood and sand have infilled areas of the scarp to form a small incipient dune with a driftwood core that fronts the large eroded established dune. A subsequent erosive event has removed most of this incipient dune, as evidenced by the small (~0.25 m), grassy sediment bench that separates two major scarps on the established foredune (Figure 4.16). This second scarp has been infilled with sand and driftwood, thereby creating a matrix for incipient dune formation.

Figure 4.12: Aerial photograph of Woodruff Bay beach (#BCC04002, 2004). S_1 is measured along the approximate position of mean water level.

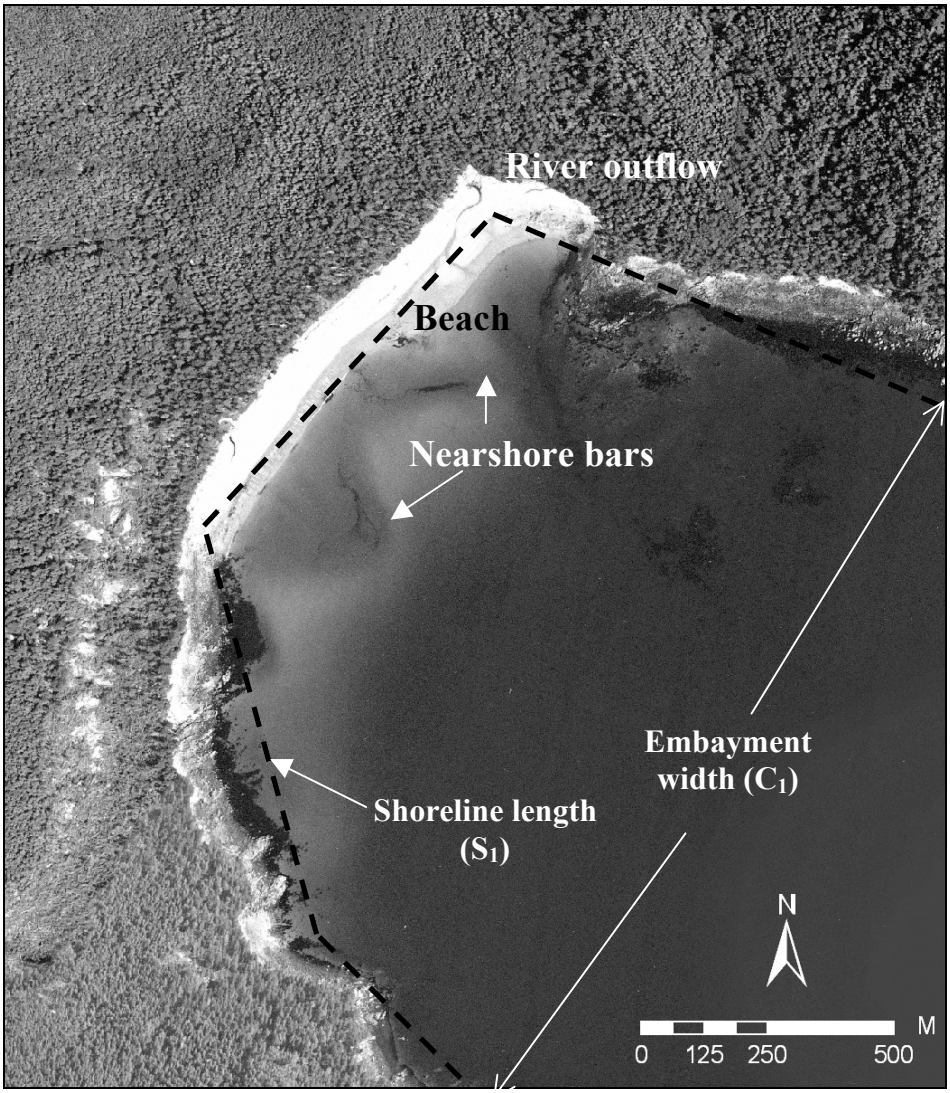

Figure 4.13: Cross-sectional profile of Woodruff Bay beach including the backshore, modern eroded foredunes, and large relict foredune ridges (June, 2006). (Vertical exaggeration = 6X).

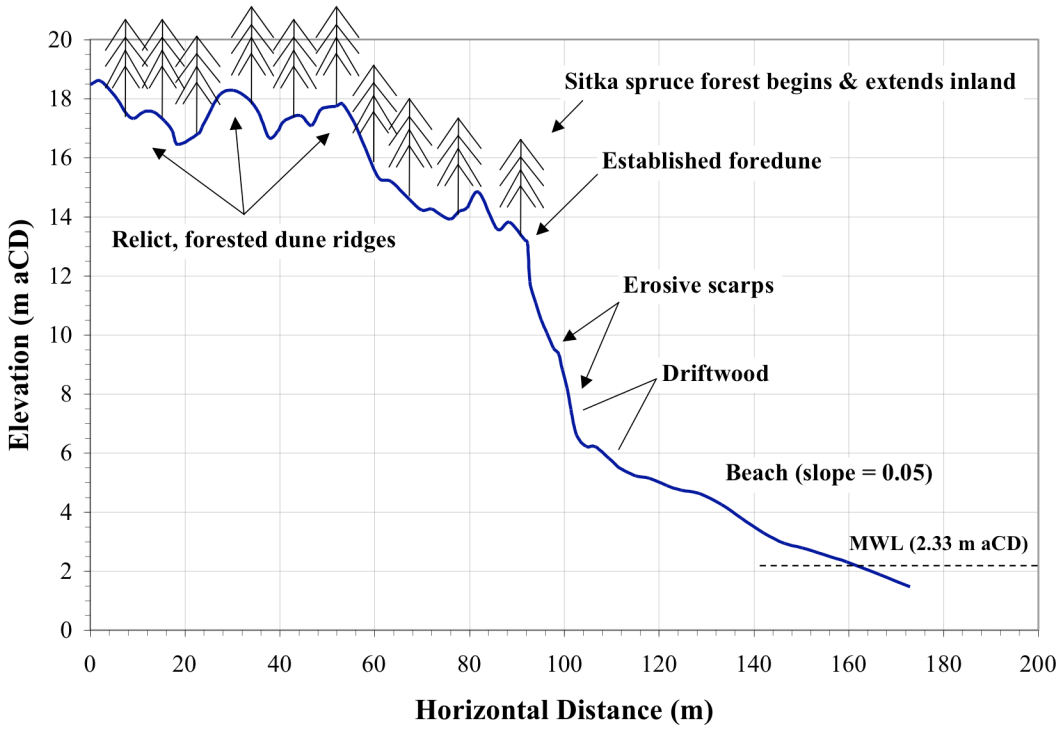

Figure 4.14: Cross-sectional topographic and bathymetric profile of Woodruff Bay (June, 2006). (Vertical exaggeration = 30X).

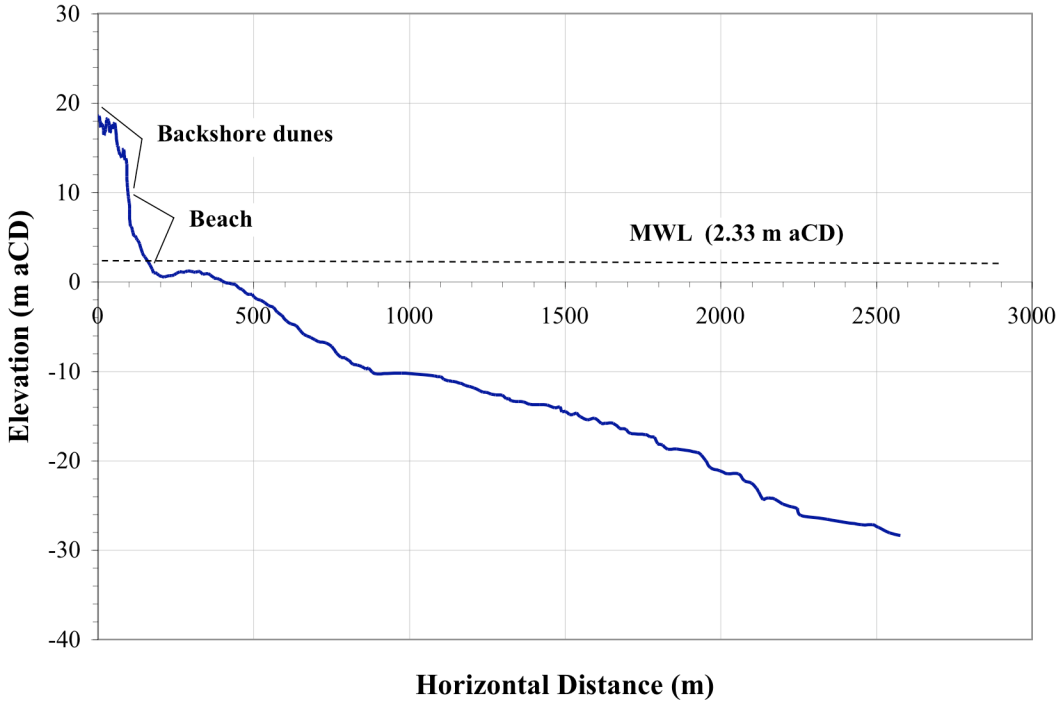

Figure 4.15: Photo along the Woodruff Bay beach profile illustrating the large eroded foredune and the modern infilling and driftwood jam that has also subsequently been eroded.

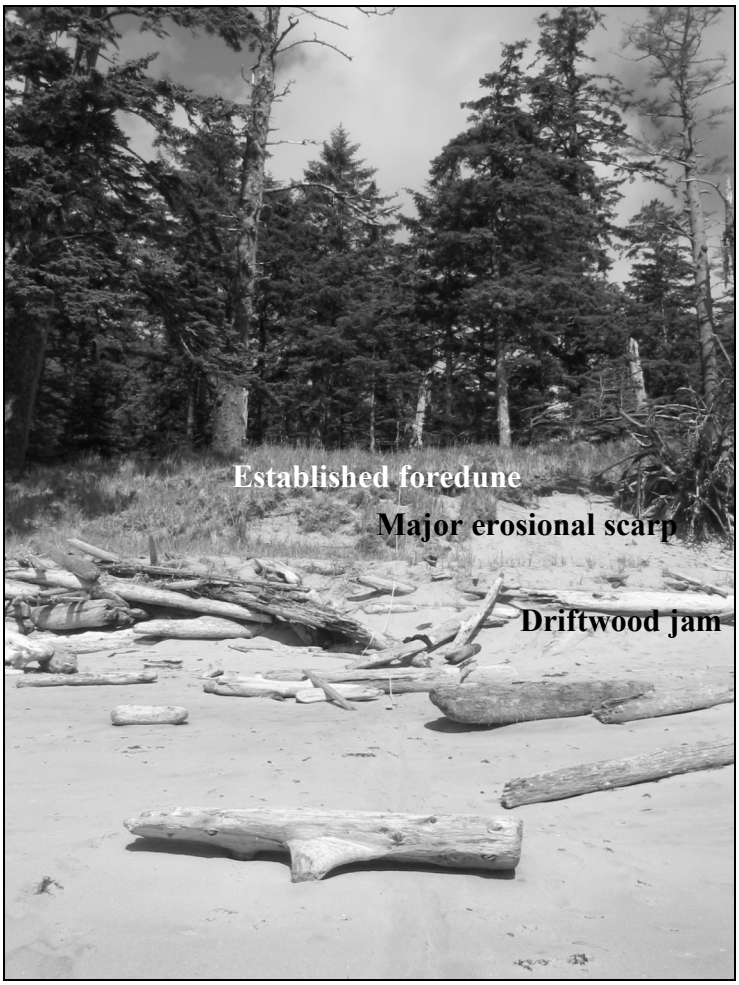

Figure 4.16: Grassy sediment bench between two erosional scarps on the established foredune at Woodruff Bay beach, with driftwood fronting the active foredune.

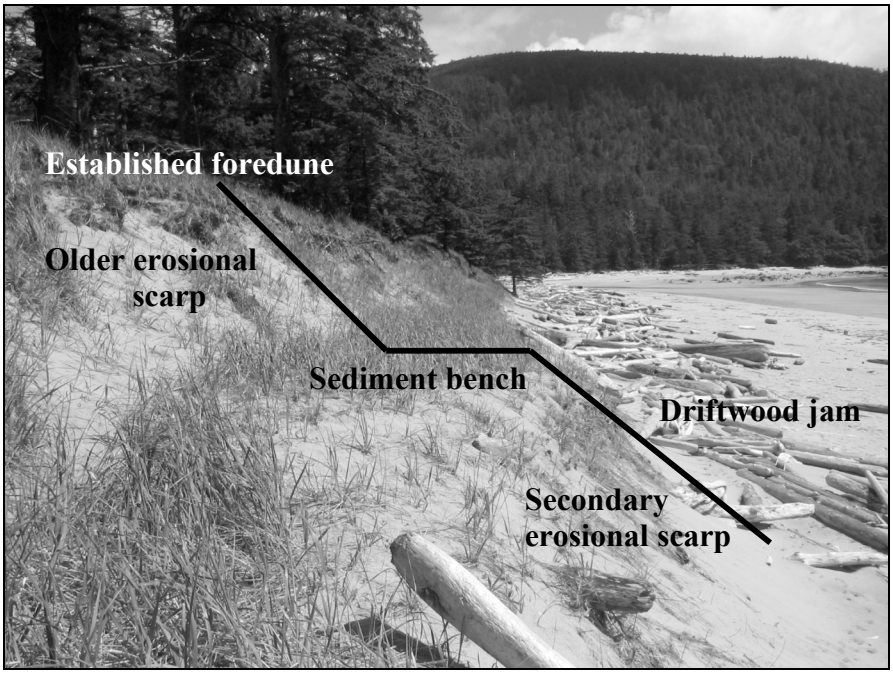

The NE end of the beach hosts a dynamic fluvial outflow that frequently alters its course. Between June 2005 and June 2006, the river outflow migrated from its relatively straight, shore-normal position to a more sinuous alongshore outflow towards the SW (Figure 4.17). A smaller, ephemeral fluvial system also flows out at the south end of the beach. The river at the north end is actively eroding the relict dunes and transporting this sediment back into the active beach-dune system, similar to what is happening at Gilbert Bay beach. This river system enters the beach through a very large, dense log jam that surrounds several large boulders (Figure 4.18).

The nearshore bathymetry shown in Figure 4.14 does not show any distinct bars in the nearshore, although the aerial photograph (Figure 4.12) indicates that there are large, crescentic sand bars in the nearshore. These bars may change size and position seasonally in response to changes in the local circulation patterns from winter storm conditions, but more detailed bathymetric data is required to more accurately assess the morphodynamics of these bars.

Sediment Budget

Much like the sediment budget at Gilbert Bay, the relict dunes that back the modern beach-dune system likely act as the primary sediment source in this system. Aeolian sands are eroded from the relict dunes during river migration and are transported into the littoral zone of the modern beach system. Some sediment appears to be stored in the large crescentic nearshore bars, which act as temporary sediment sources and sinks. Further research is required to understand the morphodynamics of these rhythmic bars. Tidal currents, wave swash, and aeolian action then reworks the sandy sediment in the nearshore and transports it onshore to the beach and into the

scarp on the established foredune. The accretion zone around the modern driftwood jam fronting the established foredune also acts as a sediment sink. Some sediment may also be lost offshore.

Figure 4.17: Woodruff Bay beach river outflow June, 2006 illustrates the dense driftwood accumulation and fluvial down-cutting of the beach (person for scale).

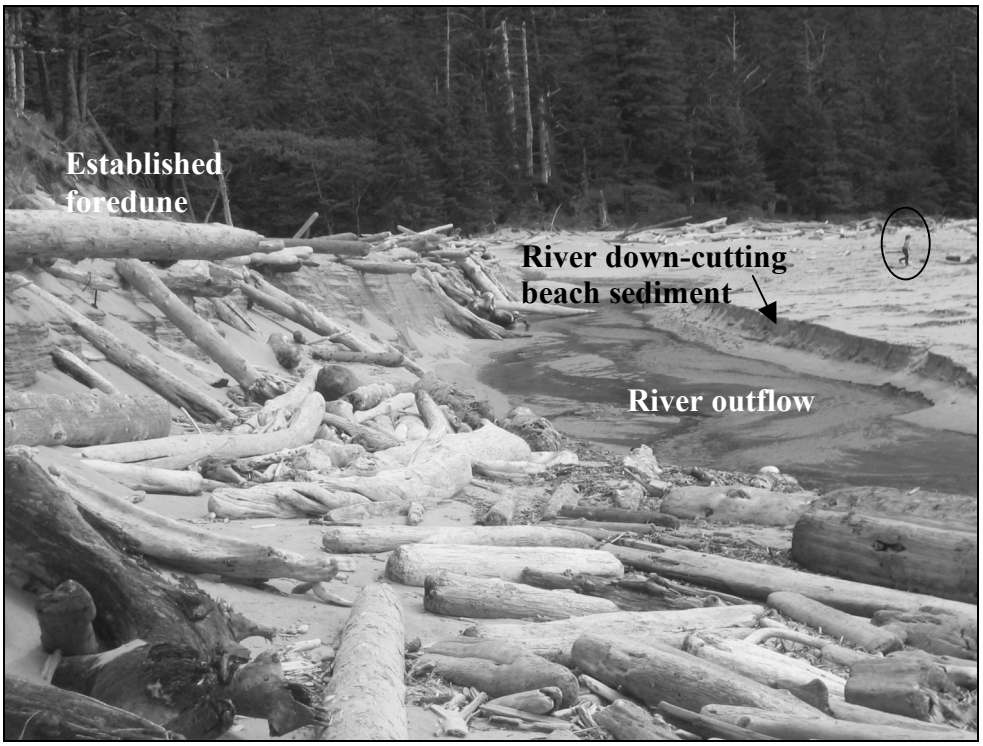

Figure 4.18: Log jam at river outflow on north end of Woodruff Bay beach.

4.2.2.1 Classification

The foredune system at Woodruff Bay is characterized by two historic erovsive events that have been recently infilled. According to Hesp's (2002) model (Figure 2.5), this system appears to be in Stage 3b given the historic scarps as well as more recent accretion in the driftwood jam at the base of the foredune. Portions of the dune system toward the south-west end of the beach, however, appear to be in Stage 4, with no infilling following the major erosive event. Under future erosive water levels, the long-term morphology of this system may exhibit continued erosion and landward migration for the foredune (see Chapter 5).

Using an average significant wave height and the Short and Masselink (1999) breaker wave height calculation (H_b=1.8 m), Woodruff Bay beach is classified as reflective. Based on the topographic beach profile (Figure 4.9), the beach appears to have a reflective to intermediate morphology. Using average winter (September through February) significant wave height (3.9 m), the Masselink and Short (1993) model classifies this beach as reflective to intermediate (RTR = 1.7, Ω = 1.2). This illustrates that high-energy beaches are classified more accurately by using the average winter (stormy) significant wave height rather than the annual average.

Figure 4.19: Southern section of the eroded dune system at Woodruff Bay representing Hesp's (2002) Stage D of foredune evolution.

4.3 Summary

This chapter provides baseline documentation of the geomorphology and classification of two significant sandy beach-dune systems in GH-NPR. The information presented shows that these two intermediate, high-energy systems are responding differently to the morphodynamic regime of the CSJ region, despite their numerous geomorphic similarities. There is clear on-site evidence that Gilbert Bay beach is actively prograding, while Woodruff Bay beach has experienced major historical erosive events. Controlling factors such as embayment size, aspect to incident wind and wave conditions, and sediment supply influence the distinct geomorphic responses of these systems. To assess the processes that drive these systems, Chapter 5 details the morphodynamic regime of the CSJ region including an assessment of the wind regime, sediment drift potential, and erosive water levels.

5.0 Morphodynamic Regime of Cape St. James Region

This chapter describes the morphodynamic regime of the Cape St. James (CSJ) region of Haida Gwaii (HG) and provides comparison to that of the Rose Spit (RS) region. First, the aeolian activity within the beach-dune systems of Woodruff and Gilbert Bays is examined by characterizing the annual and monthly wind regime using regional meteorological data from CSJ and applying a common sediment drift potential model (Fryberger, 1979). Second, the regional erosive water level regime is examined using the regional water level record from Winter Harbour, translated to CSJ, and calculations of wave runup. Combined, these objectives characterize the erosive and potential dune maintenance/rebuilding regimes of these beach-dune systems.

These results are compared to those from previous work on the aeolian regime on NE Graham Island, HG along East Beach toward RS (Pearce, 2005) and on the regional water level trends at Prince Rupert (PR) (Abeysirigunawardena and Walker, unpublished data, 2007). This comparison provides a broader understanding of the regional morphodynamic regime of HG. Finally, the impacts of projected erosive water level scenarios for 2020, 2050, and 2080 are discussed for Gilbert and Woodruff Bay beaches based on long-term regional mean and maximum water level trends and calculated runup values.

5.1 Aeolian transport regime

This section characterizes the aeolian sediment transport regime of southern HG (CSJ region) and compares it to that of the north (RS region, Pearce 2005). From

this, discussion is provided on how these local regimes influence beach-dune geomorphology at Gilbert and Woodruff Bay beaches in the south, and East Beach in the north. These results describe the capacity of the morphodynamic regimes at CSJ and RS to transport and deposit sediment in the backshore, thereby maintaining or rebuilding the local beach-dune systems following an erosive event. Section 5.3 compliments these results by characterizing the erosive capacity of total water levels on these beach-dune systems.

5.1.1 Wind regime

Cape St. James

CSJ experiences a year-round, high-energy wind regime. For the complete available record (1953-2006), the annual average wind speed recorded at CSJ is 8.9 m s^{-1}. This annual average wind speed may be an overestimate of wind conditions in this region because of its location 93 m above sea level. Combined with the steep terrain of St. James Island, this elevation may cause flow acceleration. Figure 5.1a shows the annual wind rose for CSJ for 1995-1999. This time period is the same interval used by Pearce (2005), and was selected for ease of comparison with the wind regime at RS. The interval is assumed to be broadly representative of the long-term wind regime based on qualitative comparisons with the entire available record (1953-2006).

The average annual wind speed for the 1995-1999 time interval is 8.5 m s^{-1}. The annual wind rose from CSJ indicates a strong, bimodal wind regime with a primary mode from WNW (17% of the total wind record) and a secondary mode from the S (14%) (Figure 5.1a). Other modes in the annual wind regime include high

magnitude (>18 m s^{-1}) storm winds from the SSE and moderate (6-18 m s^{-1}) winds from the NNW.

The monthly wind roses (Figure 5.2) portray the seasonally opposed wind regime of this region. The high magnitude S to SE wind occurs from October to April (winter), while WNW to NW wind dominates from May to September (summer). Average monthly wind speed ranges from a minimum of 6.5 m s^{-1} in August to a maximum 10.6 m s^{-1} in December. The monthly trends for average wind speed and percent competent winds (>6 m s^{-1}) at CSJ are similar (Figure 5.4a, Table 5.1).

Table 5.1: Annual and monthly wind regime summary of CSJ and RS (1995-1999).

	Average wind speed (m/s)		Percent competent winds (>6 m/s)		Primary modal direction		Secondary mode	
	CSJ	RS	CSJ	RS	CSJ	RS	CSJ	RS
Annual	**8.87**	**8.1**	**61.6**	**62.3**	**WNW**	**SSE**	**S**	**W**
January	9.65	8.71	70.2	69.4	S	SSE	SSE	ESE
February	10.24	9.17	69.3	68.6	SSE	SSE	S	S
March	8.90	8.37	60.8	65.5	S	SSE	NNW	S
April	8.51	7.97	56.1	59.0	S	SSE	WNW	S
May	7.30	7.48	52.7	52.9	NNW	W	WNW	SE
June	7.72	7.99	60.2	66.6	WNW	W	NNW	SE
July	7.19	7.03	57.3	57.4	WNW	W	NNW	SE
August	6.48	6.37	47.9	45.5	WNW	W	NNW	SE
September	6.69	6.97	49.4	51.6	WNW	SSE	SSW	W
October	9.56	8.69	69.3	62.2	S	SSE	WNW	S
November	9.43	9.08	69.1	69.6	S	SSE	SSE	S
December	10.57	9.68	77.6	70.3	SSE	SSE	S	E

Figure 5.1: a) The annual wind rose from CSJ (1995-1999) indicates a strong, bimodal wind regime with the greatest magnitude winds from the south-southeast and a second mode of lower magnitude, higher frequency winds from the northwest. b) The annual wind rose from RS (1995-1999) illustrates that the strongest magnitude winds are from the southeast with a secondary mode of lower magnitude winds from the west. [Pearce (2005:97), with permission].

(a)

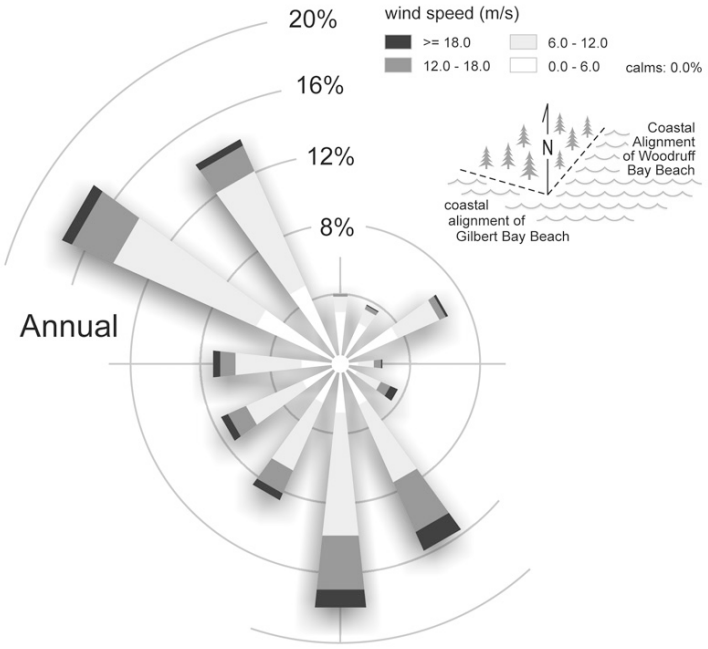

(b)

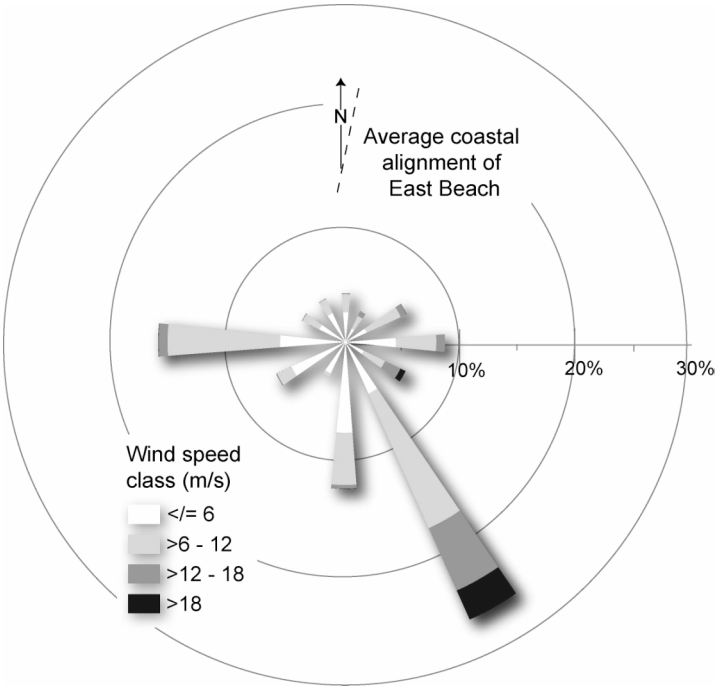

Figure 5.2: The monthly wind roses from CSJ (1995-1999) illustrate a seasonal shift in the wind regime from predominantly high magnitude south-southeast wind in the winter to lower magnitude north-northwest wind in the summer.

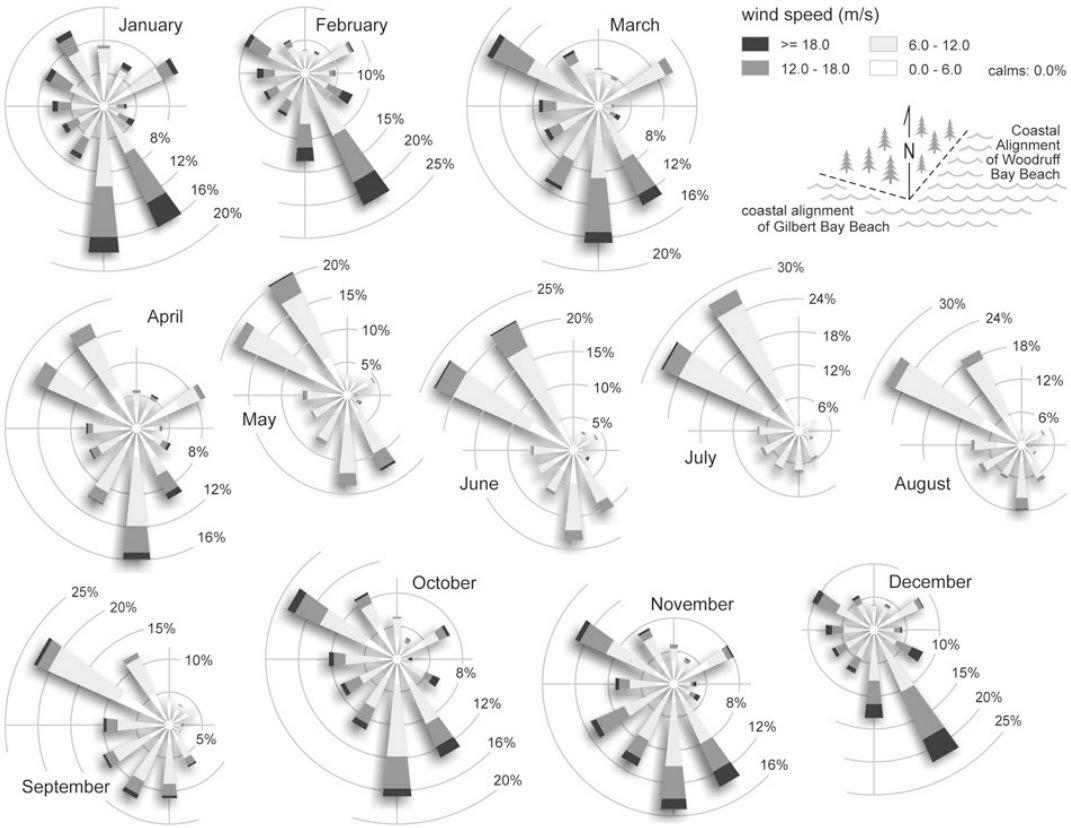

Figure 5.3: The monthly wind roses from RS (1995-1999) show a seasonal shift in the wind regime. During the winter, fall and early spring strong southeast winds are dominant, while during the late spring and summer, lower magnitude west winds dominate. [Pearce (2005: 91), with permission].

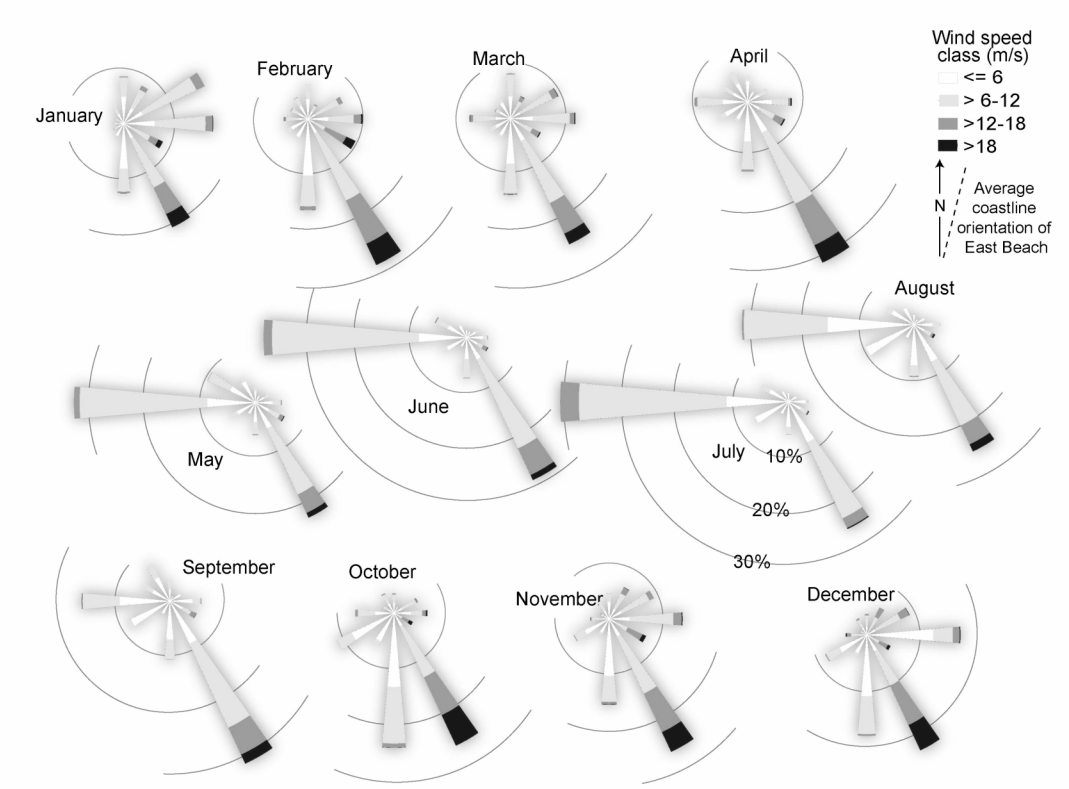

Figure 5.4: Mean monthly wind speeds and percent monthly wind competence from a) CSJ and b) RS (1995-1999) show a distinct seasonal shift from high magnitude winds in the winter to low magnitude winds in the summer. [RS graph modified from Pearce, 2005].

(a)

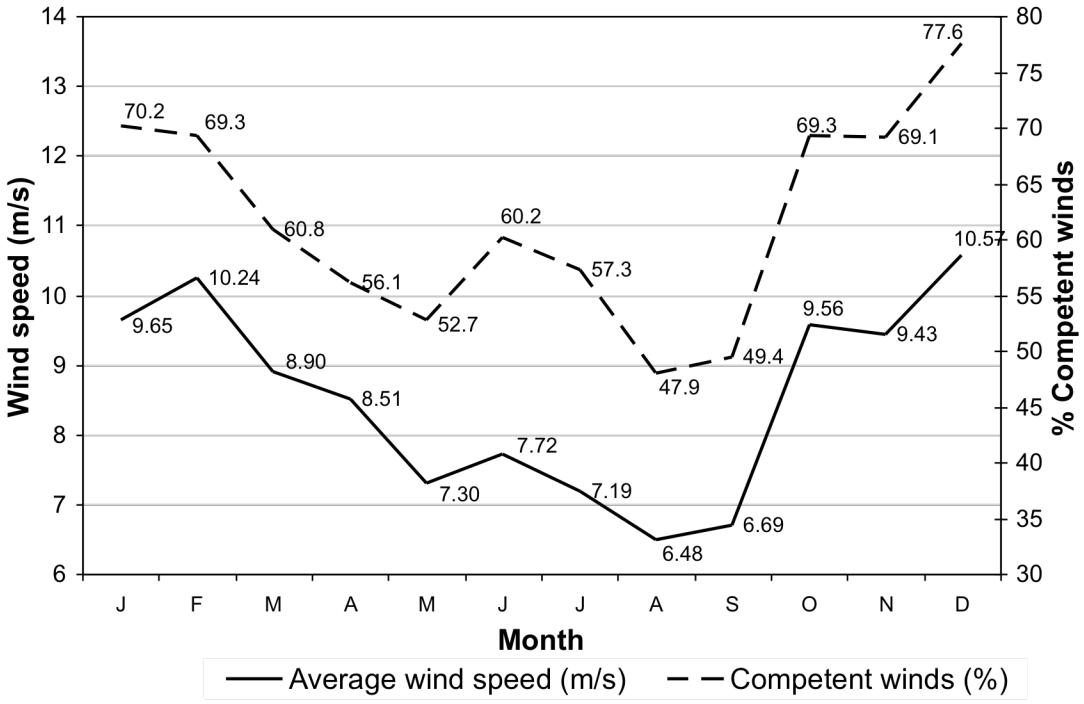

(b)

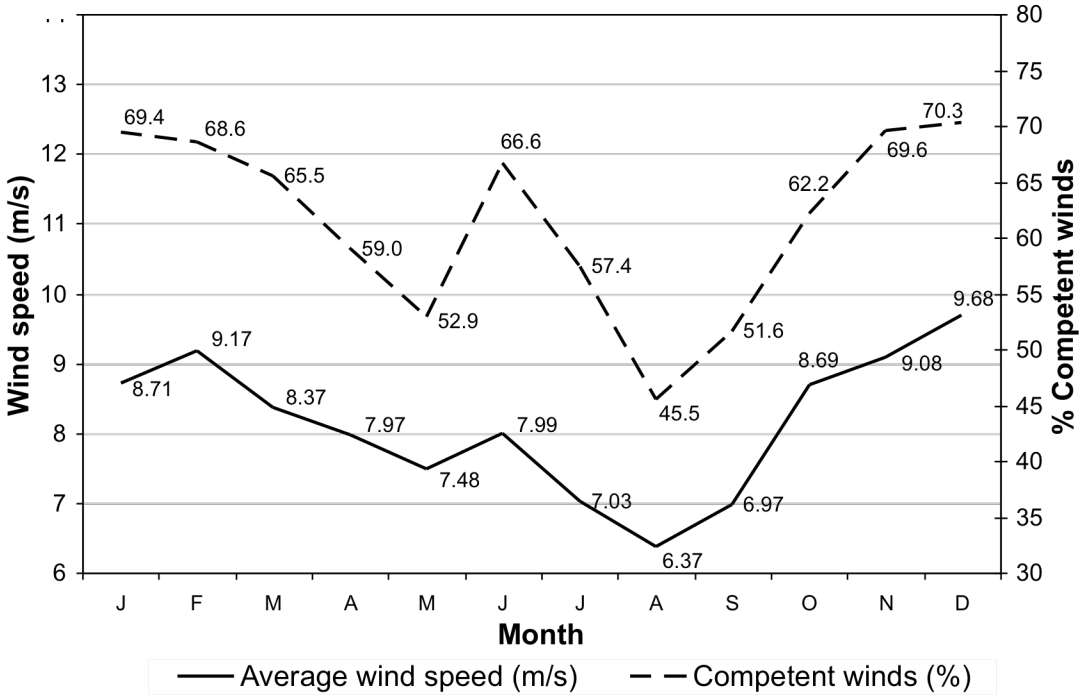

Rose Spit

An analysis of the wind regime at RS provides a regional comparison to the regime at CSJ (Pearce, 2005). RS also experiences a high, year-round wind regime, with an average wind speed of 8.5 m s^{-1} and frequent (62%) transporting winds (i.e., >6 m s^{-1}). The annual (1995-1999) wind rose from RS shows a strong bimodal regime with a primary mode from the SE and a secondary mode from the W (Figure 5.1b). The monthly wind roses portray the seasonally opposed wind regime at RS (Figure 5.3). The greatest magnitude winds are from the SE and occur from September to April. The lesser magnitude westerly winds prevail in May through August, though the SE winds still show the highest magnitude. Figures 5.1b, 5.3, and 5.4b illustrate the details of the wind regime, and are discussed in more detail in Pearce (2005).

5.1.2 Fryberger's (1979) sediment drift potential model

Cape St. James

When applied to CSJ wind data for 1995-1999, the Fryberger (1979) sediment drift potential model yields an annual average DP of 4570 VU, an RDP of 1542 VU toward a resultant drift direction (RDD) of 46°, and an RDP/DP ratio of 0.34 (Table 5.2). According to Fryberger's (1979) classification, the CSJ region has a high wind energy regime that is obtuse to acute bimodal. The annual drift rose (Figure 5.5a) illustrates the predominant sediment drift direction is from the SW. There are also strong drift vectors from the NW and SE, but almost no drift vectors from the NE.

There is high seasonal variability in the sediment drift regime of this region. The monthly drift roses (Figure 5.6) illustrate that the highest potential for sediment

transport is from October to April, when all DP values are >300 VU, with a maximum DP of 726 VU in December (Table 5.2). The lowest potential for sediment transport occurs in August, with a DP value of 138 VU.

The RDD is toward the NE for the winter months (October to April), with a dramatic shift to the SE in May (Figure 5.6, Table 5.2). The NE drift directions during October to April are onshore to oblique onshore at Gilbert Bay beach and along shore at Woodruff Bay beach (Figure 5.6). The summer SE drift directions from May to August are offshore to oblique offshore at both beaches. There are limitations in assuming that the wind conditions at CSJ accurately represent the conditions at each beach (see Section 5.3.1 for further discussion).

Table 5.2: Summary of annual and monthly results from the Fryberger (1979) sediment drift potential model for CSJ and RS (1995-1999). [Source of RS data: Pearce, 2005].

	DP (VU)		RDP (VU)		RDD (degrees to true north)		RDP/DP	
	CSJ	RS	CSJ	RS	CSJ	RS	CSJ	RS
Annual	**4570**	**3176**	**1542**	**1826**	**46**	**317**	**0.34**	**0.58**
January	575	292	300	201	17	291	0.52	0.69
February	609	340	339	260	21	311	0.56	0.77
March	432	310	140	196	25	300	0.32	0.63
April	349	266	167	210	32	321	0.48	0.79
May	188	195	42	78	122	358	0.22	0.40
June	222	249	81	107	137	4	0.36	0.43
July	165	183	125	87	162	35	0.76	0.48
August	138	160	54	99	132	337	0.39	0.62
September	154	182	49	132	84	324	0.32	0.73
October	517	298	217	213	59	321	0.42	0.71
November	494	346	197	249	32	302	0.40	0.72
December	726	364	286	209	59	299	0.39	0.57

Figure 5.5: Annual Fryberger (1979) sediment drift potential drift rose for a) CSJ and b) RS (1995-1999), shows significant drift toward the northeast. DP = drift potential, RDP = resultant drift potential, and RDD = resultant drift direction. [RS figure from Pearce (2005: 95), with permission].

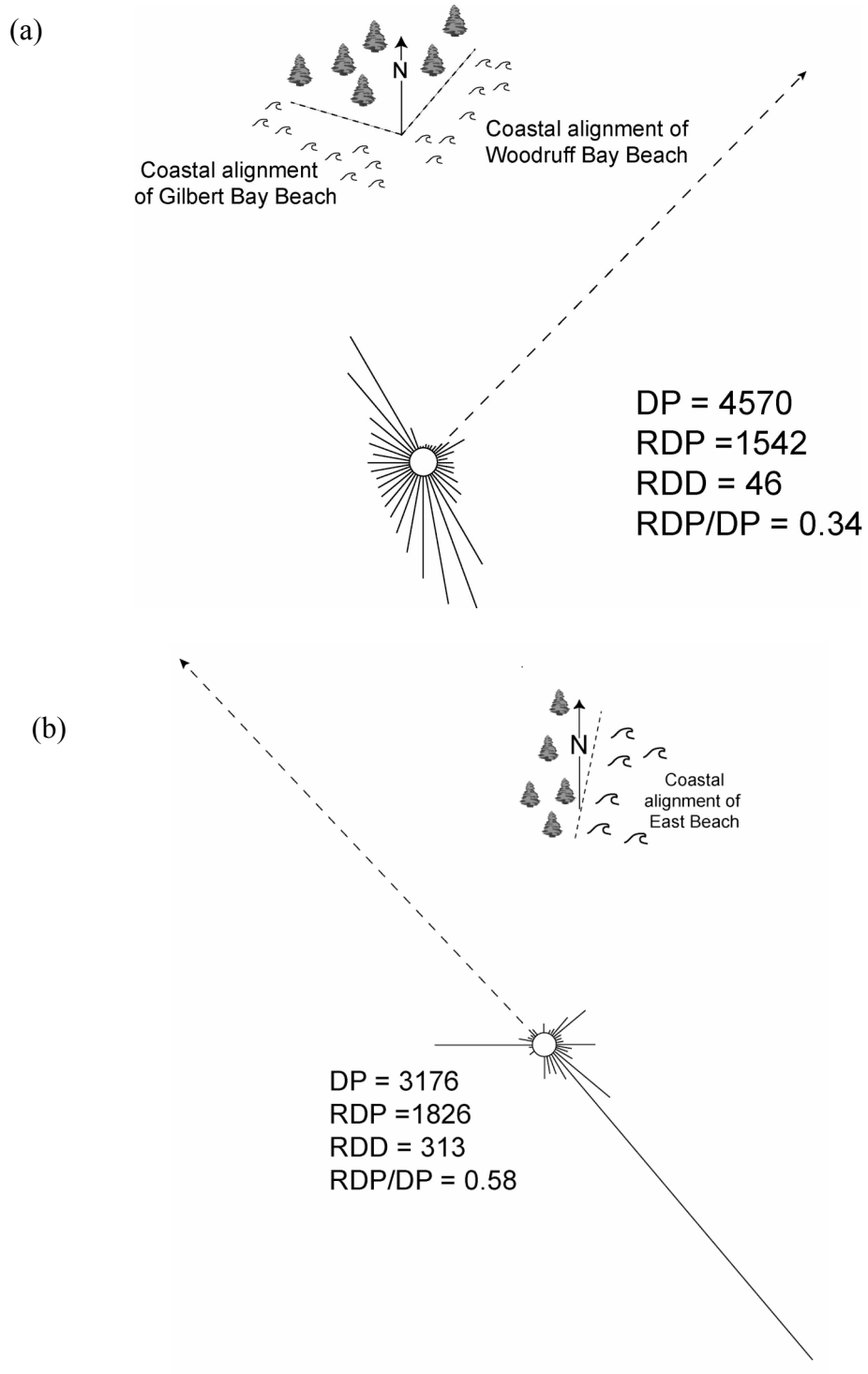

Figure 5.6: Monthly Fryberger (1979) sediment drift roses for CSJ (1995-1999) show a notable seasonal shift from a northeast drift direction in the winter to a southeast drift direction in the summer. DP = drift potential, RDP = resultant drift potential, RDD = resultant drift direction, and PPT = total monthly precipitation (mm).

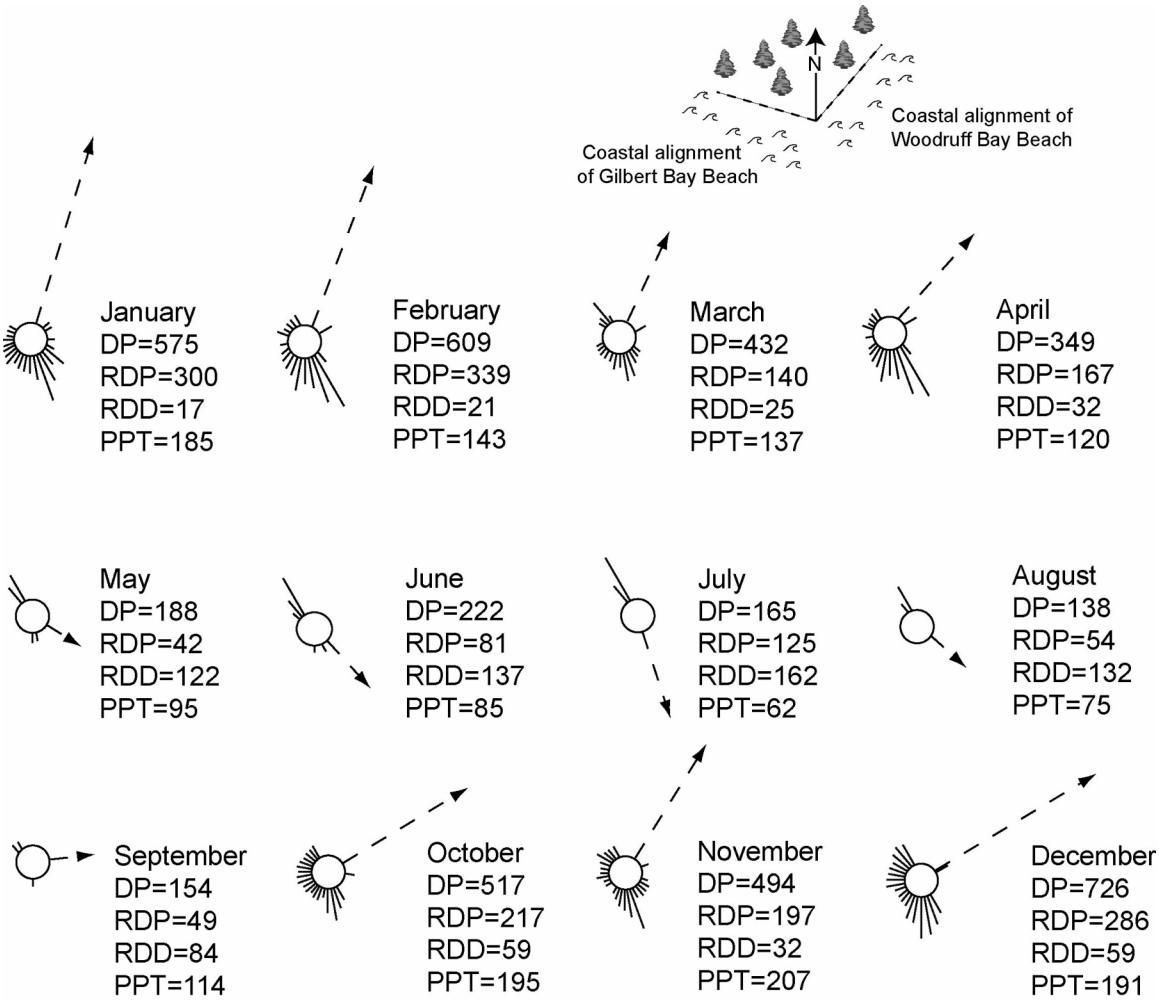

Figure 5.7: Monthly Fryberger (1979) sediment drift potential drift roses for RS (1995-1999) show a notable seasonal shift from a northeast drift direction in the winter to a southeast drift direction in the summer. DP = drift potential, RDP = resultant drift potential, and RDD = resultant drift direction. [Pearce (2005: 97), with permission].

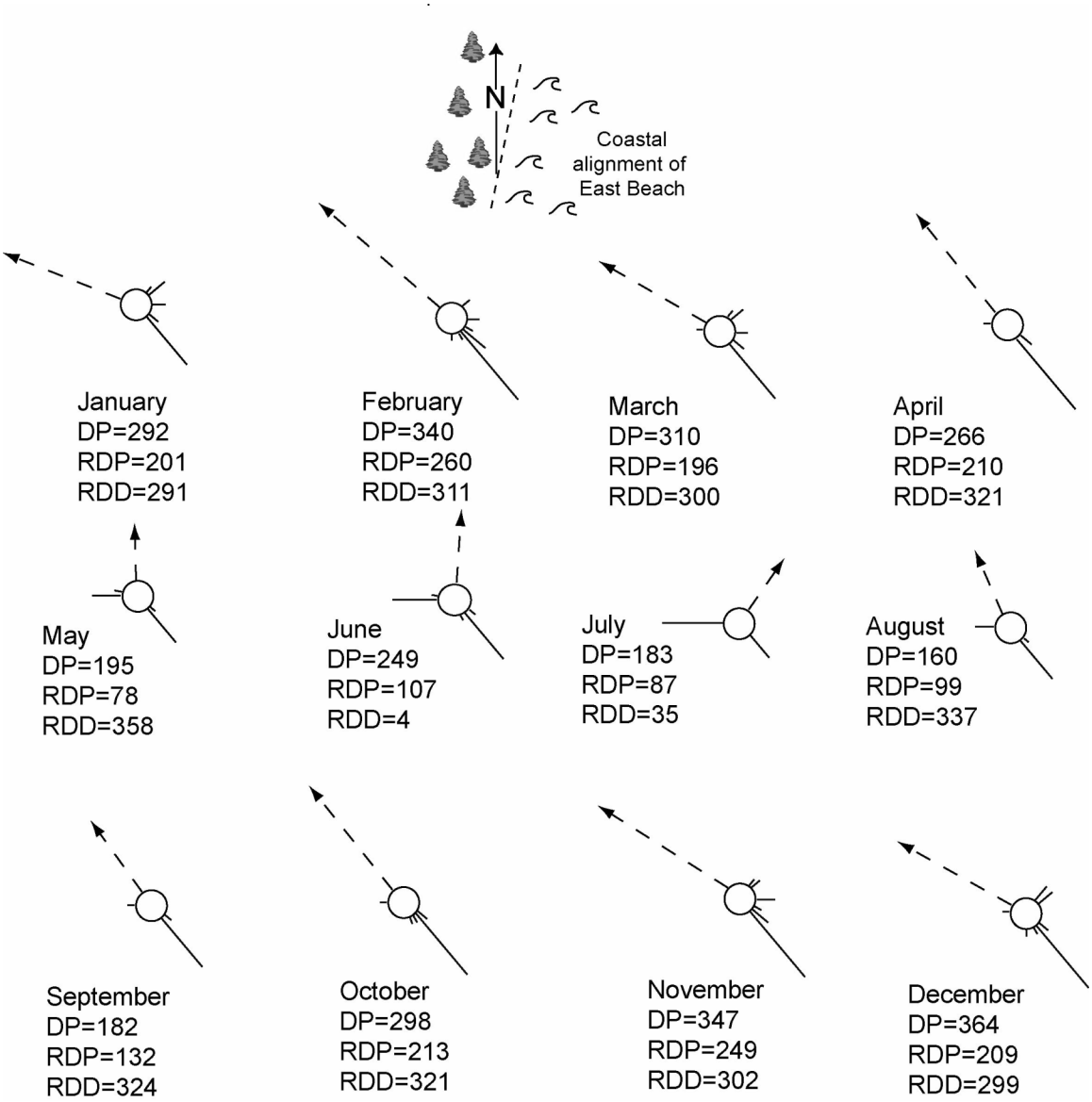

Rose Spit

The results for the Fryberger sediment transport potential model applied to the 1995-1999 wind record from RS from Pearce (2005) are summarized here to allow comparison to CSJ. Using wind data from 1995-1999 from RS, the Fryberger (1979) model yields an annual average DP of 3176 VU, an RDP of 1826 VU toward an RDD of 313°, and an RDP/DP ratio of 0.58 (Figure 5.5b, Table 5.2). This indicates a high wind energy environment with an obtuse to acute bimodal regime. The drift rose illustrates the dominant NW drift direction, with a secondary drift vector from the W (Figure 5.5b). There is notable seasonal variability in the sediment drift regime at RS. The monthly drift roses indicate that the greatest drift potential is from September through February, when all DPs > 200 VU (Figure 5.7, Table 5.2). Figures 5.5b and 5.7 illustrate the annual and monthly RDPs for RS, and are discussed in more detail in Pearce (2005).

5.2 Erosive water level regime

This section discusses the erosion potential of the CSJ region by examining trends in high water level events for the CSJ region combined with wave runup estimates for Gilbert Bay and Woodruff Bay beaches. The results presented here illustrate the estimated capacity of the morphodynamic regime at CSJ to erode the backshore of these beach-dune systems. Figures 5.8a and b portray each beach-dune cross-sectional profile showing positions of HHWLT, LLWLT, MWL, HHWLT + runup, and elevation of the beach-dune junction[12]. Runup values were derived using

[12] Beach-dune junction is defined as the point on the cross-sectional profile where aeolian processes dominate (i.e., the seaward edge of the driftwood jam).

Equation 2, described in section 3.3. These profiles illustrate historical average water level conditions in the CSJ region and provide a context for future trends and extreme scenarios discussed later in the chapter.

Results from long-term water level trend analysis for CSJ and PR are presented, as well as results from extreme water level recurrence analysis and wave runup estimation. The trends in average annual (AAWL) and maximum annual water levels (MaxWL) have important implications for the morphodynamics of beach-dune systems in this region and their potential responses to known climate variability events (e.g., El Niño) and climate change-induced sea level rise (see Chapter 6). Results from wave runup analysis for Gilbert and Woodruff Bay beaches are also presented.

Figure 5.8: Topographic profiles of a) Gilbert Bay beach and b) Woodruff Bay beach with lines indicating Lowest Low Water Large Tide (LLWLT), Highest High Water Large Tide (HHWLT), mean water level (MWL), estimated runup elevation, and HHWLT plus runup based on water level data from CSJ.

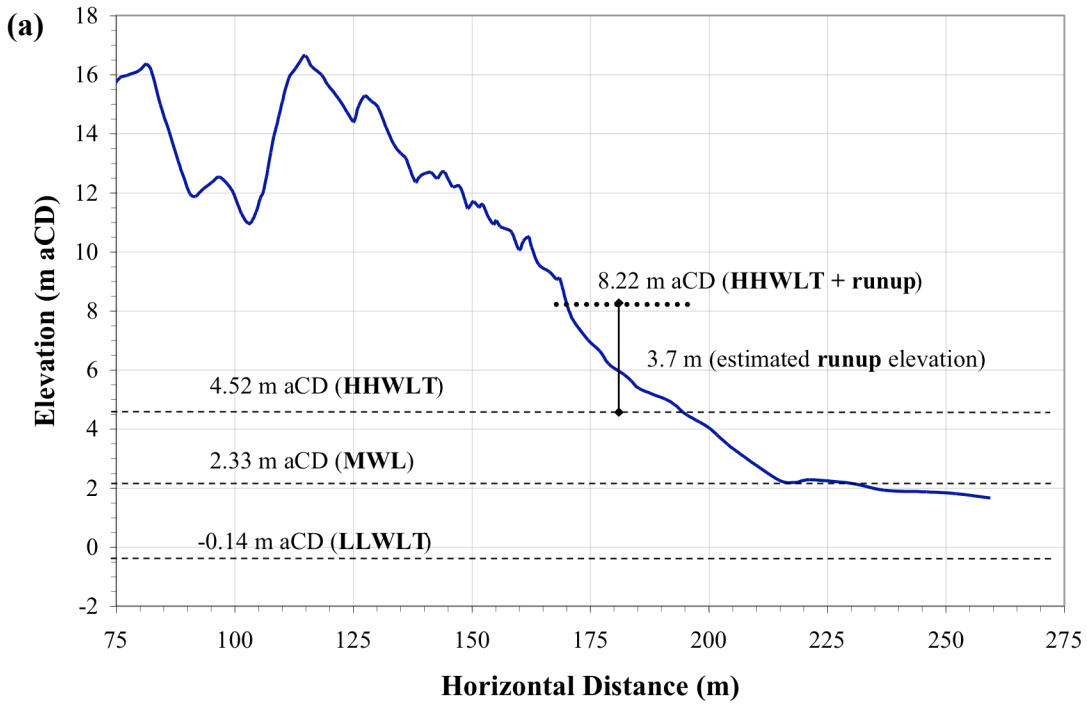

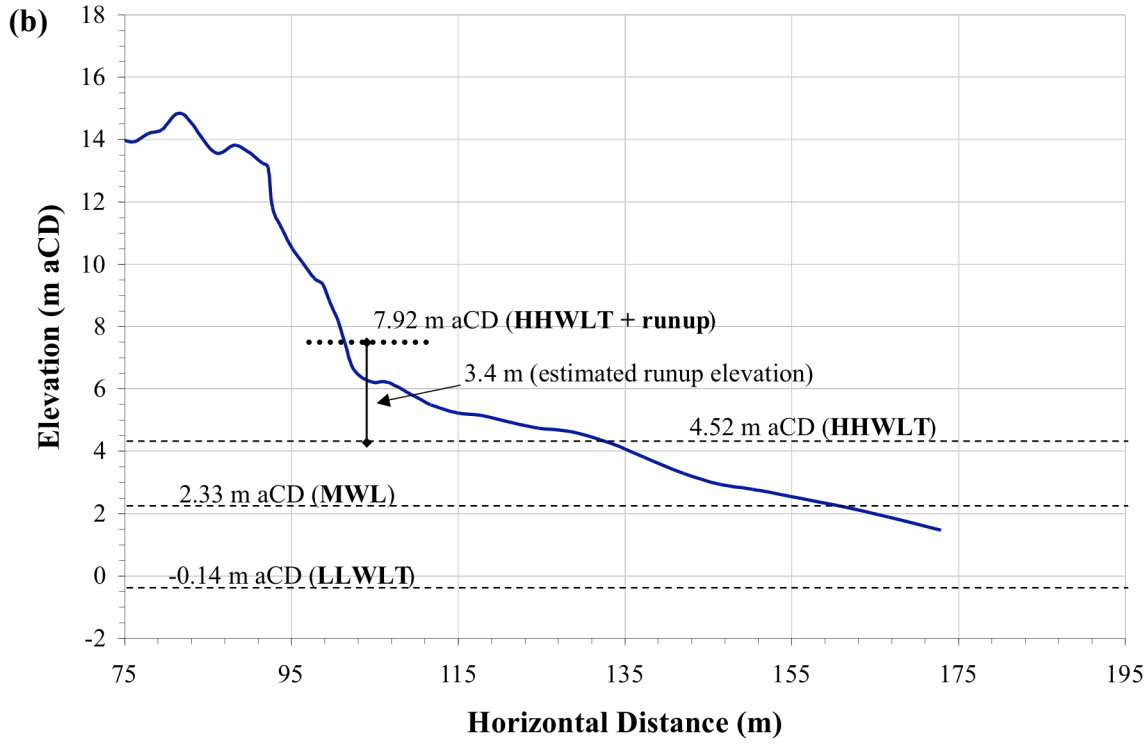

5.2.1 Long-term mean and maximum water level trends

Applying a linear regression model to the available adjusted water level record for CSJ is limited because the record is only 17 years long. There is an increasing trend of +0.7 mm yr^{-1} in AAWL at CSJ (Figure 5.9a), but the reliability of the trend is limited because it is not statistically significant. The simple linear regression model based on MaxWL at CSJ, however, yields a significant ($p < 0.05$) trend of +16.7 mm yr^{-1} (Figure 5.9b).

For comparison, the measured total water level record at PR is 71 years long (1909-2003, with some years removed due to gaps in the data). Based on statistical analysis by Abeysirigunawardena and Walker (unpublished data, 2007), the longer-term regional water level record yields a significant ($p < 0.05$) trend of +1.6 mm yr^{-1} in AAWL and a significant ($p < 0.05$) trend of +3.4 mm yr^{-1} in annual MaxWL. The

PR water level trends are assumed to be broadly representative of the regional sea level response characteristics of the northern coast of BC with 95% confidence intervals ranging from +1.0 to 2.33 mm yr^{-1} (Abeysirigunawardena and Walker, unpublished data, 2007).

Due to the short length of the CSJ water level record, a linear regression model was applied to the same time interval (1989-2006) for the PR data in order to compare the results to CSJ. The resulting AAWL trend for PR (+1.7 mm yr^{-1}) from 1989-2006 was not statistically significant (Figure 5.9c), while the MaxWL regression for this time interval at PR yields a significant trend of +5.8 mm yr^{-1} (Figure 5.9d).

Figure 5.9: Simple linear regression models for: (a) AAWL at CSJ (1989-2006), (b) MaxWL at CSJ (1989-2006), (c) AAWL at PR (1989-2006), and (d) MaxWL at PR (1989-2006).

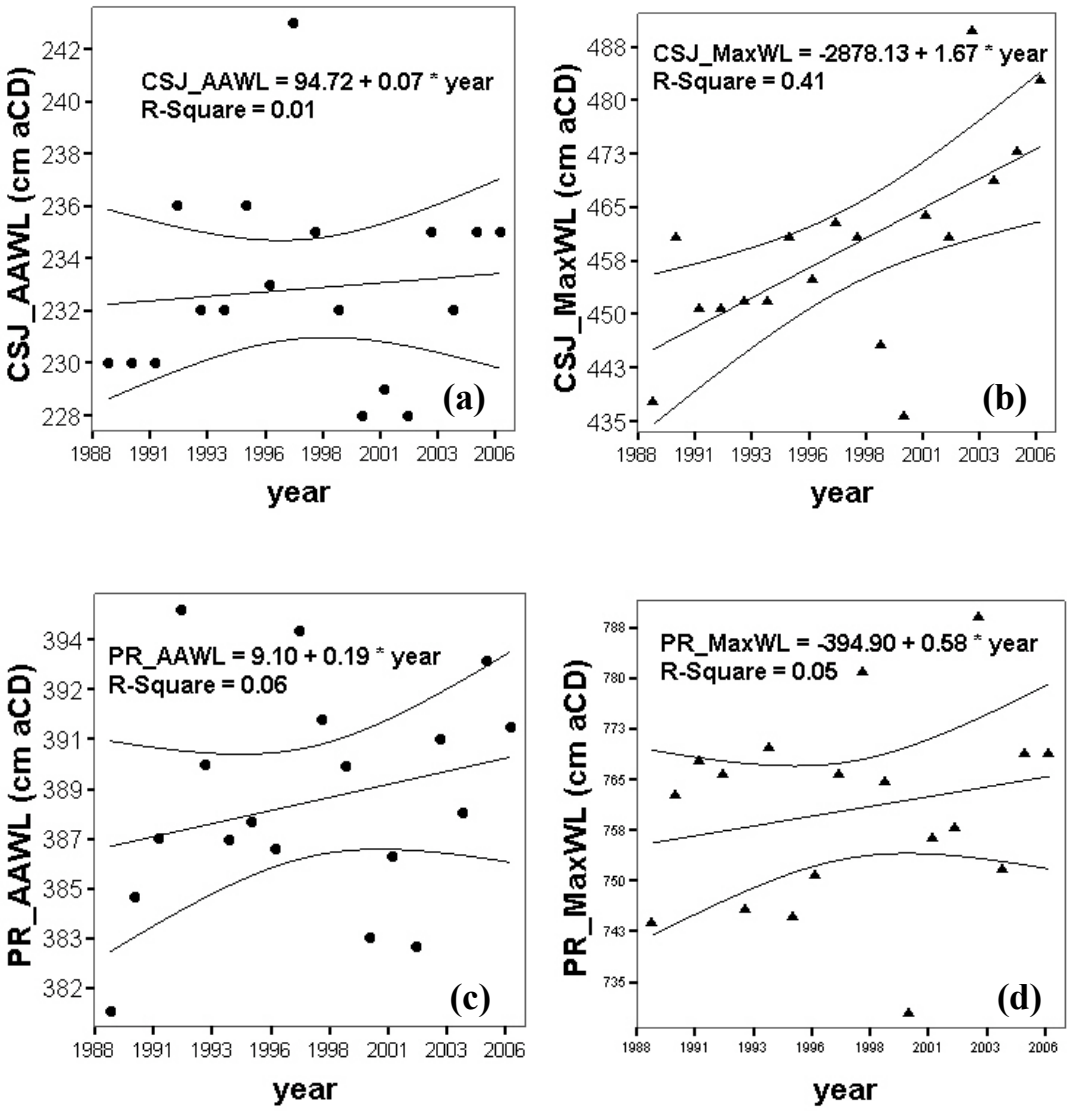

5.2.2 Extreme water level regime

The linear regression analyses discussed above indicate that the beach-dune systems in the CSJ region are experiencing significant increases in the magnitude of annual maximum water levels. Decomposition analysis of the influence of surge and astronomical tides on extreme water levels shows a notable trend at CSJ, with annual maximum surge events occurring mostly at low to intermediate tidal stages, while MaxWL events occur at high tidal stages (Figure 5.10). This tidal dominance of the extreme water level regime supports similar results from water levels at PR (Abeysirigunawardena and Walker, unpublished data, 2007).

Using the Extreme Value Toolkit (Gilleland et al., 2000), an extreme water level recurrence curve was produced for CSJ based on a non-linear GEV distribution (Figure 5.11). The curve projects an extreme annual water level (R = 1) of 4.52 m aCD and a 10-year maximum water level projection (R = 10) of 4.78 m aCD. Because this curve is only based on 17 annual maximum water level data points (1989-2006), the confidence intervals are too large for R > 10, and water level projections cannot be made. Alternatively, the PR record provides a much longer (71-year) maximum water level record. Using the same approach, Abeysirigunawardena and Walker (unpublished data, 2007) estimate an annual maximum water level (R = 1) of 7.13 m aCD and a 10-year maximum water level (R = 10) of 7.78 m aCD at PR. The projected 100-year extreme water level (R = 100) at PR is 7.9 m aCD. Basing CSJ extreme water level projections on results from PR is limited because there are significant differences in the tidal ranges (7 m at PR vs. 5 m at CSJ) and MWL (3.8 m aCD at PR vs. 2.3 m aCD at CSJ) at each site. Additionally, site-specific environmental conditions such as fetch development distances and tidal

current interactions cause the extreme water level trends at each site to differ substantially.

5.2.3 Wave runup

The measured water level data for CSJ represent deep-water conditions and therefore do not account for the additional water elevation caused by wave runup on sloping beaches. On beaches, observed water levels represent the elevation of the measured water level plus the elevation of wave runup (Figure 2.1). The runup ($R_{2\%}$, Equation 2; Ruggiero et al., 1997, 2001) elevation value for Gilbert Bay beach is 3.7 m and for Woodruff Bay beach is 3.4 m (See Figures 5.8a and b). These values are calculated based on the available significant wave height record (1993-2006) and the inter- to sub-tidal beach slope. In calculating these wave runup values, it is assumed that significant wave height measured at the EC-South Moresby buoy (C46147, see Figure 1.2) is representative of wave conditions for Gilbert and Woodruff Bay beaches.

Figure 5.10: Decomposition of surge-tide components of annual maximum water level events (circles) and annual maximum surge events (triangles), indicating the maximum water level events are dominated by extreme tides and there is a consistent occurrence of extreme surge events at low to mid tides.

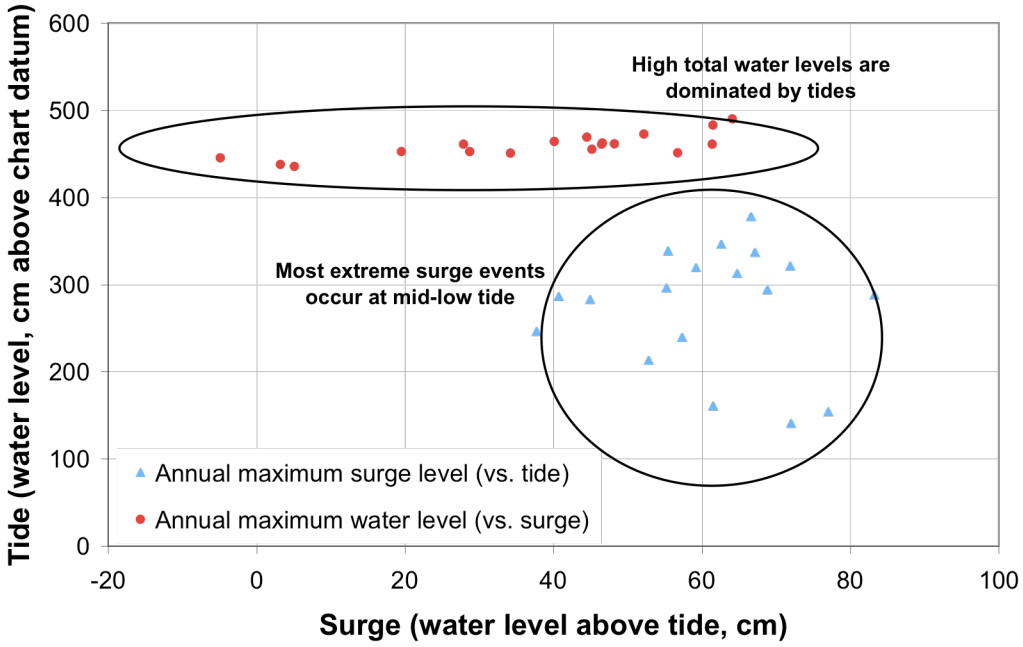

Figure 5.11: Maximum water level recurrence curve for CSJ produced using the Extreme Values Toolkit with a non-linear GEV distribution.

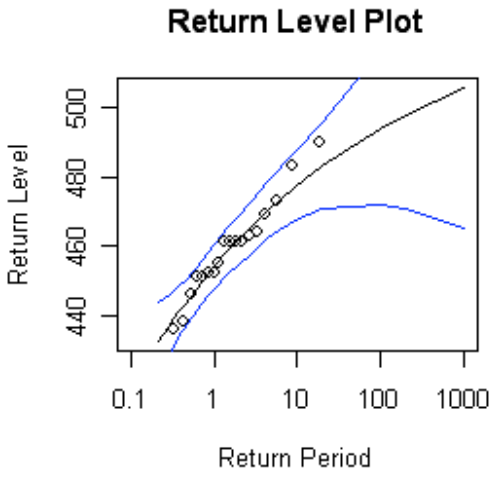

Recurrence interval (years)	1	5	10
Return level (m aCD)	4.52	4.65	4.78
95% confidence limit (m)	±0.05	±0.06	±0.1

5.3 Discussion

The second objective of this thesis was to estimate the erosional and depositional regimes of Gilbert Bay and Woodruff Bay beaches and to compare them to northern HG in order to assess the broader regional morphodynamics. The results presented in this chapter address this objective through detailed analysis of the regional wind regime, sediment drift potential, long-term water level trends, maximum water level recurrence, and wave runup.

Backshore morphodynamics and dune evolution can only be accurately understood by considering the effects of aeolian sediment transport *and* the magnitude and frequency of occurrence of erosive high water levels (Ruz and Meur-Ferec, 2003). The analyses of the aeolian regime and sediment drift potential presented in this chapter estimate the capacity of these beach-dune systems to maintain and build dunes via onshore sediment transport. Conversely, the water level analysis estimates the potential for erosive events that will scarp the dunes backing the beach systems and move sediment into the nearshore.

5.3.1 Aeolian regime

The wind regime at CSJ is similar in average strength and seasonality to the regime at RS, but notably different in directionality (Figure 5.12). Both locations experience a year-round, high-energy wind regime that is seasonally bimodal. The strongest and most frequent winds at RS are from the southeast (direct onshore) in the winter and from the west in the summer, while at CSJ the strongest and most frequent winds are from south to southeast in the winter and the northwest in the summer. During the summer months (May – September), the wind regime at CSJ is more uni-

directional than at RS. The net result of this difference is that the annual wind rose for CSJ has a primary mode from the N-NW, despite a high frequency of S-SE winds in the winter months (October – March). At RS most of the summer months have a bi-directional wind regime with a primary mode from the west and a secondary, but significant, mode from the SE. At both locations, the strongest winds (i.e., >18 ms^{-1}) occur in the winter months from the S-SE. The wind regime at both locations is influenced by the position and strength of the Aleutian Low pressure system in the winter and the anti-cyclonic wind pattern generated by the Pacific High in the summer.

Fryberger's (1979) regional drift potential model for both CSJ and RS indicates that, regionally, beach-dune systems in HG experience strong aeolian sediment transport regimes. The annual and monthly drift directions at CSJ, however, are markedly different from that at RS. Figure 5.12 illustrates this difference through a cumulative monthly RDP diagram that also incorporates monthly RDD. The diagram for RS indicates that East Beach, in northern HG, experiences a very high onshore sediment transport regime most of the year (September through March) due to the southeast aspect of the beach to dominant onshore transporting winds. This is evidenced by large, southeast-facing, aeolian dunes that characterize East Beach. Gilbert Bay beach also experiences a high onshore sediment transport regime with its SW aspect and net drift direction to the NE. Again, like on East Beach, the active, southwest facing foredunes and incipient dunes that back this beach provide strong evidence of this onshore (NE) sediment drift. Based on the RDP analysis from CSJ, Woodruff Bay beach experiences a primarily alongshore sediment

drift direction due to its SE aspect. The aeolian dunes at Woodruff Bay beach, however, indicate otherwise.

The large relict and active foredunes at Woodruff Bay beach (Figure 4.13) provide an indication of a strong onshore sediment transport regime, unlike what is indicated by the RDP diagram in Figure 5.12 (i.e., an alongshore RDD). Using the wind data from CSJ for RDP analysis for an embayed system such as this has limitations. The wind record at CSJ may not accurately characterize the wind experienced by each of the beach-dune systems because topographic steering and forcing create a localized flow field at each beach that may deviate significantly from the regional wind direction (Tsoar, 1983; Tsoar and Yaalon, 1983). The beach at Woodruff Bay, for example, probably experiences a net drift potential similar to East Beach (i.e., onshore oriented to the northwest) and there may be a reduced strength of winds from the north-northwest on the beach. Woodruff Bay beach is embayed and backed by steep terrain that may block incident winds from the north and northwest from reaching the beach (offshore). Wind data recorded above the surface on-site at Woodruff Bay beach would provide a more accurate representation of the wind regime experienced by the sediment at this beach. Unfortunately, there is no wind record available specifically for Woodruff Bay beach. The only available data is recorded from 10 m above the surface on St. James Island, which is at 93 m above sea level. This introduces additional limitations because the height of the station and the steep topography of the island may locally accelerate the wind, thereby overestimating the regional wind speeds.

Secondary flow effects generated by dune topography may play an important role in dune rebuilding and maintenance during offshore and alongshore wind events. Topographic steering and flow acceleration during offshore and alongshore wind events can result in landward (i.e., onshore) sediment transport into the dune system (Gares et al., 1996; Nordstrom et al., 1996; Walker et al., 2006). Offshore to oblique onshore winds can be steered alongshore and then deflected back towards the foredune. During competent winds (i.e., >6 m s^{-1}), this steering can transport sediment into the dunes (Walker et al., 2006). Additionally, flow stagnation from airflow interaction with dune topography can cause decreased wind speeds and thereby promote sediment deposition at the toe of the dunes, resulting in scarp infilling and dune rebuilding. The complexities introduced by secondary flow effects are important to consider when assessing the morphodynamic regime of any beach-dune system. For this study, it appears that, although the annual RDP is alongshore at Woodruff Bay beach, secondary flow effects may enable the frequent offshore and alongshore (W to N) winds to cause onshore sediment transport, thereby promoting dune maintenance and rebuilding.

Figure 5.12: A comparison of monthly RDP (in brackets) and RDD variation from CSJ (top) and RS (bottom) (Pearce, 2005) shows the distinct directional differences in the sediment drift potential in the two areas. Arrows represent unitless RDP vector units.

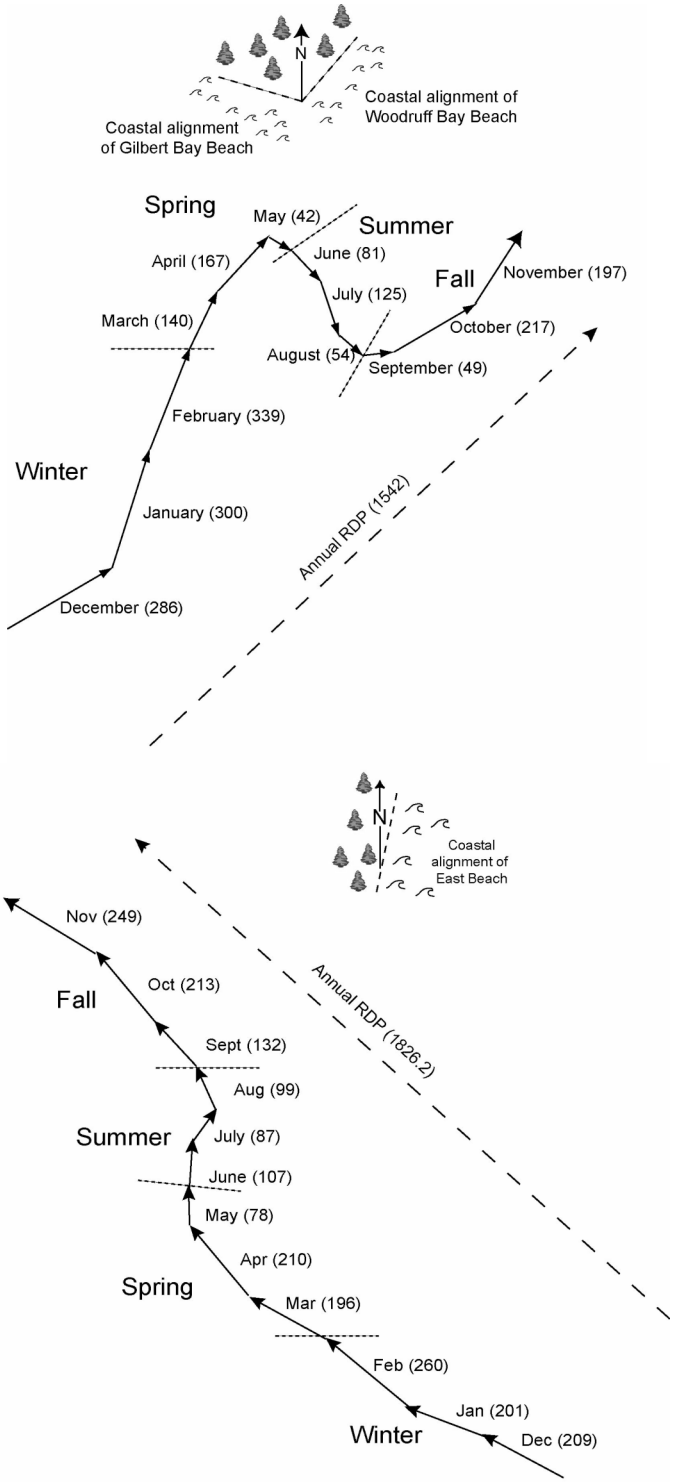

5.3.2 Water level regime

Although the long-term water level record at CSJ does not yield a statistically significant trend (because of the short record, n = 17), the results from PR (n = 71) represent the broader regional water level trends for both AAWL (+1.6 mm yr^{-1}) and MaxWL (+3.4 mm yr^{-1}) (Abeysirigunawardena and Walker, unpublished data, 2007). These trends, therefore, indicate that HG is experiencing a significant increase in erosive water levels (i.e., capable of exceeding the beach-dune junction). The regional AAWL trend is close to the global rate of sea level rise according to the Intergovernmental Panel on Climate Change (IPCC) (+1 to 2 mm yr^{-1}; IPCC, 2001). Due to site-specific conditions (e.g., fetch generation distances, current interactions) there are limitations in assuming that the PR water level trends accurately represent trends at CSJ. These assumptions were made based on the limited availability of long-term regional water level data.

The MaxWL trend indicates that, due to increased frequency and magnitude of storm events in the region (Graham and Diaz, 2001), extreme water levels are increasing at twice the rate of the mean sea level trend (Abeysirigunawardena and Walker, unpublished data, 2007). Decomposition analysis indicates that, in this region, MaxWL events are dominated by tides, unlike storm-generated surge events, which tend to occur at lower tide stages (Figure 5.10). There appears to be a coupling between astronomical tides and surge events, which supports similar results from the regional water level record at PR (Abeysirigunawardena and Walker, unpublished data, 2007). At this point, the mechanisms behind this are not well understood and discussions in the literature remain hypothetical (Heap, 1983). Further analysis of this coupling is beyond the scope of this thesis.

5.3.3 Response of beach-dune systems to sea-level rise

Climate-change induced variations in regional water levels have important implications for beach-dune morphodynamics. Most efforts to predict the impacts of sea level rise on beaches have relied on the simple conceptual model presented by Bruun (1962, 1988) that predicts erosion of the upper beach and offshore deposition proportional to the increase in sea level (Equations 9 and 10, Figure 2.11). Without addressing the critical role of the beach-dune sediment budget (i.e., onshore sediment movements by wind action and resulting dune rebuilding from erosive events), this model fails to accurately model the morphological response of many sandy coasts to sea level rise (Cooper and Pilkey, 2004; Davidson-Arnott, 2005).

An alternative model presented by Davidson-Arnott (2005) suggests that the beach-dune sediment budget plays an essential role in the response of sandy systems to sea level rise (Figure 2.12). Most sandy beaches, like those at Gilbert and Woodruff Bay, are backed by foredunes and the exchange of sediment between these two regions of the beach is common (Davidson-Arnott, 2005). Wave erosion of incipient and/or established foredunes from high water level events results in a transfer of sediment from the dune to the beach (Psuty, 1988; Nickling and Davidson-Arnott, 1990; Sherman and Bauer, 1993; Davidson-Arnott, 2005). This sediment is transported back to the dune by aeolian action, provided there is a sufficiently competent wind regime. For foredune-backed beach systems, Davidson-Arnott (2005) argues that all sediment eroded from a beach by high water levels is not simply deposited on the nearshore profile. Rather, eroded sediment will be transferred landward into the dunes by aeolian action, resulting in a landward migration of the foredune. Additionally, because the volume of sediment transferred landward is equal

to the volume transferred into the nearshore, the dune will maintain its overall volume (Davidson-Arnott, 2005).

Based on this model, the results presented in this chapter suggest that in southern HG, the beach-dune systems may respond to the increasing water level trends by migrating landward a distance 16-20X sea level rise (Equation 10). Despite a documented erosive water level regime at CSJ, the fluvial erosion of the relict dunes combined with a strong aeolian regime (represented by a large RDP) may be able to provide a persistent enough sediment supply to the backshore so that the beach-dune profile will transfer landward and keep pace with rising sea-level.

Storm-driven nearshore bars will also migrate onshore as water depth increases with rising sea level (Davidson-Arnott, 2005). High-energy beach-dune systems essentially require extreme storm events to cause morphological change (Cooper et al., 2004). Given the increasing trend of mean and maximum annual water levels at CSJ, extreme events will likely produce severe erosion of the foredunes at Gilbert and Woodruff Bay beaches. This erosion will remove the vegetation from the seaward slope of the foredunes, which will enable the high magnitude S-SE winds that dominate in southern HG, to erode sand from the front of the dune and transport to the lee (Davidson-Arnott, 2005). The combined effect of this erosional action followed by onshore aeolian sediment transport may result in landward migration and preservation of the dunes under the water level trends described in Section 5.2. Empirical support for this potential dune migration comes from Davidson-Arnott and Law (1996), Law and Davidson-Arnott (1990), and Aagaard et al. (2004) and observations in the RS region by Pearce (2005) where 1-3

m of vertical accretion occurred via onshore aeolian transport to the lee of retreating foredunes on East Beach. Subsequent work by Anderson and Walker (2006) showed that appreciable quantities of sediment (up to 110 kg m^{-2}) can move as far as 250 m onshore via modified saltation and/or suspension.

Figure 5.13a presents a conceptual model of a possible future state of Gilbert Bay beach based on Bruun (1962) and Davidson-Arnott (2004), under a plausible 20 cm rise in sea level. Gilbert Bay beach could increase slightly in elevation as the sediment stored in the incipient dune is eroded and moved into the nearshore. The driftwood-cored incipient dune could be removed and the seaward-most vegetated dune ridge could also be eroded. This eroded sediment may be stored in the nearshore and potentially transported onshore by swash, bar migration, and competent winds at lower tide stages. This aeolian action will result in a landward migration of the modern prograding dune ridges by up to 3.5 m, based on the beach slope of 0.06 (SCOR working group 89, 1991). Provided sufficient winds persist in this region, some sediment may be transported into the forested backshore. The dense forest on the large relict dunes will likely keep this region of the beach-dune profile from migrating.

Figures 5.13b provides a conceptual representation of a possible future state of Woodruff Bay beach under a plausible 20 cm rise in sea level. Like at Gilbert Bay beach, the nearshore at Woodruff Bay will likely increase slightly in elevation due to removal of sediment from the infilled scarp and deposition onto the beach portion of the profile. The large scarp will likely migrate landward as extreme water levels continue to erode the foredune. As this occurs the established vegetation on the

foredune may be removed. This removal will increase the amount of aeolian sediment transport into the forested dune complex causing accretion and infilling of the interdune troughs. Landward of the trough the forest will remain and very little sediment transport and accretion will occur in this portion of the relict dunes.

It is important to recognize that if the rate of erosion from extreme water level events exceeds the ability of the aeolian regime to maintain the foredunes, landward migration may not occur and these systems could respond via net erosion and loss of the foredunes. More generally, it is essential to acknowledge that predictions about beach-dune response to long-term climate change are subject to intrinsic uncertainty. These uncertainties are numerous, but can be generalized in three categories (Cowell et al., 2006): i) uncertainties about climate change; ii) uncertainties about the effect of climate change on sea levels and wave climates; and, iii) uncertainty in modeling beach response on climate change timescales (e.g., decades to millennia). Additionally, caution must be used when generalizing about regional-scale beach-dune response to climatic change due to the site-specific influence of numerous factors such as, aspect to incident wind and wave conditions, and shoreline shape (e.g., embayed) (Cooper et al., 2004).

Figure 5.13 Conceptual model of the possible future state of a) Gilbert Bay beach and b) Woodruff Bay beach. Solid black line represents modern beach-dune profile, dashed line represents possible future profiles given a 20 cm rise in sea level. Mean Water Level (MWL) and Higher High Water Large Tide (HHWLT) shown.

a)

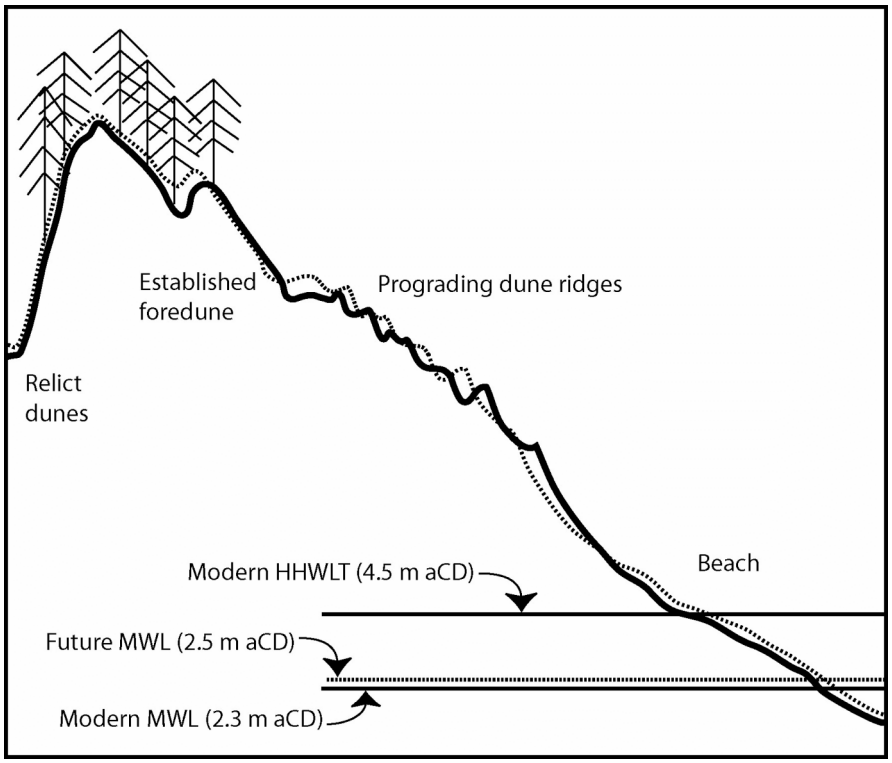

b)

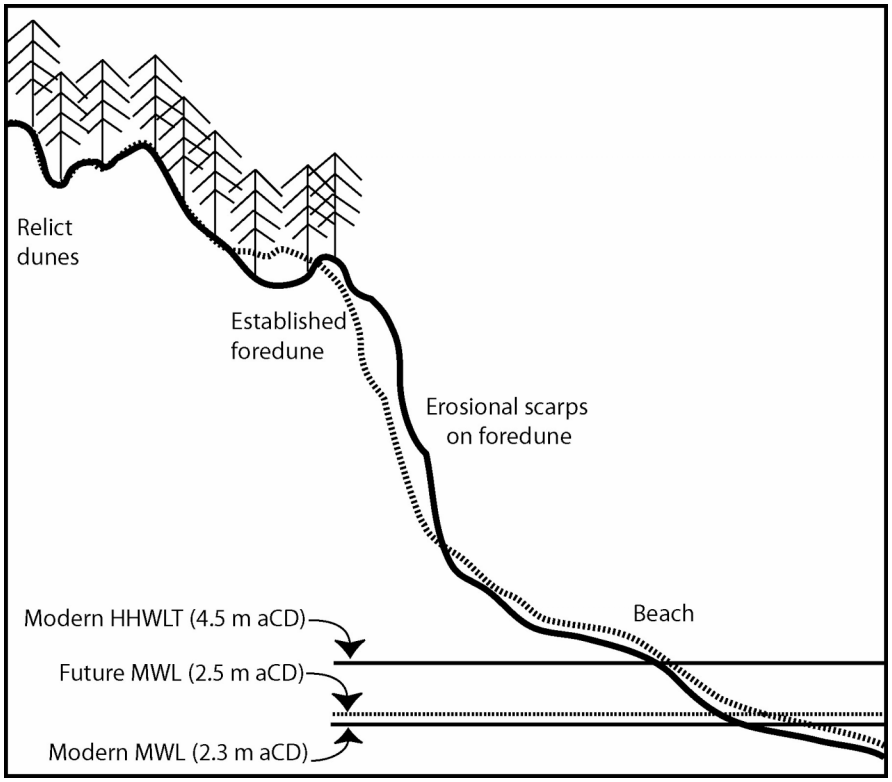

5.3.4 Projected future water level scenarios

Combining the estimated runup values for Gilbert and Woodruff Bay beaches with the long-term regional water level trends enables projections of future water level scenarios to be calculated (Table 5.3). Based on IPCC forecasting scenarios, MaxWL scenarios were calculated for 2020, 2050, and 2080. Projected changes in annual maximum water levels were estimated using the longer-term +3.4 mm yr^{-1} trend from PR (Abeysirigunawardena and Walker, unpublished data, 2007). Figures 5.13a and b show the position of these estimated MaxWL scenarios on the cross-sectional topographic beach-dune profiles for Gilbert and Woodruff Bay beaches, respectively. These scenarios assume no significant changes to the regional significant wave height over the projected time intervals. An increase in average significant wave height would increase the wave runup values, which would also increase the projected water level scenarios. Thus, the scenarios presented here could be considered minimum projected extreme water level elevations based on the available wave record (1993-2006). This erosive water level trend indicates the potential of these beach-dune systems to experience dune migration or loss under future sea level rise scenarios.

The historical maximum total water level plus wave runup from the December 24, 2003 winter storm is shown on both scenario plots. Figure 5.14 illustrates the mean hourly wind speed during the storm at CSJ and the resulting wind-generated storm surge from the water level record during this event. From this, the link between persistent storm-driven winds and high surge levels is clear. Storm surges are major forcing parameters of high-energy beach-dune morphodynamics as beach-dune systems experience a seasonal cycle of aeolian-driven summer accumulation and

fall/winter surge-induced erosion (Ruz and Meur-Ferec, 2003). Future scenarios for erosive water levels on these beach-dune systems must, in addition to increasing water level trends, consider the influence of enhanced storminess and the associated increase in surge elevation.

Table 5.3: a) Mean and maximum water level summaries for 2006 and projected scenarios from the CSJ water level record for 2020, 2050, and 2080 based on a +1.7 mm yr^{-1} rise in mean water level and a +3.4 mm yr^{-1} rise in maximum water level (Abeysirigunawardena and Walker, unpublished data, 2007). b) Total mean and maximum potential water level values (including runup) for 2006 and projected scenarios for 2020, 2050, and 2080 at Gilbert Bay beach and Woodruff Bay beach. Potentially erosive events are defined as those that exceed the modern elevation of the beach-dune junction.

(a)

Year	**MWL** (m aCD)	**MaxWL** (m aCD)
2006	2.3	4.6
2020	2.5	5.0
2050	3.1	6.1
2080	3.6	7.1

(b)

	Year	**Gilbert Bay Beach**	**Woodruff Bay Beach**
MWL + runup (m aCD)	**2006**	6.02	5.74
	2020	6.24	5.96
	2050	6.57	6.47*
	2080	7.26*	6.98*
MaxWL + runup (m aCD)	**2006**	8.29*	8.01*
	2020	8.73*	8.45*
	2050	9.75*	9.47*
	2080	10.77*	10.5*

* = potentially erosive WL

Figure 5.14: Topographic profile showing projected maximum water level (WL) events for 2006, 2020, 2050, and 2080 based on climate change-induced sea level rise and calculated wave runup on a) Gilbert Bay beach and b) Woodruff Bay beach. Projected MaxWLs based on a rise of +3.4 mm yr^{-1} are shown as the longer lines, while the total water level, including runup, is represented by the shorter line associated with each Max WL line. Also shown is the maximum historical water level from the December 24, 2003 storm.

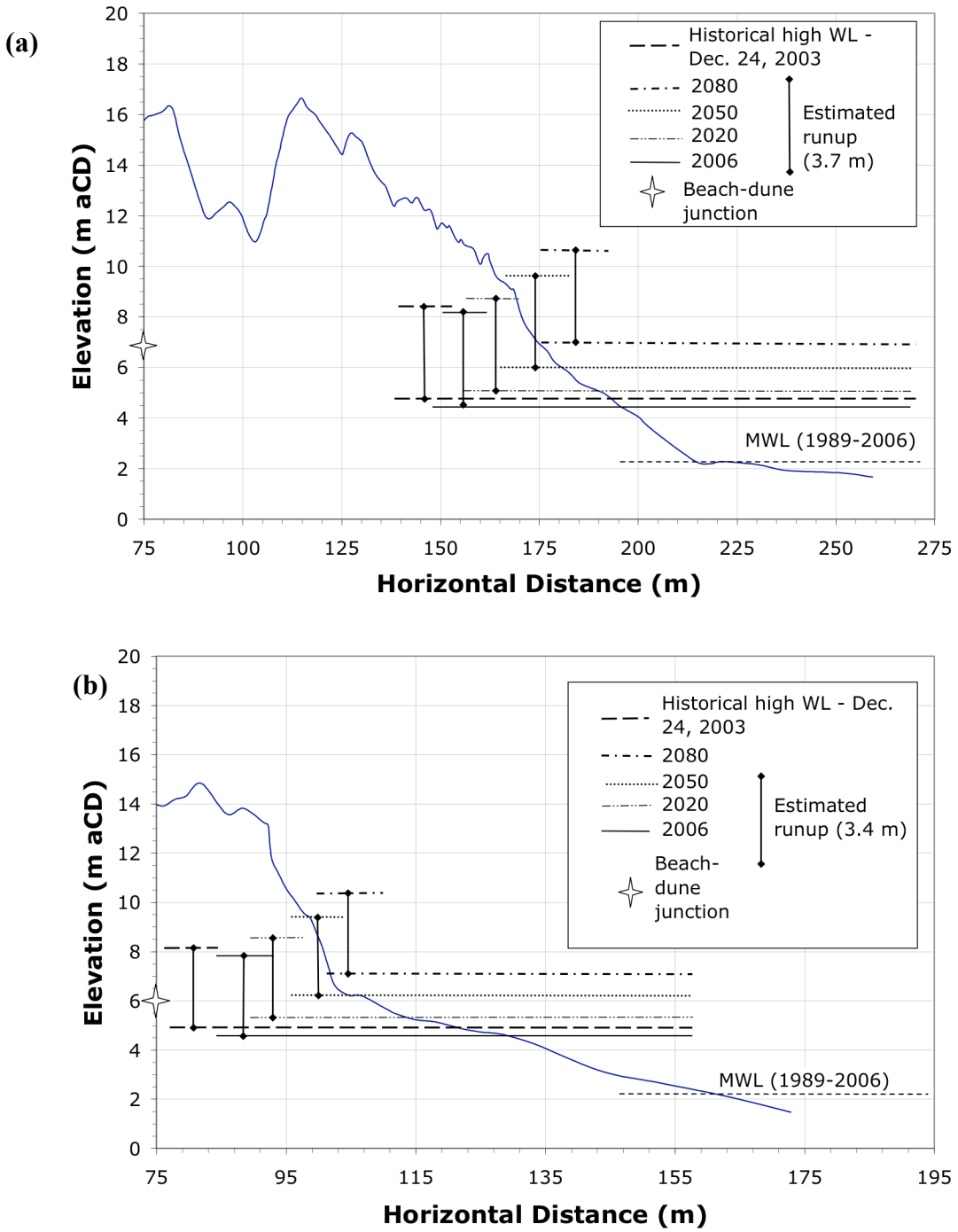

Figure 5.15: December 24, 2003 storm event as recorded at CSJ expressed by mean hourly wind speed (m s^{-1}) and surge (m). Indicates the influence of high persistent high winds on storm-induced high water levels.

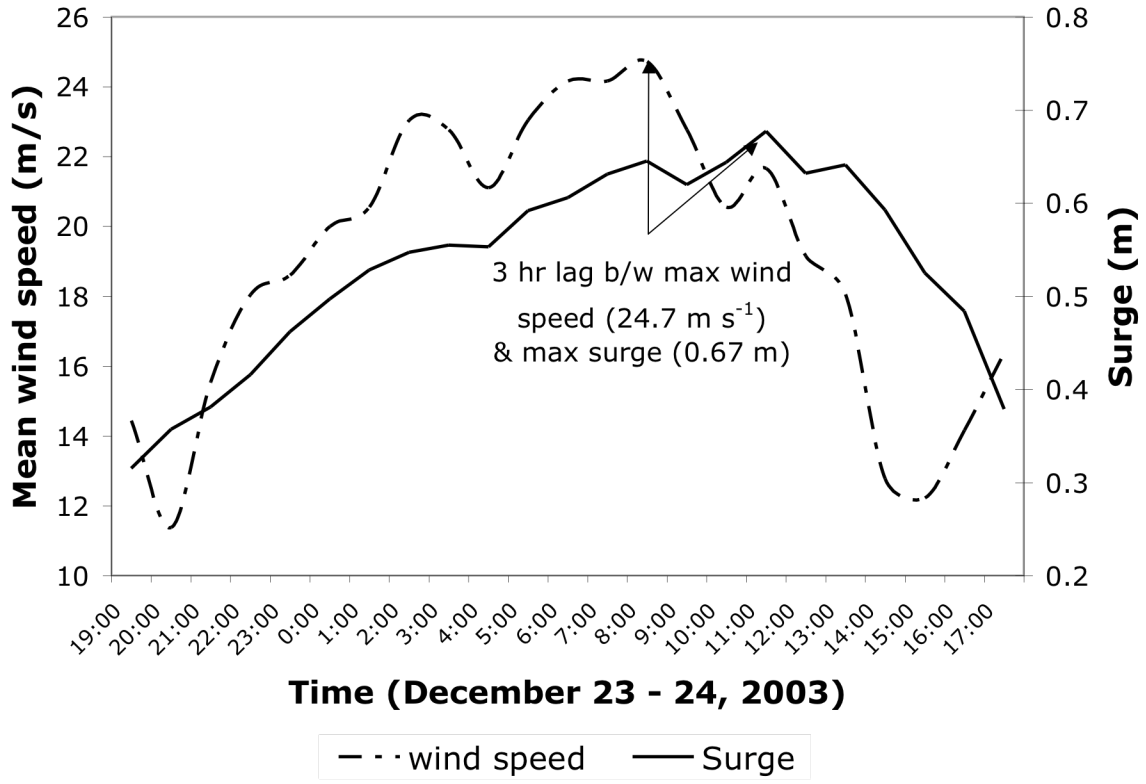

5.4 Summary

This chapter provides evidence that beach-dune systems in the CSJ region of HG experience a high-energy wind regime with a strong, primarily onshore RDP. The RDP at RS, in northern HG, is stronger than at CSJ because of more persistent, year-round competent (i.e., >6 m s^{-1}) SE winds. The large dunes at each beach-dune system provide evidence for the results from Fryberger's (1979) model, with the largest dunes on East Beach where the RDP is strongest (and sediment supply is unlimited) and smaller dunes in the embayed beach systems of the south (CSJ), where sediment supply is limited and RDP is slightly less due to higher directional variability in the competent wind regime.

The water level regime in both southern and northern HG is trending to more erosive conditions given climate change-induced rising sea levels and extreme water level events. This erosive regime combined with the generally strong onshore sediment supply indicates these systems may experience landward migration based on future projections of extreme water level unless the erosive water level rate increases such that onshore sediment transport cannot keep pace and result in a net dune loss. Coastal managers monitoring for climate change-induced changes in the morphodynamic regime of HG should consider several key factors, including: sea level rise, trends in erosive water levels, wave runup, storminess and associated surge levels, and variation in the regional wind regime (magnitude, frequency and direction).

6.0 Climate Variability Signals

This chapter examines regional climate variability signals in the water level regime at CSJ as a method for exploring the atmosphere-ocean drivers that may influence beach-dune morphodynamics within GH-NPR. The statistical techniques employed to generate the results in this chapter are used as a scoping tool to explore statistically significant relationships between water level data and climate variability index values. More rigourous statistical analyses are beyond the scope of this thesis, but are recommended for future research to gain a deeper understanding of the relationships identified here. Non-linear statistical techniques such as cumulative sum analysis and superposed epoch analysis, for example, may provide enhanced understanding of the regional climate variability regime shifts. Due to the limited length of the water level record for CSJ (1989-2006), longer-term water level and climate variability correlations derived from PR by Abeysirigunawardena and Walker (unpublished data, 2007) are used to provide a longer-term context.

6.1 Water level response to climate variability

6.1.1 Correlation analysis

Simple correlation analysis shows significant ($p < 0.01$) linear relationships between the averaged annual CSJ water level record and annual climate variability indices (Table 6.1). In the following results sections, $r < 0.3$ is considered a poor correlations, $0.3 > r > 0.6$ is considered a moderately strong correlation, and >0.6 is considered a strong correlation. These distinctions are qualitative in nature, based on similar exploratory statistical analysis (Abeysirigunawardena and Walker,

unpublished data, 2007). There is a moderate positive correlation between average annual water levels (AAWL) and MEI ($r = 0.532$), a strong positive correlation between AAWL and PDO ($r = 0.680$), a moderate negative correlation ($r = -0.547$) between NOI values and AAWL (Table 6.1), and a moderate positive correlation ($r = 0.398$) between ALPI and AAWL. Recall from Section 2.4 that positive MEI values and negative NOI values represent El Niño conditions. Annual MEI, NOI, PDO, and ALPI values do not provide any statistically significant correlations with maximum annual water levels (MaxWL).

Seasonal correlation analysis indicates that there is a moderately strong positive correlation ($r = 0.523$) between averaged winter (September to February) MEI values and winter average water levels (winter AWL) (Table 6.1). Additionally there is a significant ($p < 0.05$) strong negative correlation between average winter NOI values and winter AWL ($r = -0.623$) (Table 6.1). Summer (March-August) PDO values correlate significantly with summer average water levels (summer AWL) ($r = 0.784$) and summer maximum water levels (summer MaxWL) ($r = 0.623$). Summer AWL and summer MaxWL correlate moderately with summer NOI values ($r = -0.506$ and -0.499, respectively) (Table 6.1).

ALPI values moderately correlate with December to March AWL ($r = 0.576$) (Table 6.1). December to March MaxWL also correlates moderately ($r = 0.537$) with annual ALPI values (which are a manifestation of December to March conditions). Additionally, there is a strong positive correlation ($r = 0.779$, $p < 0.01$) with average annual surge values (measured total water level minus predicted tidal water level) and ALPI values (Table 6.1).

Table 6.1: Pearson's correlation coefficients for relations between annual, winter (September – February), and summer (March-August) average MEI, NOI, PDO, and ALPI levels and average annual and winter water level (AAWL) for CSJ (1989-2006) and PR (1932-2003; statistically significant ($p < 0.05$) relationships are highlighted. Note: Winter ALPI correlations are based on December – March average water levels and the annual ALPI values (which are derived from December to March conditions). PR data source: Abeysirigunawardena and Walker (unpublished data, 2007).

		MEI		NOI		PDO		ALPI	
		CSJ	PR	CSJ	PR	CSJ	PR	CSJ	PR
Annual AWL	Pearson's r	0.532	0.569	-0.547	-0.577	0.680	0.650	0.398	0.483
	Sig.	0.023	0.000	0.019	0.000	0.002	0.000	0.102	0.000
Annual MaxWL	Pearson's r	0.288	n/a	-0.061	n/a	0.369	n/a	0.075	n/a
	Sig.	0.247	n/a	0.809	n/a	0.132	n/a	0.766	n/a
Winter AWL	Pearson's r	0.523	0.640	-0.623	-0.654	0.358	0.477	0.576	n/a
	Sig.	0.026	0.000	0.006	0.000	0.145	0.000	0.012	n/a
Winter MaxWL	Pearson's r	0.309	n/a	-0.353	n/a	0.359	n/a	0.537	n/a
	Sig.	0.213	n/a	0.151	n/a	0.144	n/a	0.022	n/a
Winter Surge	Pearson's r	0.294	n/a	-0.407	n/a	0.420	n/a	0.784	n/a
	Sig.	0.237	n/a	0.093	n/a	0.083	n/a	0.000	n/a
Summer AWL	Pearson's r	0.348	0.478	-0.506	-0.481	0.784	0.628	n/a	n/a
	Sig.	0.158	0.000	0.032	0.000	0.000	0.000	n/a	n/a
Summer MaxWL	Pearson's r	0.23	n/a	-0.499	n/a	0.623	n/a	n/a	n/a
	Sig.	0.359	n/a	0.035	n/a	0.006	n/a	n/a	n/a

Correlation coefficients between MEI, PDO, NOI, ALPI, and AAWL at PR are also presented in Table 6.1 (from Abeysirigunawardena and Walker, unpublished data, 2007). These results are based on 71 years of data from the PR water record, and thus provide stronger statistical relationships (i.e., lower p-values, based on a larger sample size) than those for the CSJ record, which is only 17 years (1989-2006). As such, these correlation coefficients from PR provide a statistical extension of the regional picture for the results from CSJ. The results from PR indicate that there are statistically significant ($p < 0.01$) correlations between AAWL and MEI ($r = 0.569$), NOI ($r = -0.577$), PDO ($r = 0.650$), and ALPI ($r = 0.483$) (Table 6.1). This analysis also reveals seasonal relationships between climate variability indices and water levels at PR. There are statistically significant ($p < 0.01$) correlations between winter

AWLs (September to February) and winter MEI (r = 0.640), NOI (r = -0.654), and PDO (r = 0.477) averages. Similarly, there are statistically significant correlations between summer AWLs (March to August) and summer MEI (r = 0.478), NOI (r = -0.481), and PDO (r = 0.628) averages. In their statistical analysis, Abeysirigunawardena and Walker (unpublished data, 2007) do not provide correlation coefficients for maximum water levels or surge.

Several correlations from PR support those from CSJ. The correlation for winter AWL and winter MEI, for example, is positive and moderate to strong for data from both locations, with r = 0.640 at PR and r = 0.523 at CSJ. Also, all three (average, winter, and summer) correlation coefficients for NOI and average water level are significant at both sites. That is, at both sites there is a moderately strong correlation (r = -0.577 at PR and r = -0.547 at CSJ) between water levels and NOI. At both locations, there are also significant correlations between NOI and summer AWL (r = -0.481 at PR and r = 0.506 at CSJ) and NOI and winter AWL (r = -0.654 at PR and r = -0.623 at CSJ). Summer AWLs also show strong positive correlation with summer PDO averages (r = 0.628 at PR and r = 0.784 at CSJ).

6.1.2 Simple linear regression analysis

Linear regression models applied to the statistically significant linear relationships identified above provide an indication of the degree of influence that the climate variability signals (independent variable) have on water levels (dependent variable). For example, 28% of the variation in AAWL can be explained by ENSO as expressed by positive MEI values ($R^2 = 0.28$) (Figure 6.1a). Similarly, negative NOI values show a moderately strong linear relationship with AAWL ($R^2 = 0.30$) (Figure

6.1b). The strongest linear relationship with AAWL is with the PDO (R^2 = 0.46) (Figure 6.1c).

Seasonal analysis of water levels and climate index values also identifies some strong associations as indicated by moderate to high R^2 values. The strongest linear relationship exists between summer AWL (March to August) and summer average PDO values (R^2 = 0.61) (Figure 6.2a). There is an equally strong association between annual surge values (observed total water level minus predicted tidal water level) and the strength of the Aleutian Low as expressed by the annual ALPI value (R^2 = 0.62) (Figure 6.3c). Weaker associations were also found in the linear regression model for winter AWLs and ENSO, represented by the -NOI and +MEI (R^2 = 0.39 and 0.27, respectively) (Figures 6.2c and d).

The association between winter AWL (September to February) and PDO is weak (R^2 = 0.12). Linear regression analysis of summer averages does indicate, however, that PDO forcing may account for ~61% of the variation in summer AWL (R^2 = 0.61) and ~39% of variation in summer MaxWL (R^2 = 0.39) (Figures 6.2a and b). Summer AWL and summer MaxWL are moderately associated with summer NOI (R^2 = 0.26 and 0.25, respectively).

Figures 6.3a-c represent the significant effects of the Aleutian Low on water levels at CSJ. There is a moderately strong association between December to March AWL (R^2 = 0.33) and ALPI as well as December to March MaxWL and ALPI (R^2 = 0.29) (Figures 6.3a and b). The strongest linear association for ALPI is with annual surge (R^2 = 0.62).

Figure 6.1: Simple linear regression models for: a) AAWL vs. annual average MEI, b) AAWL vs. average annual NOI, and c) AAWL vs. average annual PDO. 95% confidence intervals shown.

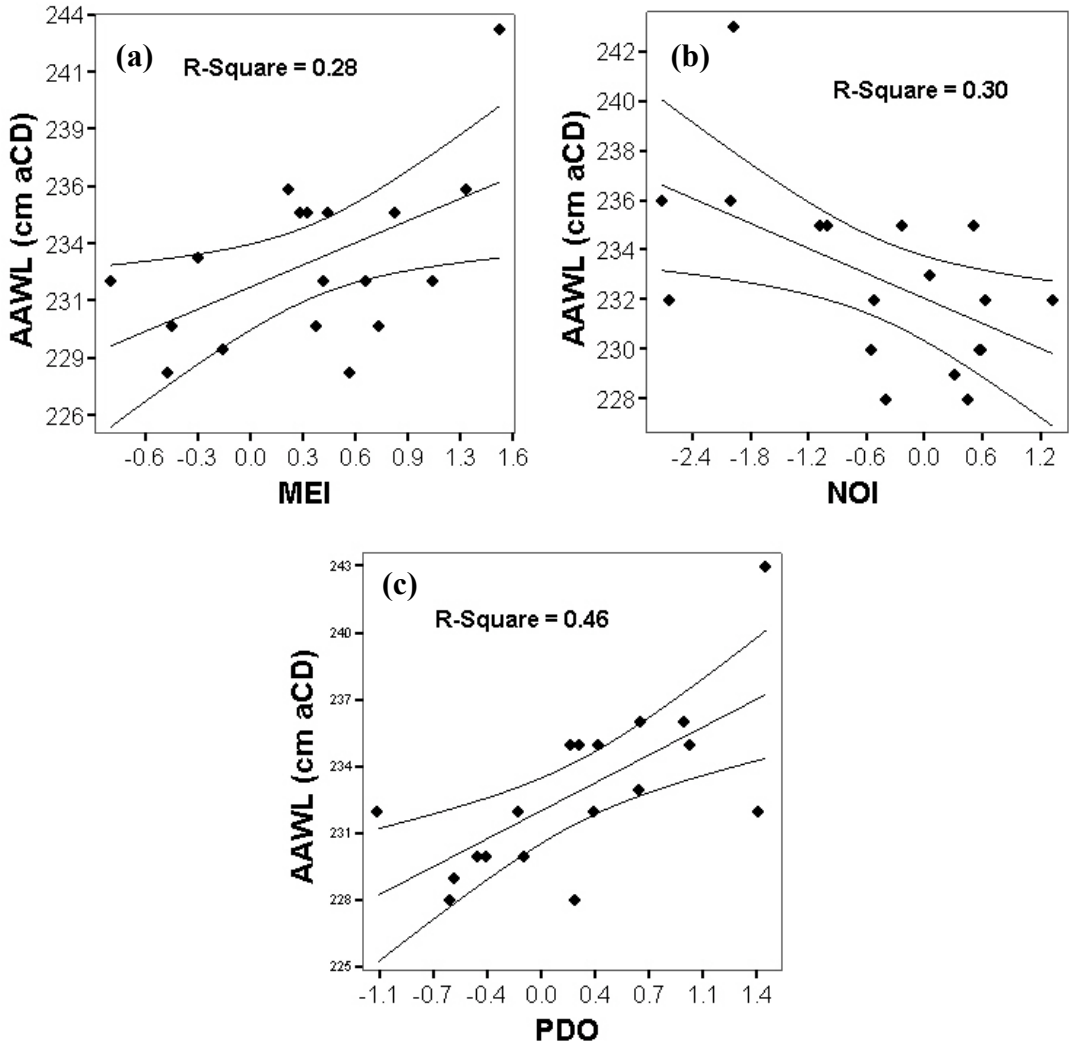

Figure 6.2: Simple linear regression models for: a) summer AWL (March to August) vs. summer average PDO; b) summer MaxWL vs. summer average PDO; c) winter AWL (September to February) vs. winter average MEI; and d) winter AWL vs. winter average NOI at CSJ. 95% confidence intervals shown.

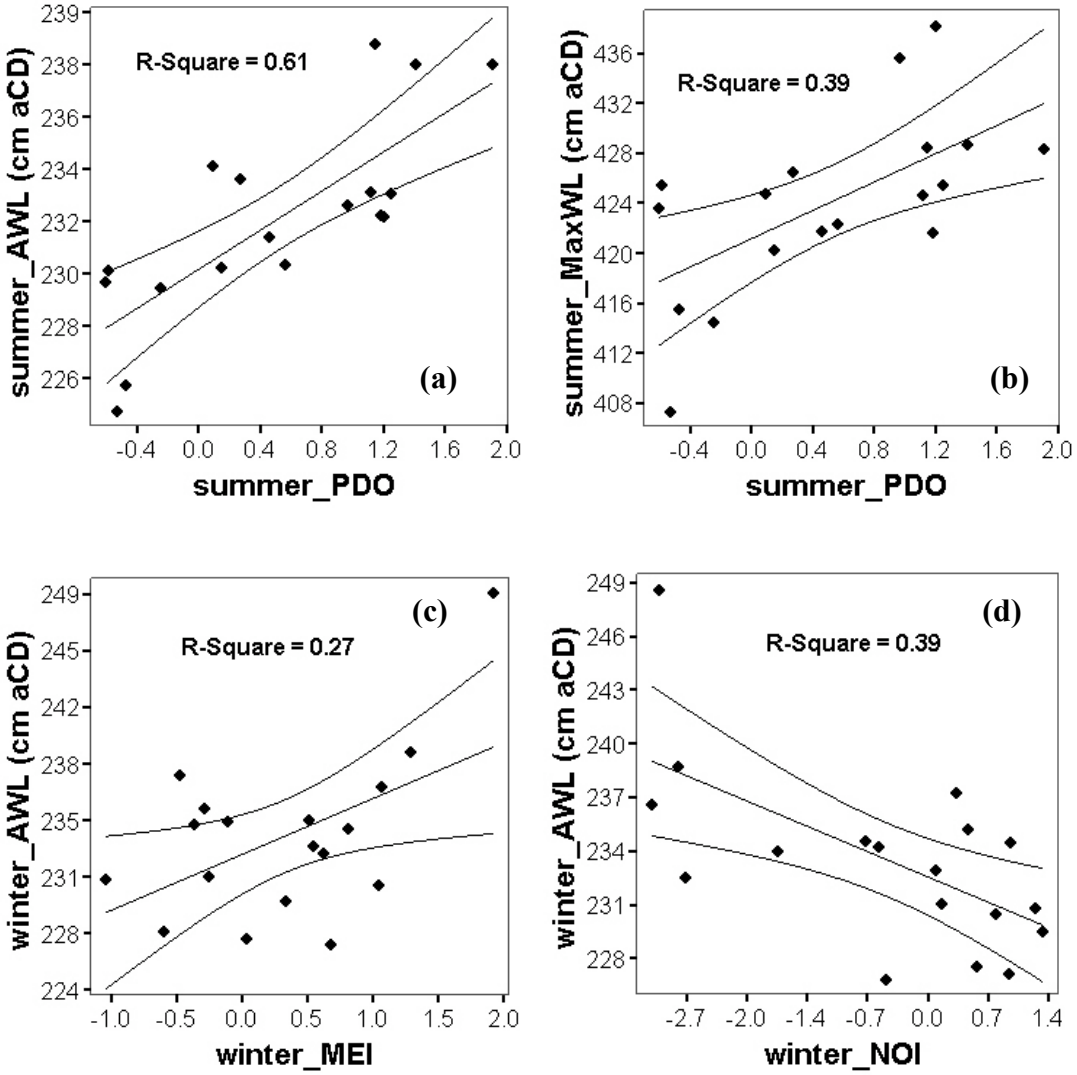

Figure 6.3: Simple linear regression models at CSJ for: a) December to March AWL vs. ALPI; b) December to March MaxWL vs. ALPI; and c) annual average surge vs. ALPI. 95% confidence intervals shown.

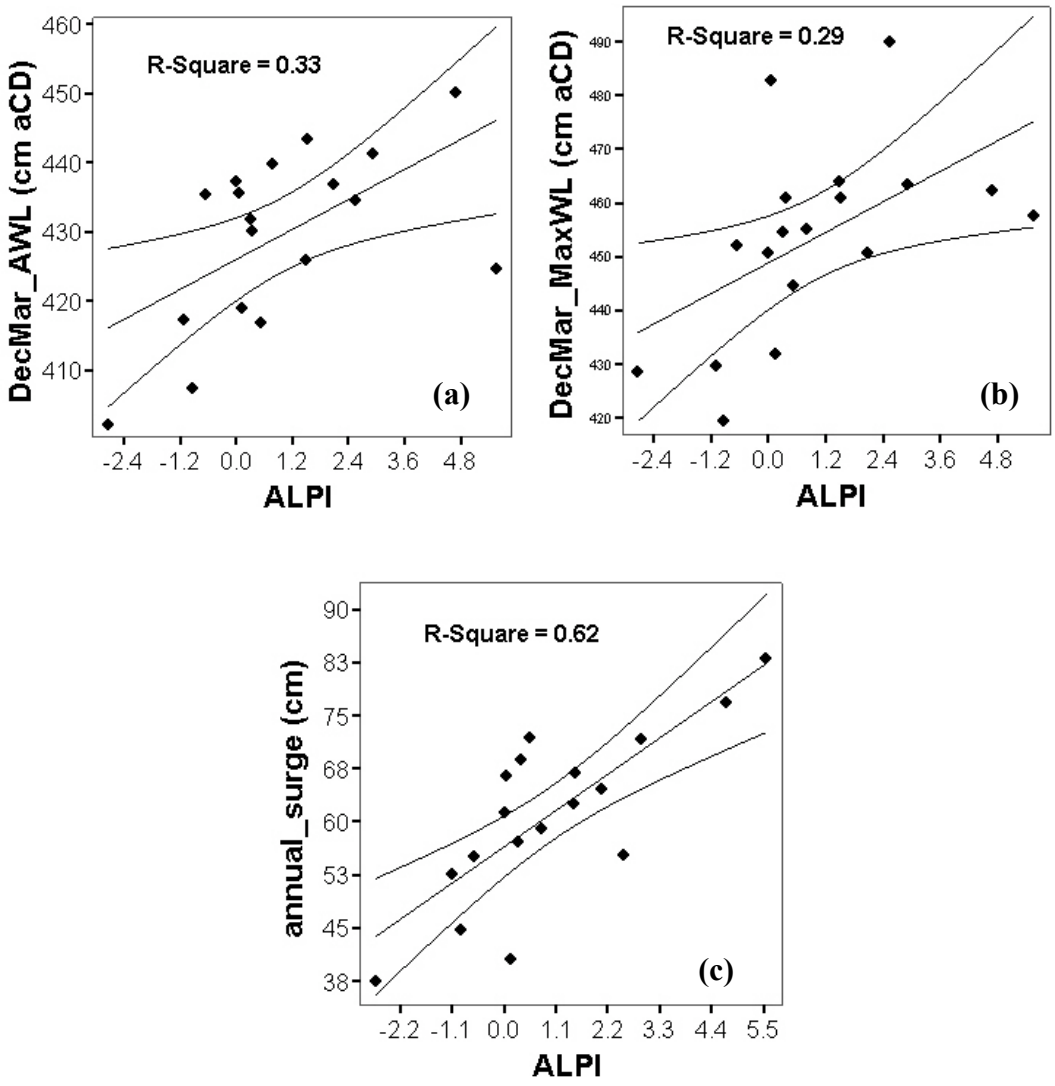

6.1.3 Graphical analysis of residuals

Graphical analysis of residual (i.e., the difference from the long-term average) annual climate variability index values and residual mean annual water levels at CSJ yields qualitative results that provide additional information about the regional climate variability signals at CSJ (Figures 6.4a-c). Figure 6.4a shows the temporal similarities in the residual AAWL and MEI trends. There is a coinciding peak in both AAWL and MEI strength in 1992 and 1997. There are dramatic decreases in both values in 1998 (a strong El Niño year). This decrease is followed by gradual increases in both trends until 2003, followed by variable trends through to 2006. Generally, when water levels are higher than average, MEI values are also stronger than average.

There is a strong temporal relationship between AAWL and NOI residual values (Figure 6.4b). In this plot, the negative relationship between NOI values and AAWL is apparent in the opposition of the trend lines. Years with anomalously low (-) NOI values (El Niño conditions) correspond to years with anomalously high AAWL values and, similarly, years with high NOI residuals correspond to years with low residual AAWL values.

The residual plot for AAWL and PDO values illustrates that strong positive PDO years correspond to years with high AAWL (Figure 6.4c). In particular, the PDO and AAWL residuals are very similar in 1997.

Figure 6.4: Residual annual average water levels (AAWL) from CSJ (1989-2006) with a) residual NOI values, b) residual MEI values, and c) residual PDO values. AAWL values above the standard deviation (SD) bars indicate strong +/- climate variability events.

(a)

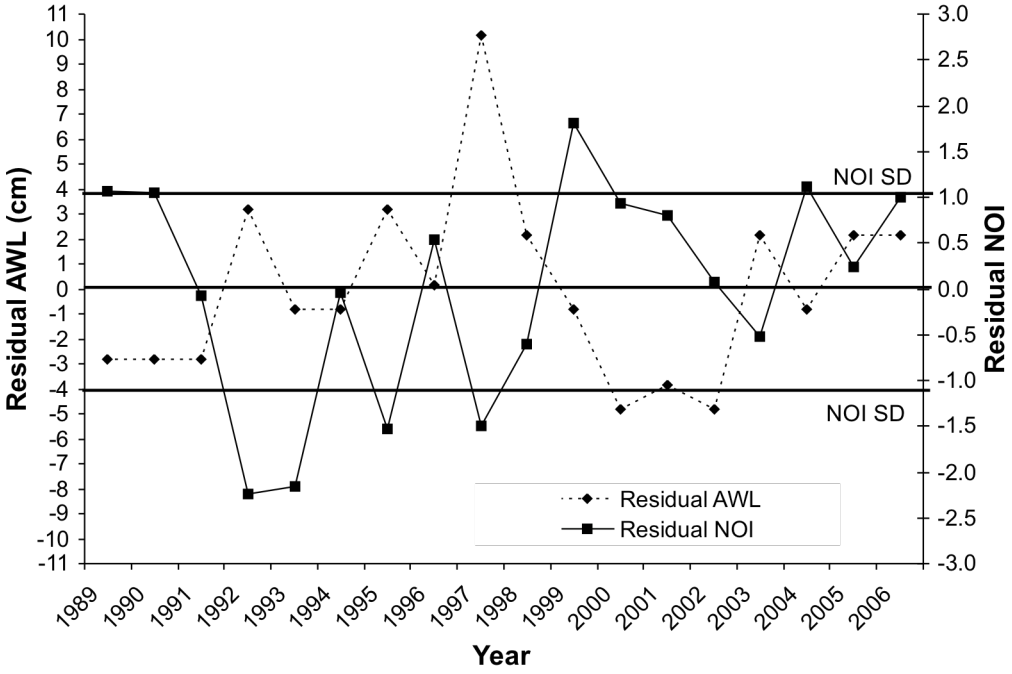

(b)

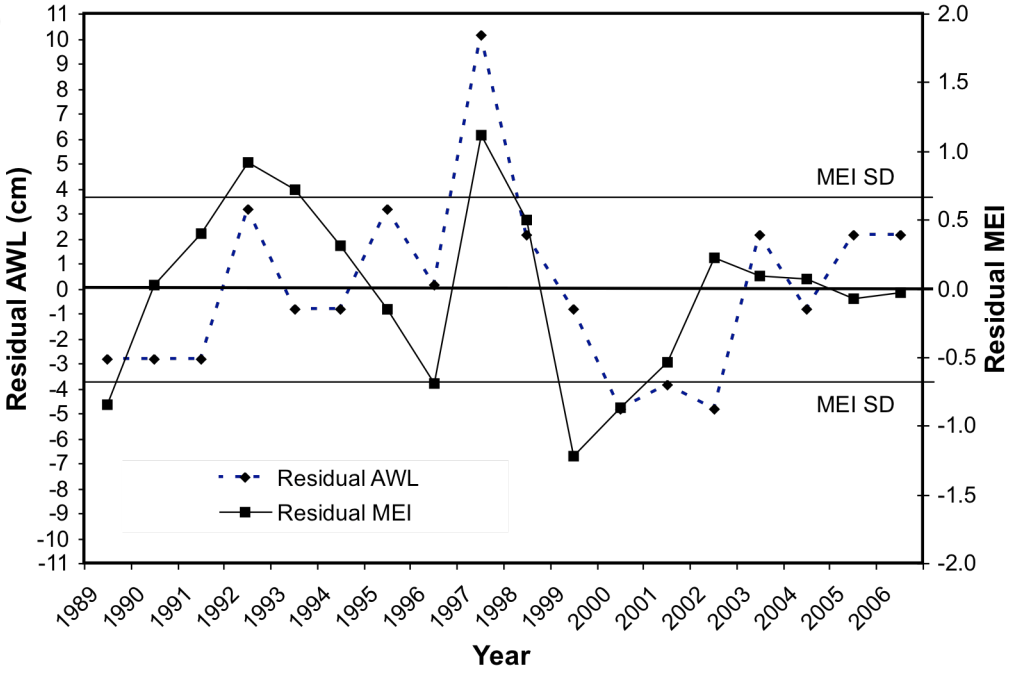

(c)

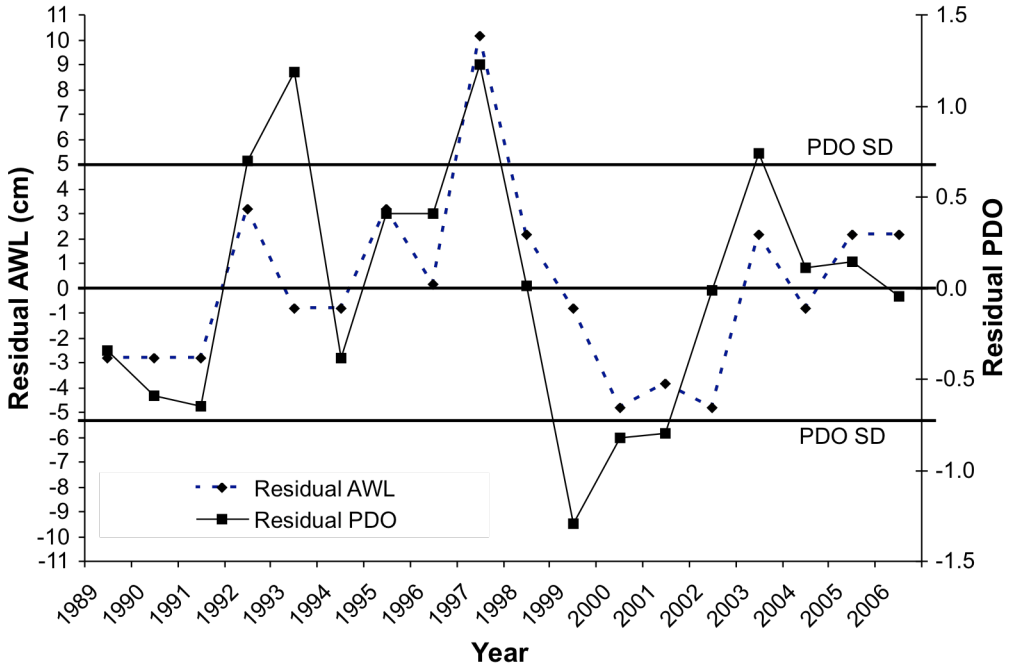
Residual AWL (cm)
Residual PDO
Year
PDO SD
PDO SD
Residual AWL
Residual PDO
11
10
9
8
7
6
5
4
3
2
1
0
-1
-2
-3
-4
-5
-6
-7
-8
-9
-10
-11
1.5
1.0
0.5
0.0
-0.5
-1.0
-1.5
1989
1990
1991
1992
1993
1994
1995
1996
1997
1998
1999
2000
2001
2002
2003
2004
2005
2006

6.2 Discussion

The third objective of this thesis was to identify regional climatic variability signals in the total water level regime at CSJ and to compare these to the long-term, regional water level signal from PR. Results from the analysis presented in this chapter indicate that ENSO, PDO, and ALPI climate variability signals exert control on regional annual average water levels at CSJ. This study, combined with results from PR (Abeysirigunawardena and Walker, unpublished data, 2007), also illustrates that atmospheric and oceanic forcing of regional water levels varies seasonally.

Strong El Niño events are characterized by elevated sea levels along the west coast of North America (Crawford et al., 1999; Storlazzi and Griggs, 2000; Subbotina et al., 2001; Allan and Komar, 2002, 2006; Abeysirigunawardena and Walker, unpublished data, 2007). ENSO-related sea level variability along the west coast of the Americas occurs due to a combination of oceanic poleward propagation of coastally trapped waves and atmospheric teleconnections (Subbotina et al., 2001). North from the equator to the coast of central California, oceanic forcing (e.g., Kelvin wave propagation) dominates, while north of this region, atmospheric teleconnections (e.g., large-scale atmospheric pressure fields and/or the accompanying oceanic wind field) appear to drive sea level response (Emery and Hamilton, 1985; Ruggiero et al., 1997; Overland et al., 2001; Subbotina et al., 2001). During strong ENSO events, there is also a known intensification of the Aleutian Low in the North Pacific, particularly in the winter (Emery and Hamilton, 1985; Byshev and Lebedev, 2000). This intensification contributes to elevated average water levels on the west coast of North America during strong ENSO events (e.g., 1997-98) via warmer coastal SST

(thermal expansion effects) and enhanced SE sea surface winds (Trenberth and Hurrell, 1994; King et al., 2000).

At CSJ, ENSO-related water level forcing is illustrated in the synchronicity between residual AAWL and strong +MEI values (Figure 6.4a) and in the asynchronous trends between residual AAWL and strong -NOI values (Figure 6.4b). There is a notably stronger synchronicity between AAWL and the El Niño phases of the climate indices (+MEI, -NOI). Because the NOI represents the extra-tropical expression of ENSO in the NE Pacific, the correlation between water levels and climate variability index values is, as anticipated, stronger than for MEI, which is not regionally specific. Negative NOI values represent strong ENSO years. As such, Figure 6.4b exemplifies (qualitatively) how ENSO appears to be a key driver of AAWL in this region, as expressed in the +/- NOI residuals and the corresponding +/- AAWL residuals. Every anomalously low NOI year corresponds directly to an anomalously high water level and, when the residual NOI value nears zero, so does the residual water level value.

Although there is markedly less literature assessing water level response to the PDO, on the coast of BC it appears that PDO forcing exerts an even more significant influence on annual sea level variability than ENSO (Abeysirigunawardena and Walker, unpublished data, 2007). Figure 6.4c qualitatively illustrates the PDO-related forcing of water levels at CSJ. Generally, years with strong +PDO values correspond to high AAWL. Multiple regression analysis of MEI, NOI, PDO, ALPI and AAWL reveals that the longer-term regional variation in annual water levels is most strongly correlated with the PDO (Abeysirigunawardena and Walker,

unpublished data, 2007). This oceanic forcing is caused by thermal expansion effects on the ocean caused by enhanced SST and strengthening Aleutian Low during positive PDO phases (Mantua and Battisti, 1995; Zhang et al., 1997).

Seasonal analysis indicates that in the winter, ENSO forcing dominates over PDO forcing. More than 50% of the variability in winter water levels at CSJ is controlled by ENSO (+MEI, -NOI). Similar results exist for PR, where ENSO (expressed in MEI and NOI) accounts for >60% of the seasonal water level (Abeysirigunawardena and Walker, unpublished data, 2007). Figure 6.5 illustrates the significant influence of strong ENSO events (e.g., the 1997-1998 El Niño) on the regional water levels at CSJ, particularly winter water levels. Compared to the monthly average water levels for the available record (1989-2006), the 1997-1998 monthly water levels are up to 30 cm greater (February). Crawford et al. (1999) identified a similar trend in the water level record from Tofino, BC, where, during strong El Niño winters, water levels typically rise ~10-20 cm above seasonal heights. During the 1997-1998 El Niño event, water levels in Hecate Strait rose up to 40 cm (Barrie and Conway, 2002). These elevated water levels typically remain for several months (Crawford et al., 1999).

Figure 6.5: Monthly average water levels at CSJ from the entire available record (1989-2006) and from the strong 1997-1998 El Niño event indicating strong winter ENSO forcing of elevated water levels.

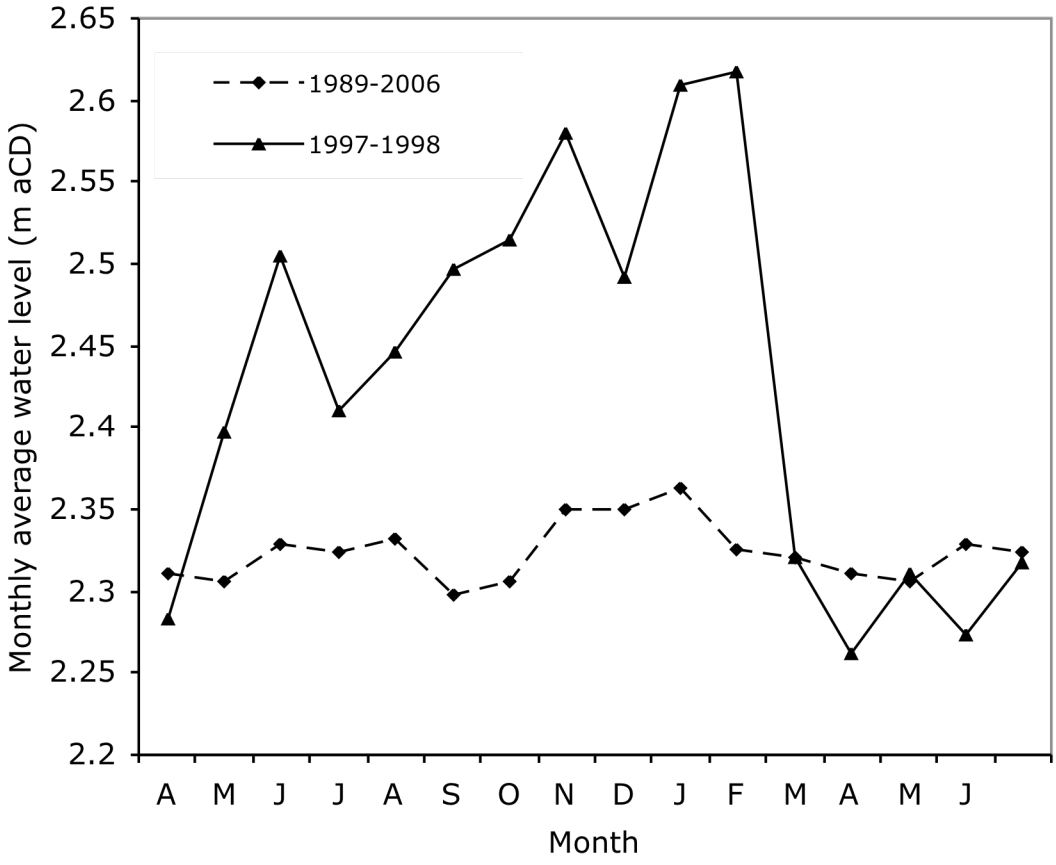

Winter (September - February) water levels in this region of the NE Pacific appear to be controlled primarily by atmospheric forcing due to amplified variations in sea level pressure and/or surface wind stress along the coastal margins during strong El Niño events (Subbotina et al., 2001). The weakened equatorial trade winds associated with El Niño events (+MEI, -NOI) cause an intensification of the jet stream, which strengthens the winter Aleutian Low and weakens the North Pacific High (Emery and Hamilton, 1985; Byshev and Lebedev, 2000). During periods with a strong Aleutian Low, storm tracks move further south and S-SE surface winds increase (Trenberth and Hurrell, 1994). The stronger winds result in enhanced storm surge development in coastal waters, which contribute to elevated winter water levels. Some of the strongest correlations between climate variability and water levels at CSJ occur from synoptic scale atmospheric forcing due to strengthening of the Aleutian Low (represented by the ALPI). ALPI, an annual value based on winter (December – March) conditions (Beamish et al., 1997), correlates significantly with December to March AWL, December to March MaxWL, as well as annual average surge values.

While atmospheric forcing related to ENSO and ALPI exerts significant control on winter water levels, oceanic (SST) forcing related to the PDO appears to seasonally control summer (March – August) water levels in this region. Statistical results from CSJ, as well as from the longer-term regional signal at PR, illustrate this seasonal forcing. Persistent SST warming from the 20-30 year PDO cycle may be the cause of this summer climate variability signal (Abeysirigunawardena and Walker, unpublished data, 2007), though a detailed understanding of the PDO phenomenon is still lacking.

Statistical analysis of the CSJ water level record and the PDO is limited because the length of the record (17 years) is shorter than the length of the phenomenon (20-30 years). The PDO regime shift that occurred in 1977, for example, is not captured by the CSJ water level record. As such, the statistical significance of the linear relationship between AAWL and PDO may be lower than if the record extended back into the 1970s. Graphically, there is a correspondence between PDO values and AAWL at CSJ (Figure 6.4c). In particular, years with strong ENSO values (+MEI, -NOI) coupled with strong PDO values are associated with the highest AAWL. That is, the water level forcing effects of ENSO and PDO appear to be additive. The influence of warmer sea surface temperatures coupled with lower pressure atmospheric conditions causes particularly high water levels (Walker, 2006).

Further analysis of statistical relationships between water levels at CSJ and the PDO is not possible without a longer record. For now, the best alternative is to utilize the longer-term regional record and climate variability signals from PR (Abeysirigunawardena and Walker, unpublished data, 2007) as a context for the more limited results from CSJ presented in this chapter. Future efforts should also consider the added resolution provided by non-linear statistical techniques applied to climate variability signal analysis.

6.3 Summary

The results in this chapter provide statistical and graphical evidence that variations in water levels at CSJ are driven by known climate variability phenomena. Generally, water levels at CSJ are primarily controlled by the PDO and ENSO

climate signals. Furthermore, atmospheric forcing from the ALPI signal exerts a strong control on winter maximum water levels and storm surge generation due to enhanced sea surface winds. Statistical correlation analysis indicates that several similarities exist in the response of water levels at PR and CSJ to atmospheric and oceanic forcing due to climate variability signals. Most notably, ENSO-related forcing of water levels dominates in the winter, while PDO-related forcing dominates in the summer. These similarities help to broaden the spatial boundaries of the regional influence of known climate variability signals (namely, ENSO, PDO, and ALPI) on water levels in NE Pacific.

The apparent influence of climate variability signals on water levels in this region has important implications for coastal erosion, especially considering that these enhanced water levels are super-imposed on longer-term sea level rise, as discussed in Chapter 5. As suggested by Abeysirigunawardena and Walker (unpublished data, 2007), smaller-scale climate variability impacts may be more hazardous to coastal areas than longer-term climate change-induced sea level rise. Coastal park managers must, therefore, consider the role of annual, inter-annual, and inter-decadal climate variability when projecting future coastal erosion regimes and hazards in this region of the NE Pacific.

7.0 Summary and Conclusions

The purpose of this research was to conduct a detailed assessment of the geomorphology and climate variability responses of two beach-dune systems in Gwaii Haanas National Park Reserve and Haida Heritage Site (GH-NPR). The research established the foundation for a park-wide geoindicator monitoring initiative that will assist park managers in understanding and adapting to climate variability and climate change-induced changes affecting the coastal systems in this area of the Pacific margin of Canada.

The specific objectives of this thesis were to: i) describe and classify the geomorphic controls and features of Gilbert and Woodruff Bay beaches, ii) estimate the erosional and rebuilding regimes of the Cape St. James (CSJ) region of Haida Gwaii (HG), and iii) identify regional climatic variability and climate-change induced signals in the water level regime of the CSJ region of HG. Based on these objectives, the key findings of this research are presented below.

- The geomorphic assessment of Gilbert Bay and Woodruff Bay beaches in Chapter 4 illustrates that these beach-dune systems in the CSJ region are responding distinctly to the regional morphodynamic conditions (e.g., wind, waves, and water levels). Gilbert Bay beach has actively prograding dune ridges, while Woodruff Bay beach has large erosive scarps on the established foredune. Aspect to the erosive water level regime and competent wind regime and embayment size appear to control these distinct geomorphic responses.

- In comparison to the northern region of HG (e.g., Rose Spit and East Beach), the geomorphology in GH-NPR is significantly different primarily due to differences in sediment supply as a result of variations in the Quaternary glacial history of these

two regions. The large dunes on East Beach have a continuous sediment supply from the eroding glacial outwash sediments stored in cliffs along the coast of NE Graham Island (e.g., Cape Ball). In the south, however, most beach-dune systems are embayed and have a limited and episodic sediment supply.

- The northern and southern regions of HG have strong dune rebuilding potential due to their highly energetic onshore aeolian wind regimes. The southern (CSJ) region of HG experiences a strong (annual average wind speed = 8.9 m s^{-1} and RDP = 1542), seasonally bimodal wind regime with high onshore (at Gilbert Bay beach) and alongshore (at Woodruff Bay beach) aeolian sediment transport potential.

- The CSJ region is characterized by an increasingly erosive water level regime, with annual average water levels increased by at least +1.6 mm y^{-1}, and annual maximum water levels increasing by +3.4 to +16.7 mm y^{-1}. This water level regime is driven by ENSO- and PDO-driven climate variability events. These climate variability signals appear to exert seasonal forcing on regional water levels with PDO forcing dominating in the summer and ENSO forcing in the winter. These results support similar findings from the longer-term regional record at PR.

- Combined, the aeolian sediment transport potential and the erosive water level regime at CSJ suggest that beach-dune systems in this region may respond by migrating landward, keeping pace with increasing sea level (per Davidson-Arnott, 2005). This landward migration will only occur if there is a sufficient sediment supply. Alternatively, if sea levels rise too quickly or if sediment supply decreases, the dune systems may not be able to keep pace, which will result in a net loss of sediment and erosion of the dune systems may occur. Under rising sea levels, these beach-dune systems could see net coastal retreat of 16-20X the amount of sea level rise considering beach slopes of 0.05-0.06 (per Bruun, 1964; SCOR working group 89, 1991).

- Figure 5.13 provides conceptual illustration of the possible future states of Gilbert and Woodruff Bay beaches under a plausible 20 cm rise in sea level. Provided sufficient winds persist in this region, aeolian delivery could result in a landward migration of the modern prograding dune ridges at Gilbert Bay beach by up to 3.5 m, based on the beach slope of 0.06. At Woodruff Bay beach, the large scarp could migrate landward as extreme water levels continue to erode the foredune. On Woodruff Bay beach, 20 cm of sea level rise could result in landward migration of the beach-dune profile up to 4 m, based on the beach slope of 0.05.

7.1 Future considerations

This research successfully establishes the baseline geomorphic and morphodynamic assessments of the CSJ region of GH-NPR. In doing so, several future research considerations are identified, including:

- Continued monitoring via repeat (annual and seasonal) topographic profile surveys at both beaches will increase the capacity of future efforts to estimate rates of dune growth, migration, progradation, or erosion.

- More rigourous bathymetric surveys and sediment sampling at both sites will enable assessment of nearshore geomorphology and sedimentary composition.

- Optical dating of the relict dune ridges at Gilbert and Woodruff Bays will estimate a minimum date of dune stabilization and rates of dune progradation which will strengthen the understanding of the historic and pre-historic morphodynamics of these beach-dune systems.

- Site-specific wind data collection and onsite aeolian sediment transport and erosion/accretion measurements at Gilbert Bay and Woodruff Bay beaches will enhance understanding of local aeolian rebuilding potential and dune maintenance. In turn, this will help verify the representativeness of the RDP calculation for this region.

- Non-linear statistical analysis of the regional water level record and climate variability indices would enhance the significance of the relationships identifies in the exploratory analysis presented in this thesis.

References

Aagaard, T., Davidson-Arnott, R., Greenwood, B., and Nielsen, J., 2004. Sediment supply from the shoreface to dunes linking sediment transport measurements and long-term morphological evolution. Geomorphology 60: 204-224.

Abeysirigunawardena, D.S., and Walker, I.J., unpublished data, 2007. Sea level response to climatic variability and change in Northern British Columbia. Manuscript submitted to Atmosphere-Ocean.

Allan, J.C., and Komar, P.D., 2002. Extreme storms on the Pacific Northwest coast during the 1997-98 El Niño and 1998-9 La Niña. Journal of Coastal Research 18: 175-193.

Allan, J.C., and Komar, P.D., 2006. Climate controls on US west coast erosion processes. Journal of Coastal Research 22: 511-529.

Anderson, J., and Walker, I.J., 2006. Airflow and sand transport variations within a backshore-parabolic dune plain complex: NE Graham Island, British Columbia, Canada. Geomorphology 77: 17-34.

Anthony, E.J., 1998. Sediment-wave parametric characterization of beaches. Journal of Coastal Research 14: 347-352.

Anthony, E.J., 2000. Marine sand supply and Holocene coastal sedimentation in northern France between the Seine estuary and Belgium. In: Pye, K., and Allen, J.R.L. (Editors), Coastal and Estuarine Environments - Sedimentology, Geomorphology and Geoarchaeology. Special Publications of the Geological don. Geological Society of London, London, UK.

Anthony, E.J., and Orford, J.D., 2002. Between wave- and tide-dominated coasts: the middle ground revisited. Journal of Coastal Research SI 36: 8-15.

Arens, S.M., 1994. Aeolian Processes in the Dutch Foredunes. Unpublished Ph.D. Thesis, University of Amsterdam, Amsterdam.

Arens, S.M., 1996. Patterns of sand transport on vegetated foredunes. Geomorphology 17: 339-350.

Arens, S.M., van Kaam-Peters, H.M.E., and van Boxel, J.H., 1995. Airflow over foredunes and implications for sand transport. Earth Surface Processes and Landforms 20: 315-332.

Arens, S.M., Jungerius, P.D., and Van Der Meulen, F., 2001. Coastal dunes. In: A. Warren, and French, J.R. (Editors), Habitat Conservation: Managing the Physical Environment. John Wiley & Sons Ltd., Chichester, UK.

Aubrey, D. G., 1979. Seasonal patterns of onshore/offshore sediment movement. Journal of Geophysical Research 84, 6347-6354.

Bagnold, R.A., 1941. The Physics of Blown Sand and Desert Dunes. Methuen, London.

Ballantyne, A., personal communication, 2006. Canadian Hydrographic Service, Pacific Region. Fisheries and Oceans Canada.

Barrie, J.V., and Conway, K., 2002. Rapid sea level change and coastal evolution on the Pacific margin of Canada. Sedimentary Geology 150: 171-183.

Barrie, V.J., Conway, K.W., Josenhans, H.W., Clague, J.J., Mathewes, R.W. and Fedje, D., 2005. Late Quaternary geology of Haida Gwaii and surrounding marine areas. In: Fedje, D.W., and Mathewes, R.W. (Editors). Haida Gwaii: Human history and environment from the time of Loon to the time of the Iron People. University of British Columbia Press, Vancouver, B.C.

BCMWLAP (Ministry of Water, Land and Air Protection), 2002. Indicators of climate change for British Columbia. Government of British Columbia, Victoria. 48pp. Accessed January 12, 2006 from http://www.env.gov.bc.ca /air/climate/indicat/index.html.

Beamish, R.J., and Bouillon, D.R., 1993. Pacific salmon production in relation to climate. Canadian Journal of Fisheries and Aquatic Sciences 50: 1002-1016.

Beamish, R.J., Neville, C.M., and Cass, A.J., 1997. Production of Fraser River sockeye salmon (*Oncorhynchus nerka*) in relation to decadal-scale changes in the climate and the ocean. Canadian Journal of Fisheries and Aquatic Sciences 54: 543-554.

Bernabeu, A.M., Medina, R. and Vidal, C., 2003a. A morphological model of the beach profile integrating wave and tidal influences. Marine Geology 197: 95-116.

Bernabeu, A.M., Medina, R., and Vidal, C., 2003b. Wave reflection on natural beaches: an equilibrium beach profile model. Estuarine Coastal and Shelf Science 57: 577-585.

Blaise, B., Clague, J.J., and Mathewes, R.W., 1990. Time of maximum late Wisconsin glaciation, West coast of Canada. Quaternary Research 34: 282-295.

Blumberg, D.G., and Greeley, R., 1993. Field studies of aerodynamic roughness length. Journal of Arid Environments 25: 39-48.

Brown, E. D., 2002. Effects of climate on Pacific herring, *Clupea pallasii*, in the northern Gulf of Alaska and Prince William Sound, Alaska. In: PICES-GLOBEC International Program on Climate Change and Carrying Capacity Report of 2001 BASS/MODEL, MONITOR and REX Workshops and the 2002 MODEL/ REX Workshop. PICES-North Pacific Marine Science Organization, Sidney, BC.

Bruun, P., 1962. Sea level rise as a cause of shore erosion. Journal of Waterways and Harbors Division (ASCE) 88: 116-130.

Bruun, P., 1988. The Bruun Rule of erosion by sea-level rise: A discussion on large scale two- and three-dimensional usages. Journal of Coastal Research 4: 627-648.

Bullard, J., 1997. A note on the use of the "Fryberger Method" for evaluating potential sand transport by wind. Journal of Sedimentary Research 67: 499-501.

Byshev V.I., and Lebedev, M.M., 2000. Probabilistic response of the atmosphere of the Northern Hemisphere to El Nino events. Oceanology 40: 631-638.

Carter, R.W.G., 1977. The rate and pattern of sediment interchange between beach and dune. In: Tanner, W.F. (Editor), Coastal Sedimentology. Florida State University, Tallahassee.

Carter, R.W.G., Hesp, P.A., and Nordstrom, K.F., 1990. Erosional landforms in coastal dunes. In: K.F. Nordstrom, Psuty, N.P., and Carter, R.W.G. (Editors), Coastal Dunes, Form and Process. John Wiley and Sons, London, UK.

Clague, J.J., 1991. Quaternary glaciation and sedimentation. In: Gabrielse, H., and Yorath, C.J. (Editors), Geology of the Cordilleran Orogen in Canada. Geology of Canada No. 4. Geological Survey of Canada. Ottawa, ON.

Cooper, J.A.G., Jackson, D.W., Navas, F., McKenna, J., and Malvarez, G., 2004. Identifying storm impacts on an embayed, high-energy coastline: examples from western Ireland. Marine Geology 210: 261-280.

Cooper, J.A.G., and Pilkey, O.H., 2004. Sea-level rise and shoreline retreat: time to abandon the Bruun Rule. Global and Planetary Change 43: 157-171.

Cooper, J.A.G., and Pilkey, O.H., 2004. Alternatives to the mathematical modeling of beaches. Journal of Coastal Research 20: 641-644.

Cowell, P., Thom, B., Jones, R., Everts, C., and Simanovic, D., 2006. Management of uncertainty in predicting climate-change impacts on beaches. Journal of Coastal Research 22: 232-245.

Crawford, W.R., Cherniawkey, J., Foreman, M., and Chandler, P., 1999. El Niño sea level signals along the west coast of Canada. North Pacific Marine Science Organization (PICES), Scientific Report No. 10. Sidney, BC.

Dally, W.R., and Dean, R.G., 1984. Suspended sediment transport and beach profile evolution. Journal of Waterway, Port, Coastal and Ocean Engineering 110: 15-33.

Davidson-Arnott, R., 2005. Conceptual model of the effects of sea level rise on sandy coasts. Journal of Coastal Research 21: 1166-1172.

Davidson-Arnott, R.G., and Law, M.N., 1996. Measurement and prediction of long-term sediment supply to coastal foredunes. Journal of Coastal Research 13: 654-663.

Davidson-Arnott R.G.D., MacQuarrie K., and Aagaard, T., 2005. The effect of wind gusts, moisture content and fetch length on sand transport on a beach. Geomorphology 68: 115-129.

Davis, R.A., and Hayes, M.O., 1984. What is a wave-dominated coast? Marine Geology 60: 313-329.

Dean, R.G., 1977. Equilibrium beach profiles: US Atlantic and Gulf Coasts. Ocean Engineering Report No. 12, University of Delaware, Newark.

Dean, R.G., 1991. Equilibrium beach profiles: Characteristics and applications. Journal of Coastal Research 7: 53-84.

Dingler, J.R., and Reiss, T.E., 2002. Changes to Monterey Bay beaches from the end of the 1982-83 El Niño through the 1997-98 El Niño. Marine Geology 181: 249-263.

Emery, W.J., and Hamilton, K., 1985. Atmospheric forcing of interannual variability in the northeast Pacific ocean – connections with El Niño. Journal of Geophysical Research – Oceans 90: 857-868.

Fedje, D.W., 1993. Sea-levels and Prehistory in Gwaii Haanas. Unpublished M.A. Thesis, University of Calgary, Canada.

Fedje, D.W., and Christensen, T., 1999. Modeling paleoshorelines and locating early Holocene coastal sites in Haida Gwaii. American Antiquity 64: 635-652.

Ferguson R.I., and Church M., 2004. A simple universal equation for grain settling velocity. Journal of Sedimentary Research 74: 933-937.

Folk, R.L., and Ward, W.C., 1957. Brazos River Bar: a study of the significance of grain size parameters. Journal of Sedimentary Petrology 27: 3-26.

Fryberger, S.G., 1979. Dune forms and wind regime. In: McKee, E.D. (Editor), A Study of Global Sand Seas. USGS Professional Paper 1052, Washington DC.

Gares, P.A., 1992. Topographic changes associated with coastal dune blowouts at Island Beach State Park, New Jersey. Earth Surface Processes and Landforms 17: 598-604.

Gares, P.A., Davidson-Arnott R.G.D., and Bauer B.O., 1996. Alongshore variations in aeolian sediment transport: Carrick Finn Strand, Ireland. Journal of Coastal Research 12: 673-682.

Gedalof, Z., and Smith, D., 2001. Interdecadal climate variability and regime-scale shifts in Pacific North America. Geophysical Research Letters 28: 1515-1518.

Gershunov, A., and Barnett, T.P., 1998. Interdecadal modulation of ENSO teleconnections. Bulletin of American Meteorological Society 79: 2715-2725.

Gilleland, E., Katz., R., and Young, G., 2003. Extremes Toolkit: Weather and Climate Applications of Extreme Value Statistics. Accessed February 26, 2006 from http://www.isse.ucar.edu/extremevalues/evtk.html.

Graham, N.E., and Diaz, H.F., 2001. Evidence for intensification of North Pacific winter cyclones since 1948. Bulletin of the American Meteorological Society 82: 1869-1893.

Gumbel, E.J., 1958. Statistics of Extremes. Columbia University Press, NY.

Harper, J., 2006. Wave climate. In: Sloan, N.A., and Harper, J.R. (Editors), Living marine legacy of Gwaii Haanas. V: Coastal zone values and management around Haida Gwaii. Parks Canada Technical Reports in Ecosystem Science. Parks Canada, Ottawa.

Harper, J., and Bartier, P., 2006. Geology. In: Sloan, N.A., and Harper, J.R. (Editors), Living marine legacy of Gwaii Haanas. V: Coastal zone values and management around Haida Gwaii. Parks Canada Technical Reports in Ecosystem Science. Parks Canada, Ottawa.

Harper, J.R., Austin, W.C., Morris, M.C., Reimer, P.D., and Reitmeier, R., 1994. Ecological Classification of Gwaii Haanas - Biophysical Inventory of Coastal Resources. Report prepared for Parks Canada, Calgary, Alberta by Coastal and Ocean Resources Inc., Sidney, BC.

Hebda, R. J.,1995. British Columbia vegetation and climate history with focus on 6 KA BP. Geographie Physique et Quaternaire 49: 55–79.

Hesp, P.A., 1988. Surfzone, beach, and foredune interactions on the Australian south east coast. Journal of Coastal Research SI 3: 15-25.

Hesp, P., 2002. Foredunes and blowouts: initiation, geomorphology and dynamics. Geomorphology 48: 245-268.

Hesp, P.A., Walker, I.J., Davidson-Arnott, R.G., and Ollerhead, J., 2005. Flow dynamics over a vegetated foredune at Prince Edward Island, Canada. Geomorphology 65: 71–84.

Hosier, P.E., and Cleary, W.J., 1977. Cyclic geomorphic patterns of washover on a barrier island in southeastern North Carolina. Environmental Geology 2: 23-31.

Houser, C.A., and Greenwood, B., 2005. Profile response of a lacustrine multiple barred nearshore to a sequence of storm events. Geomorphology 69: 118-137.

Hsu, S., 1971. Wind stress criteria in aeolian sand transport. Journal of Geophysical Research 76: 8684-8686.

Inman, D.L., Elwany, S.H.M., and Jenkins, S.C., 1993. Shorerise and bar-berm profiles on ocean beaches. Journal of Geophysical Research 98: 18181-18199.

IPCC (International Commission on Climate Change), 2001. Climate Change 2001: Impacts, Adaptation and Vulnerability. Cambridge University Press, Cambridge, UK.

Jackson, N.L., and Nordstrom, K.F., 1998. Aeolian transport of sediment on a beach during and after rainfall, Wildwood, NJ, USA. Geomorphology 22: 151-157.

James, R.W., 1969. Abnormal changes in wave height. Mariners Weather Log 13: 252-255.

Josenhans, H.W., Fedje, D.W., and Conway, K.W., 1995. Post glacial sea levels on the western Canadian continental shelf – Evidence for rapid change, extensive subaerial exposure, and early human habitation. Marine Geology 125: 73-94.

Josenhans, H., Fedje, D., and Pienitz, R., 2000. Early humans and rapidly changing Holocene sea levels in the Queen Charlotte Islands, Hecate Strait, British Columbia, Canada. Science 277: 71-74.

King, J., McFarlane, G., and Beamish, R., 2000. Decadal-scale patterns in the relative year class success f sablefish. Fisheries Oceanography 9: 62-70.

Klein, A., and Menezes, J., 2001. Beach morphodynamics and profile sequence for a headland bay coast. Journal of Coastal Research 17: 812-835.

Klein, A., Filho, L., and Schumacher, D.H., 2002. Short-term beach rotation processes in distinct headland bay beach systems. Journal of Coastal Research 18: 442-458.

Lancaster, N., 1988. Controls of eolian dune size and spacing. Geology 16: 972-975.

Larson, M., and Kraus, N.C., 1994. Temporal and spatial scales of beach profile change, Duck, North Carolina. Marine Geology 117: 75-94.

Law, M., and Davidson-Arnott, R., 1990. Seasonal controls on aeolian processes on the beach and foredune. In: Davidson-Arnott, R.G.D. (Editor), Canadian Symposium on Coastal Sand Dunes. National Research Council of Canada, Guelph, ON.

Lettau, H.H., and Lettau, K., 1978. Experimental and micro-meteorological field studies on dune migration. In: Lettau, K. and Lettau, H.H. (Editors), Exploring the world's driest climate. University of Wisconsin-Madison, Institute for Environmental Studies, Madison.

Maia, L., Freire, G., and Lacerda, L., 2005. Accelerated dune migration and aeolian transport during El Niño Events along the NE Brazilian Coast. Journal of Coastal Research 21: 1121-1126.

Mantua N.J., and Battisti, D.S., 1995. Aperiodic variability in the Zebiak-Cane coupled ocean-atmosphere model: Air-sea interactions in the western equatorial Pacific. Journal of Climate 8: 2897-2927.

Mantua, N.J., Hare, S.R., Zhang, Y., Wallace, J.M., and Francis, R.C., 1997. A Pacific interdecadal climate oscillation with impacts on salmon production. Bulletin of the American Meteorological Society 78: 1069-1079.

Masselink, G., personal email communication, March 13, 2007.

Masselink, G., and Pattiaratchi, C.B., 2001. Seasonal changes in beach morphology along the sheltered coastline of Perth, Western Australia. Marine Geology 172: 243-263.

Masselink, G., and Short, A.D., 1993. The effect of tide range on beach morpho-dynamics and morphology: a conceptual model. Journal of Coastal Research 9: 785-800.

Mathewes, R. W., and Heusser, L. E., 1981. A 12,000 year palynological record of temperature and precipitation trends in southwestern British Island, Queen Charlotte Islands, British Columbia. Canadian Journal of Botany 59: 707–710.

McKenna Neuman, C., and Scott, M.M., 1998. A wind tunnel study of the influence of pore water on aeolian sediment transport. Journal of Arid Environments 39: 403-419.

McLaren, P., and Bowles, D., 1985. The effects of sediment transport on grain-size distributions. Journal of Sedimentary Petrology 55: 457-470.

McPhaden, M.J., 2002. Encyclopedia of Global Environmental Change El Niño and La Niña: Causes and Global Consequences. John Wiley and Sons, Chichester, UK.

Nickling, W.G., and Davidson-Arnott, R.G.D., 1990. Aeolian sediment transport on beaches and coastal sand dunes. Symposium on Coastal Sand Dunes. Coastal Zone Engineering, Institute for Mechanical Engineering, National Research Council, Guelph, Ontario.

Noerlinger, P.D. and Brower, K.R., 2007. The melting of floating ice raises the ocean level. Geophysical Journal International 170: 145–150.

Nordstrom, K.F., and Jackson, N.L., 1993. The role of wind direction in eolian transport on a narrow sandy beach. Earth Surface Processes and Landforms 18: 675-685.

Nordstrom, K.F., Bauer, B.O., and Davidson-Arnott, R.G.D., 1996. Offshore aeolian transport across a beach: Carrick Finn Strand, Ireland. Journal of Coastal Research 12: 664-672.

Parks Canada, 2000. Unimpaired for future generations? Protecting ecological integrity with Canada's national parks, 2. Setting a new direction for Canada's national parks. Report of the Panel on the Ecological Integrity of Canada's National Parks. Parks Canada, Ottawa, Canada.

Pearce, K., 2005. Aeolian Geomorphology of Northeast Graham Island, Haida Gwaii, British Columbia. Unpublished MSc Thesis, University of Victoria.

Pellatt, M.G., and Mathewes, R.W., 1997. Holocene Tree Line and Climate Change on the Queen Charlotte Islands, Canada. Quaternary Research 48: 88-99.

Pojar, J., and Mackinnon, A. (Editors), 1994. Plants of Coastal British Columbia including Washington, Oregon and Alaska. Lone Pine Publishing, Edmonton, Alberta.

Psuty, N.P., 1988. Sediment budget and dune/beach interaction. Journal of Coastal Research SI 3: 1-4.

Psuty, N.P., 1993. Foredune morphology and sediment budget, Perdido Key, Florida. In: Pye, K. (Editor), Dynamics and Environmental Context of Aeolian Sedimentary Systems. Geological Society of London, London, UK.

Psuty, N.P., 2004. The Coastal Foredune: A morphological basis for regional coastal dune development. In: Martinez, M.L., and Psuty, N.P. (Editors), Ecological Studies Coastal Dunes, Ecology and Conservation. Springer-Verlag, Berlin.

Ranasinghe, R., McLoughlin, R., Short, A., and Symonds, G., 2004. The Southern Oscillation Index, wave climate, and beach rotation. Marine Geology 204: 273-287.

Rasmussen, K.R., 1989. Some aspects of flow over coastal dunes. Proceedings of the Royal society of Edinburgh 96B: 129-147.

Regnauld, H., and Louboutin, R., 2002. Variability of sediment transport in beach and coastal dune environments, Brittany, France. Sedimentary Geology 150: 17-29.

Ritter, D.F., Kochel, R.C., and Miller, J.R., 2002. Process Geomorphology. McGraw Hill, Boston, MA.

Ruggiero, P., Kaminsky, G.M., Komar, P.D., and McDougal, W.G., 1997. Extreme Waves and Coastal Erosion in the Pacific Northwest, Ocean Wave Measurement and Analysis, 3rd International Symposium, Waves '97, Virginia Beach, Virginia.

Ruggiero, P., Komar, P., McDougal, W., Marra, J., and Beach, R., 2001. Wave runup, extreme water levels and the erosion of properties backing beaches. Journal of Coastal Research 17: 407-419.

Ruz, M.H., and Meur-Ferec, C., 2004. Influence of high water levels on aeolian sand transport: upper beach/dune evolution on a macrotidal coast, Wissant Bay, northern France. Geomorphology 60: 73-87.

Sallenger, A.H., Krabill, W., Brock, J., Swift, R., Manizade, S., and Stockdon, H., 2002. Sea-cliff erosion as a function of beach changes and extreme wave runup during the 1997-1998 El Niño. Marine Geology 187: 279-297.

Sallenger, A.H., Krabill, W., and Brock, J., 2002. Sea-cliff erosion as a function of beach changes and extreme wave runup during the 1997-1998 El Niño. Marine Geology 187: 279-297.

Sarre, R.D., 1989. Aeolian sand drift from the intertidal zone on a temperate beach: potential and actual rates. Earth Surface Processes and Landforms 14: 247–258.

Saunders, K.E., and Davidson-Arnott, R.G.D., 1990. Coastal dune response to Natural Disturbances. In: Davidson-Arnott, R.G.D. (Editor), Canadian Symposium on Coastal Sand Dunes. National Research Council of Canada, Guleph, ON.

Schwing, F.B., Murphree, T., and Green, P.M., 2002. The Northern Oscillation Index (NOI): a new climate index for the northeast Pacific. Progress in Oceanography 53: 115-139.

Shabbar, A., Bonsal, B., and Khandekar, M., 1997. Canadian precipitation patterns associated with the southern oscillation. Journal of Climate 10: 3016-3027.

Sherman, D.J., and Bauer, B.O., 1993. Dynamics of beach-dune systems. Progress in Physical Geography 17: 413-447.

Sherman, D.J., Jackson, D.W.T., Namikas, S.L., and Wang, J., 1998. Wind-blown sand on beaches: an evaluation of models. Geomorphology 22: 113-133.

Short, A.D., 1979. Three dimensional beach-stage model. Journal of Geology 87: 553-571.

Short, A.D., 1985. Rip current type, spacing and persistence, Narrabeen Beach, Australia. Marine Geology 60: 47-71.

Short, A.D., and Hesp, P.A., 1982. Wave, beach and dune interactions in southeastern Australia. Marine Geology 48: 259-284.

Short, A.D., and Trembanis, A.C., 2004. Decadal scale patterns in beach oscillation and rotation Narrabeen Beach, Australia - Time series, PCA and wavelet analysis. Journal of Coastal Research 20: 523-532.

Short, A.D., and Masselink, G., 1999. Embayed and structurally controlled beaches. In: Short, A.D. (Editor), Handbook of Beach and Shoreface Morphodynamics. John Wiley & Sons, West Sussex, UK.

Short, A.D., Cowell, P.J., Cadee, M., Hall, W., and van Dijk, B., 1995. Beach rotation and possible relation to the Southern Oscillation. In: Aung, T.H. (Editor), Ocean Atmosphere Pacific Conference. National Tidal Facility, Adelaide, Australia.

Sinnott, D., personal email communication, 2006. Canadian Hydrographic Service, Institute of Ocean Sciences, Sidney, BC.

Storlazzi, C.D., and Griggs, G.B., 2000. Influence of El Niño-Southern Oscillation (ENSO) events on the evolution of central California's shoreline. Geological Society of America Bulletin 112: 236-249.

Storlazzi, C.D., Willis, C.M., and Griggs, G.B., 2000. Comparative impacts of the 1982-3 and 1997-8 El Niño winters on the central California coast. Journal of Coastal Research 16: 1022-1036.

Storlazzi, C.D., Willis, C.M., and Griggs, G.B., 2000. Comparative impacts of the 1982-83 and 1997-98 El Niño winters on the Central California Coast. Journal of Coastal Research 16: 1022-1036.

Subbotina, M.M., Thomson, R.E. and Rabinovich, A.B., 2001. Spectral characteristics of sea level variability along the west coast of North America during the 1982-83 and 1997-98 El Niño events. Progress in Oceanography 49: 353-372.

Svasek, J.N. and Terwindt, J.H.J., 1974. Measurements of sand transport by wind on a natural beach. Sedimentology 21: 311-322.

Timmermann, A., Oberhuber, J., Bacher, A., Esch, M., Latif, M., and Roeckner, E., 1999. Increased El Niño frequency in a climate model forced by future greenhouse warming. Nature 398: 694-696.

Trenberth, K., and Hurrell, J., 1994. Decadal atmosphere-ocean variations in the Pacific. Climate Dynamics 9: 303-319.

Tsoar, H., 1983. Dynamic processes acting on a longitudinal (seif) sand dune. Sedimentology 30: 567-578.

Tsoar, H., and Illenberger, W., 1998. Re-evaluation of sand dune mobility indices. Journal of Arid Lands Studies, 7S: 265-268.

Wal, A., and McManus, J., 1993. Wind regime and sand transport on a coastal beach–dune complex, Tentsmuir, eastern Scotland. In: Pye, K. (Editor), The Dynamics and Environmental Context of Aeolian Sedimentary Systems. The Geological Society, London, UK.

Walker, I.J., unpublished Parks Canada Report, 2007. Coastal Geoindicators Monitoring Program for Climate Change and Coastal Erosion in Gwaii Haanas National Park Reserve and Haida Heritage site. Report No. GH-2006-01.

Walker, I.J., 2006. Climate; Sea level; and Sandy beach-dune systems. In: Sloan, N.A., and Harper, J.R. (Editors), Living marine legacy of Gwaii Haanas. V: Coastal zone values and management around Haida Gwaii. Parks Canada Technical Reports in Ecosystem Science. Parks Canada, Ottawa.

Walker, I.J., and Barrie, J.V., 2006. Geomorphology and sea-level rise on one of Canada's most 'sensitive' coasts: Northeast Graham Island, British Columbia. Journal of Coastal Research SI 39: 220-226.

Walker, I.J., and Nickling, W.G., 2002. Dynamics of secondary airflow and sediment transport over and in the lee of transverse dunes. Progress in Physical Geography 26: 47-75.

Walker, I.J., Hesp, P.A., Davidson-Arnott, R.G.D., and Ollerhead, J., 2006. Topographic steering of alongshore airflow over a vegetated foredune: Greenwich Dunes, Prince Edward Island, Canada. Journal of Coastal Research 22: 1278-1291.

Welch, D., 2002. Geoindicators for Monitoring Canada's National Parks. Parks Canada Ecosystem Science Review Report No. 017. Parks Canada, Ottawa.

Wiedemann, A.M., Dennis, L.R.J., and Smith, F.H., 1999. Plants of the Oregon Coastal Dunes. Oregon State University Press, Corvalis, Oregon.

Wiggs, G.F.S., Baird, A.J., and Atherton, R.J., 2004. The dynamic effects of moisture on the entrainment and transport of sand by wind. Geomorphology, 59: 13-30.

Wolter, K., and Timlin, M.S., 1993. Monitoring ENSO in COADS with a seasonally adjusted principal component index. Proceedings of the 17th Climate Diagnostics Workshop, NOAA.NMC.CAC, NSSL, Oklahoma Climate Survey. Norman, OK.

Wolter, K., and Timlin, M.S., 1998. Measuring the strength of ENSO – how does 1997/98 rank? Weather 53: 315-324.

Wright, L.D., and Short, A.D., 1984. Morphodynamic variability of surf zones and beaches - a synthesis. Marine Geology 56: 93-118.

Wright, L.D., and Thom, B.G., 1977. Coastal depositional landforms, a morphodynamic approach. Progress in Physical Geography 1: 412-459.

Zhang, Y., Wallace, J.M., and Battisti, D.S., 1997. ENSO-like interdecadal variability: 1900-93. Journal of Climate 10: 1004-1020.

Becs Cumming
UVic Dept. of Geography
PO Box 3050 STN CSC
Victoria, BC, V8W 3P5
Canada
June 1, 2007

Dear Patrick,

This letter follows from our recent emails regarding permission to reprint your figure in my Master's thesis titled, "Beach-dune morphodynamics and climatic variability in Gwaii Haanas National Park and Haida Heritage Site, British Columbia, Canada."

The University requires formal, written permission from you, the copyright owner. I would like permission to reprint the following figures in my thesis:
Hesp, P. 2002. Foredunes and blowouts: initiation, geomorphology and dynamics. Geomorphology, 48: 245-268. Figure 3 (pg. 253): A model of established foredune morphology.

The requested permission extends to any future revisions and editions of my thesis, including non-exclusive world rights in all languages and to the prospective publications of my thesis through the National Library of Canada and its agents, including University Microfilms International (UMI). These rights will in no way restrict republication of the material in any form by you or by others authorized by you. Your signing of this letter will also confirm that you own (or your company owns) the copyright to the above described material. If you agree with these arrangements, please sign this letter where indicated and return it to me at the address included in this letter.

Many thanks,
Becs Cumming

PERMISSION GRANTED FOR THE USE
REQUESTTED ABOVE:
Name: Patrick Hesp

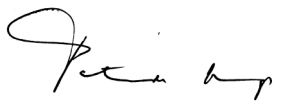

Date:15/7/2007

Becs Cumming
UVic Dept. of Geography
PO Box 3050 STN CSC
Victoria, BC, V8W 3P5
Canada
June 7, 2007

Dear Kim,

This letter is following up from our emails regarding permission to reprint your figures in my Master's thesis titled, "Beach-dune morphodynamics and climatic variability in Gwaii Haanas National Park and Haida Heritage Site, British Columbia, Canada."

The University requires formal, written permission from you, the copyright owner. I would like permission to reprint the following figures from your M.Sc. thesis:
Figure 5.1: Annual wind rose from Rose Spit
Figure 5.2: Monthly wind roses from Rose Spit
Figure 5.4: Annual drift potential from Rose Spit
Figure 5.5: Monthly drift potential from Rose Spit
Figure 5.7: Monthly RDP and RDD variation from Rose Spit

The requested permission extends to any future revisions and editions of my thesis, including non-exclusive world rights in all languages and to the prospective publications of my thesis through the National Library of Canada and its agents, including University Microfilms International (UMI). These rights will not restrict republication of the material in any form by you or by others authorized by you. Your signing of this letter will also confirm that you own the copyright to the above material. If you agree with these arrangements, please sign this letter where indicated and return it to me at the UVic geography department.

Many thanks,
Becs Cumming

PERMISSION GRANTED FOR THE USE
REQUESTED ABOVE:

Name: Kim Pearce
Date: June 21, 2007

Becs Cumming
UVic Dept. of Geography
PO Box 3050 STN CSC
Victoria, BC, V8W 3P5
Canada

June 1, 2007

Dear Gerd,

The letter follows from our recent emails regarding permission to reprint your figure in my Master's thesis titled, "Beach-dune morphodynamics and climatic variability in Gwaii Haanas National Park and Haida Heritage Site, British Columbia, Canada." The University requires formal, written permission from you, the copyright owner.

I would like permission to reprint the following figures in my thesis:
Masselink, G., and Short, A.D., 1993. The effect of tide range on beach morphodynamics and morphology: a conceptual model. Journal of Coastal Research 9: 785-800. Figure 4: Conceptual beach model.

The requested permission extends to any future revisions and editions of my thesis, including non-exclusive world rights in all languages and to the prospective publications of my thesis through the National Library of Canada and its agents, including University Microfilms International (UMI). These rights will in no way restrict republication of the material in any form by you or by others authorized by you. Your signing of this letter will also confirm that you own (or your company owns) the copyright to the above-described material.

If you agree with these arrangements, please sign this letter where indicated and return it to me at the address included in this letter.

Many thanks,

Becs Cumming

PERMISSION GRANTED FOR THE USE REQUESTED ABOVE:

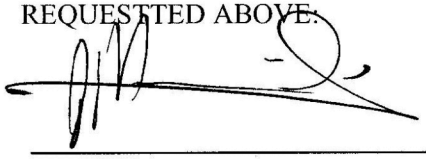

Name: Gerd Masselink
Date: 4 June 2007

BRITISH COLUMBIA
The Best Place on Earth

Ministry of Labour and Citizens' Services

Common Business Services

Intellectual Property Program
Box 9492 Stn Prov Govt
Victoria BC V8W 9N7

Copyright Permission Request Form

Date of Request 01/05/2007

File Number: 7200001861

Organization Requesting Copyright Permission:

Rebecca Cumming
Rebecca Cumming - Student
University of Victoria PO Box 3050, STN CSC
Victoria British Columbia V8W 3P5

Publication Information

Title: BC Air Photo BCC04002

ISBNNumber: ISSNNumber:

Intended Audience: N/A

Copyright Request

Number of Copies N/A Excerpt BC Air Photo

Proposed Use: Thesis

Permission/Instructions ☑ Approved ☐ Denied

Permission is granted to Rebecca Cumming ("the Requestor"), student at University of Victoria ("UVIC"), to reproduce Province of British Columbia Air Photo BCC04002 (the "Material"). It is understood that the Material will be included in the Requestor's thesis through UVIC and that the thesis will be available to learners and scholars through the National Library of Canada and UVIC.

It is further understood that the Material is being provided to the Requestor by the Province of BC "as is", without warranties or representations express or implied with respect to the Material.

Permission is not granted for the commercial publication and reproduction of the Material except under the National Library of Canada "Non-exclusive license to reproduce theses".

The following credit line is to be included: Copyright © Province of British Columbia. All rights reserved. Reprinted with permission of the Province of British Columbia. www.ipp.gov.bc.ca

Should you have any questions please contact the Intellectual Property Program by fax at 250 356-0846 or by e-mail at ipp@mail.gov.bc.ca

Victoria Heasman
A/Director

Approval Date: 01/05/2007